State University of New York Report

LES, DNS and RANS for the Analysis of High-Speed Turbulent Reacting Flows

by

P. Givi, D.B. Taulbee, V. Adumitroaie,
G.J. Sabini and G.S. Shieh

Department of Mechanical and Aerospace Engineering
State University of New York at Buffalo
Buffalo, New York 14260-4400

Annual Report Submitted to
NASA Langley Research Center

Progress Report on Activities Supported Under Grant NAG 1-1122

for the Period

September 1, 1993 - September 1, 1994

Contents

LES, DNS and RANS for the Analysis of High-Speed Turbulent Reacting Flows

P. Givi, D.B. Taulbee, V. Adumitroaie, G.J. Sabini and G.S. Shieh
Department of Mechanical and Aerospace Engineering
State University of New York at Buffalo
Buffalo, New York 14260-4400

Abstract

The purpose of this research is to continue our efforts in advancing the state of knowledge in large eddy simulation (LES), direct numerical simulation (DNS) and Reynolds averaged Navier Stokes (RANS) methods for the computational analysis of high-speed reacting turbulent flows. In the second phase of this work, covering the period: September 1, 1993 - September 1, 1994, we have focused our efforts on two research problems: (1) Developments of "algebraic" moment closures for statistical descriptions of nonpremixed reacting systems, (2) Assessments of the *Dirichlet* frequency in presumed scalar probability density function (PDF) methods in stochastic description of turbulent reacting flows. This report provides a complete description of our efforts during this past year as supported by the NASA Langley Research Center under Grant NAG-1-1122.

Technical Monitor:

Dr. J. Philip Drummond, Hypersonic Propulsion Branch, Tel: 804-864-2298 is the Technical Monitor of this Grant.

1 Introduction

While this program is associated with research on several problems of current interest in reacting turbulent flows, its primary objective is to facilitate the use of LES for the computational analyses of practical high speed transport. With the evolution of our work, sponsored by NASA for the past four years, it has become clear that to meet the needs of this program it is required to make use of advanced, yet practical, stochastic and statistical procedures in conjunctions with reliable computational procedures. The importance of the these methods have become clear through the results of our most recent work on LES of turbulent reacting flows.[1] It is now well-established that many of the conventional closures which work reasonably well in RANS[2] fail in LES. Thus, it has become clear that the first step to be taken in any meaningful LES of reacting flows is to make sure that the moments "up to the second order level" are modeled accurately. It must be noted that in none of the previous contributions in LES, was this the subject of a detailed study (see Ref.[3]). In fact, in almost all previous and concurrent contributions, only the "first" subgrid scale moment of the transport variables have been the subject of modeling. That is, the approach is based on a variation of the Smagorinsky[4] closure. Unfortunately the application of such closures does not work in LES of reacting flows. In our efforts within the past year, we have made use of the recent work of one of the Co-PI's of this proposal (D.B. Taulbee) in developing improved algebraic models. In his previous work, Taulbee[5] shows that with the modeled dynamics equations for the Reynolds stresses, it is possible to develop an improved explicit algebraic Reynolds stress model that can predict many of the flow features more accurately than the conventional models. This improvement is due to the fundamentals of the approach in that the closure is based on transport equations for the higher-order moments. Therefore, more physics is embedded in the equations. Furthermore, the extra degree of freedom provided by the closure allows more adaptability in its optimization for predictive analysis. In fact, some sample results in Refs.[1,6] do show that these new models are superior to previous closures in LES, even though the difference is not significant in RANS (also see Ref.[2]).

In LES of reacting flow phenomena in addition to the first two moments, the PDF of the

scalars within the subgrid must also be specified. Thus, we have continued our work on PDF modeling as well. Based on our extensive work in the first phase of this research[7-9] we have established that the most meaningful means of utilizing the PDF in LES is by mean of describing and solving the transport equations governing its evolution. However, it has also become clear to us the most recent PDF procedure based on the Amplitude Mapping Closure of Kraichnan[10,11] cannot be used for any type of practical applications (nor can they be utilized in basic applications in flows with nonequilibrium chemistry). Therefore, we have decided to rely and focus on the conventional Coalescence/Dispersion methodology.[12-14] Work is underway in developing numerical schemes based on the Monte Carlo methods to solve the PDF within the subgrid in LES of reacting flows. We do not have any substantiated results to report at this time. However, we do have extensive new results in PDF modeling based on "presumed methods". In particular, we have made a rather extensive study in determining the capabilities and drawbacks of the *Dirichlet* frequency in probability modeling of nonpremixed reacting flows. Our reason for this study is due to the interest at NASA LaRC in the approach. In particular, we cite the work of Gaffney *et al.*[15,16] who have used the Dirichlet density for modeling of high speed reacting systems. We feel that a detailed appraisal of this versatile density is in order, and we have made use of all recent laboratory data for this purpose.

2 Summary of Achievements

Appendix I and Appendix II provide a complete write-up on our accomplishments on the two components of this program. For the convenience of the reader, here a summary is provided:

Our efforts in (1) have been devoted towards developing closures which can be used for modeling of the "second order moments" in the contexts of both RANS and LES. In particular, explicit algebraic scalar flux models that are valid for three-dimensional turbulent flows are derived from a hierarchy of second-order moment closures. The mathematical procedure is based on the *Cayley-Hamilton* theorem and is an extension of the scheme developed by

Pope[17] and Taulbee.[5] Several closures for the pressure-scalar gradient correlations are considered and explicit algebraic relations are provided of the velocity-scalar correlations in both non-reacting and reacting flows. In the latter, the role of the Damköhler number is explicitly exhibited in turbulent flows with nonpremixed reactants. The relationship between these closures and traditional models based on the linear gradient diffusion approximation is theoretically established. The results of model predictions are assessed via comparison with available laboratory data.

In efforts related to (2), the recent experimental data in Ref.[18] pertaining to compositional structure of a turbulent reactive scalar mixing layer are reproduced by a mathematical-computational procedure utilizing the *Pearson* family (PF) of univariate and multivariate PDF's. By detailed comparisons against these data and some additional data generated by DNS of a spatially developing reacting mixing layer, an appraisal is made of the applicability and the extent of validity of PF for statistical description of reactant fluctuations. In accord with the experiment, a chemical reaction of the type $A + B \rightarrow Products$ is simulated in isothermal, incompressible flows. A wide range of the Damköhler number is considered including both frozen and equilibrium chemistry flows. The comparison of the results with laboratory data indicates that PF generated PDF's are very convenient, in the absence of better alternatives, for modeling the influence of turbulence on the reactant conversion rate. In particular, the Dirichlet frequency provides the most reasonable means of portraying the multivariate scalar PDF. The extent of agreement improves as the magnitude of the Damköhler number is increased. A more detailed comparative assessment of the model predictions against DNS data confirms the relative superiority of the Dirichlet PDF even though it is mathematically shown that this frequency is invalid in equilibrium flows. With the use of the PF generated PDF, the autospectral density function and the cross-spectra density function (including both the coherence and the phase) of the reacting scalars under equilibrium chemistry are related to frequency spectra of a conserved mixture fraction. This relation is very convenient and is favored over previous models for predicting the spectral characteristics of reacting scalars in the central region of the laboratory mixing layer and in any other homogeneous flow configurations.

The results of our work in both (1) and (2) are complete. Two papers have been written and are submitted for publication.

3 Work in Progress

In addition to the main two topics discussed in the appendixes, work is in progress in two other research areas: (1) LES by means of the Monte Carlo solution of the subgrid scalar PDF, and (2) LES by means of mechanistic models. In (1), we have just completed the development of a combined finite difference-Monte Carlo procedure for solving the PDF of scalar variables within the subgrid. At this point, we are faced with one major problem and that is the Monte Carlo solution of the advection term in the PDF transport. We have used a first order upwinding scheme for this procedure. This methods is stable, but introduces a significant amount of artificial diffusivity. In fact the amount of diffusivity introduced by the scheme is *more* that by the subgrid closure. Unfortunately, none of the higher order schemes, including all of those in Refs.[19,20] are amenable to Monte Carlo discretization. This serious problem is the subject of our current investigation.

In (2), due to our recent progress in the area of diffusion flamelet modeling (DFM)[21-23] of nonpremixed reacting flows, we have devoted a small portion of our time toward exploring the possibility of developing subgrid scale closures by means of DFM. Based on our earlier findings reported in Ref.,[24] we expect that the model should work reasonably well in the flamelet region; that is when the chemistry is fast and the thickness of the flame is very small. In such cases, the LES methodology based on DFM is expected to be satisfactory. For this purpose we have initiated a task in which typical mixing controlled chemistry models such as those developed in Ref.[25] are used in a *dynamic* subgrid model[26] for LES of homogeneous reacting flows. We have completed the mathematical formulation to accomplish this task; but we do not have any significant numerical data to report at the present time.

We hope to have results in each of these two endeavors before the deadline for our next semi-annual report.

4 Personnel

Dr. Peyman Givi is as the PI of this project. Drs. and Dale B. Taulbee and Cyrus K. Madnia serve as the Co-PI's. Of course, as before, Dr. Givi is responsible for a timely and successful completion of all the tasks.

There are two Ph.D. candidates who are supported by this grant: Mr. Virgil Adumitroaie and Mr. Craig Steinberger. In addition, the following students have contributed to various parts of the project, but are not financially supported by the NASA grant: Mr. Geoffrey Shieh, Mr. Sean Garrick and Mr. George Sabini. All these students have recently completed the requirements for M.S. degree at SUNY-Buffalo. Mr. Shieh and Mr. Garrick are continuing their studies toward Ph.D. at SUNY-Buffalo and are expected to continue the the work of Virgil Adumitroaie and Craig Steinberger. The latter two are expected to complete the requirements for Ph.D. within the 1994-1995 academic year.

References

[1] Frankel, S. H., Adumitroaie, V., Madnia, C. K., and Givi, P., Large Eddy Simulations of Turbulent Reacting Flows by Assumed PDF Methods, in Ragab, S. A. and Piomelli, U., editors, *Engineering Applications of Large Eddy Simulations*, pp. 81–101, ASME, FED-Vol. 162, New York, NY, 1993.

[2] Taulbee, D. B., Engineering Turbulence Models, in George, W. K. and Arndt, R., editors, *Advances in Turbulence*, pp. 75–125, Hemisphere Publishing Co., New York, NY., 1989.

[3] Galperin, B. and Orszag, S. A., editors, *Large Eddy Simulations of Complex Engineering and Geophysical Flows*, Cambridge University Press, Cambridge, U.K., 1993.

[4] Smagorinsky, J., General Circulation Experiments With the Primitive Equations. I. The Basic Experiment, *Monthly Weather Review*, **91**(3):99–164 (1963).

[5] Taulbee, D. B., An Improved Algebraic Reynolds Stress Model and Corresponding Nonlinear Stress Model, *Phys. Fluids A*, **4**(11):2555–2561 (1992).

[6] Frankel, S. H., Probabilistic and Deterministic Description of Turbulent Flows with Nonpremixed Reactants, Ph.D. Thesis, Department of Mechanical and Aerospace Engineering, State University of New York at Buffalo, Buffalo, NY, 1993.

[7] Madnia, C. K., Frankel, S. H., and Givi, P., Reactant Conversion in Homogeneous Turbulence: Mathematical Modeling, Computational Validations and Practical Applications, *Theoret. Comput. Fluid Dynamics*, **4**:79–93 (1992).

[8] Frankel, S. H., Madnia, C. K., and Givi, P., Comparative Assessment of Closures for Turbulent Reacting Flows, *AIChE J.*, **39**(5):899–903 (1993).

[9] Miller, R. S., Frankel, S. H., Madnia, C. K., and Givi, P., Johnson-Edgeworth Translation for Probability Modeling of Binary Scalar Mixing in Turbulent Flows, *Combust. Sci. and Tech.*, **91**(1-3):21–52 (1993).

[10] Kraichnan, R. H., Closures for Probability Distributions, *Bull. Amer. Phys. Soc.*, **34**:2298 (1989).

[11] Chen, H., Chen, S., and Kraichnan, R. H., Probability Distribution of a Stochastically Advected Scalar Field, *Phys. Rev. Lett.*, **63**(24):2657–2660 (1989).

[12] Pope, S. B., An Improved Turbulent Mixing Model, *Combust. Sci. and Tech.*, **28**:131–145 (1982).

[13] Kosály, G. and Givi, P., Modeling of Turbulent Molecular Mixing, *Combust. Flame*, **70**:101–118 (1987).

[14] McMurtry, P. A. and Givi, P., Direct Numerical Simulations of Mixing and Reaction in a Nonpremixed Homogeneous Turbulent Flow, *Combust. Flame*, **77**:171–185 (1989).

[15] Gaffney, R. L., White, J. A., Girimaji, S. S., and Drummond, J. P., Modeling of Turbulent/Chemistry Interactions Using Assumed PDF Methods, AIAA Paper 92-3638, 1992.

[16] Gaffney, R. L., White, J. A., Girimaji, S. S., and Drummond, J. P., Modeling of Temperature and Species Fluctuations in Turbulent, Reacting Flow, *Computing Systems in Engineering*, **5**(2):117–113 (1994).

[17] Pope, S. B., A More General Effective-Viscosity Hypothesis, *J. Fluid Mech.*, **72**:331–340 (1975).

[18] Bilger, R. W., Saetran, L. R., and Krishnamoorthy, L. V., Reaction in a Scalar Mixing Layer, *J. Fluid Mech.*, **233**:211–242 (1991).

[19] Carpenter, M. H., A High-Order Compact Numerical Algorithm for Supersonic Flows, in Morton, K. W., editor, *Twelfth International Conference on Numerical Methods in Fluid Dynamics, Lecture Notes in Physics*, Vol. 371, pp. 254–258, Springer-Verlag, New York, NY, 1990.

[20] Carpenter, M. H., Gottlieb, D., and Abarbanel, S., The Stability of Numerical Boundary Treatment for Compact High-Order Finite Difference Schemes, ICASE Report 91-71, NASA Langley Research Center, Hampton, VA, 1991.

[21] Williams, F. A., Recent Advances in Theoretical Description of Turbulent Diffusion Flames, in Brodkey, R. S., editor, *Turbulence in Mixing Operations*, pp. 189–209, Academic Press, New York, NY, 1975.

[22] Peters, N., Laminar Diffusion Flamelet Models in Non-Premixed Turbulent Combustion, *Prog. Energy Combust. Sci.*, **10**:319–339 (1984).

[23] Peters, N., Laminar Flamelet Concepts in Turbulent Combustion, in *Proceedings of 21st Symp. (Int.) on Combustion*, pp. 1231–1250, The Combustion Institute, Pittsburgh, PA, 1986.

[24] Steinberger, C. J., Vidoni, T. J., and Givi, P., The Compositional Structure and the Effects of Exothermicity in a Nonpremixed Planar Jet Flame, *Combust. Flame*, **94**:217–232 (1993).

[25] Givi, P., Turbulent Reacting Flows, Ph.D. Thesis, Carnegie Tech., Pittsburgh, PA., 1984.

[26] Germano, M., Turbulence: The Filtering Appraoch, *J. Fluid Mech.*, **238**:325–336 (1992).

APPENDIX I

Explicit Algebraic Scalar-Flux Models for Turbulent Reacting Flows

V. Adumitroaie, D.B. Taulbee and P. Givi
Department of Mechanical and Aerospace Engineering
State University of New York at Buffalo
Buffalo, NY 14260-4400

Abstract

Explicit algebraic scalar flux models that are valid for three-dimensional turbulent flows are derived from a hierarchy of second-order moment closures. The mathematical procedure is based on the *Cayley-Hamilton* theorem and is an extension of the scheme developed by Pope[1] and Taulbee.[2] Several closures for the pressure-scalar gradient correlations are considered and explicit algebraic relations are provided of the velocity-scalar correlations in both non-reacting and reacting flows. In the latter, the role of the Damköhler number is explicitly exhibited in turbulent flows with non-premixed reactants. The relationship between these closures and traditional models based on the linear gradient diffusion approximation is theoretically established. The results of model predictions are assessed via comparison with available laboratory data.

PACS: 47.27.Eq (Turbulence simulation and modeling), 47.70.Fw (Chemically reactive flows), 47.27.Qb (Turbulent diffusion), 47.27.Nz (Boundary layer and shear turbulence), 47.27.Wg (Jets) 02.10.Sp (Matrix theory).

I Introduction

Despite extensive recent contributions in direct and large eddy simulations of turbulent reacting flows, the application of such simulations is limited to "simple flows".[3–5] Based on this fact, it is now widely recognized that the "statistical" approach is *still* the most practical means in computational turbulence, and future capabilities in predictions of engineering turbulent combustion systems depend on the extent of developments in statistical modeling.

The literature on computational prediction of nonreactive turbulent transport is abundant with schemes based on single-point statistical closures for moments up to the second-

order.[6–10] The presence of scalar contaminant and/or chemical reactions generates additional length and time scales which have to be considered.[3,11–16] To account for these scales in a second-order moment formulation the solution of a large number of transport equations is required. This could potentially make the approach less attractive, but can be alleviated by utilizing "algebraic closures".[1,2,17–22] Such closures are either derived directly from the modeled transport equations of the respective moments, or other types of representations that lead to anisotropic "eddy-diffusivities".[23–26] In this manner, the number of equations is reduced but the accuracy of the second-order formulation and the versatility of the approach is preserved.

In this work, we expand upon the formulation developed by Taulbee[2] (also see Ref.[22]) to provide explicit algebraic relations for the flux of scalar variables in isothermal turbulent flows. Both nonreacting and reacting flows are considered. In the latter, a second-order, irreversible chemical reaction of the type $A + B \rightarrow P$ is considered in turbulent flows with initially segregated reactants. The closure explicitly accounts for the influence of the Damköhler number and, of course, includes the mixing solution in the limit of zero Damköhler number. Several closures for the pressure-scalar gradients correlations are considered and the predicted results are compared with available experimental data in nonreacting and reacting turbulent shear flows.

II Theoretical Background

With the convention that the angle brackets, $\langle\ \rangle$ represent the ensemble mean value of a transport variable and the prime denotes its fluctuations from the mean, the nondimensionalized averaged equations for incompressible, isothermal turbulent reacting flows are:

$$\frac{\partial \langle u_j \rangle}{\partial x_j} = 0, \tag{1}$$

$$\frac{\partial \langle u_i \rangle}{\partial t} + \frac{\partial \langle u_i \rangle \langle u_j \rangle}{\partial x_j} = -\frac{\partial \langle u_i' u_j' \rangle}{\partial x_j} - \frac{1}{\langle \rho \rangle} \frac{\partial \langle p \rangle}{\partial x_i} + \frac{1}{Re} \frac{\partial^2 \langle u_i \rangle}{\partial x_j \partial x_j}, \quad i,j = 1,2,3 \tag{2}$$

$$\frac{\partial\langle Y_\alpha\rangle}{\partial t}+\frac{\partial\langle Y_\alpha\rangle\langle u_j\rangle}{\partial x_j}=-\frac{\partial\langle u_j'Y_\alpha'\rangle}{\partial x_j}+\frac{1}{ScRe}\frac{\partial^2\langle Y_\alpha\rangle}{\partial x_j\partial x_j}+\langle\dot{\omega}_\alpha\rangle,$$
$$\alpha=A,B. \tag{3}$$

Here u_i, P, ρ, Y_α, Re, and Sc denote the i-th component of the velocity vector, the pressure, fluid density, mass fraction of species α, the Reynolds number, and the Schmidt number, respectively. $\langle\dot{\omega}_\alpha\rangle$ represents the rate of chemical reaction ($\langle\dot{\omega}_A\rangle=\langle\dot{\omega}_B\rangle$):

$$\langle\dot{\omega}_\alpha\rangle=-Da(\langle Y_A\rangle\langle Y_B\rangle+\langle Y_A'Y_B'\rangle), \tag{4}$$

where Da is the Damköhler number. The algebraic formulation involves a two-equation scheme in which the Reynolds stresses and the scalar fluxes are expressed by nonlinear functions of the mean gradients and the time scales of the flow. The mechanical time scale is determined by the solution of transport equations for the kinetic energy of the turbulence $\langle k\rangle=\langle u_i'u_i'\rangle/2$ and for the turbulent dissipation: $\langle\epsilon\rangle=\frac{1}{Re}\langle\frac{\partial u_i'}{\partial x_j}\frac{\partial u_i'}{\partial x_j}\rangle$. For boundary-free shear flow, these equations are:[9,27]

$$\frac{\partial\langle k\rangle}{\partial t}+\frac{\partial\langle k\rangle\langle u_j\rangle}{\partial x_j}=-\frac{\partial}{\partial x_j}\left[\langle u_j'k\rangle+\frac{1}{\langle\rho\rangle}\langle p'u_j'\rangle\right]+\frac{1}{Re}\frac{\partial^2\langle k\rangle}{\partial x_j\partial x_j}$$
$$-\langle u_i'u_j'\rangle\frac{\partial\langle u_i\rangle}{\partial x_j}-\frac{1}{Re}\langle\frac{\partial u_i'}{\partial x_j}\frac{\partial u_i'}{\partial x_j}\rangle, \tag{5}$$

$$\frac{\partial\langle\epsilon\rangle}{\partial t}+\frac{\partial\langle\epsilon\rangle\langle u_j\rangle}{\partial x_j}=-\frac{\partial}{\partial x_j}\left[\langle u_j'\epsilon\rangle+\frac{2}{Re}\langle\frac{\partial p'}{\partial x_k}\frac{\partial u_j'}{\partial x_k}\rangle\right]+\frac{1}{Re}\frac{\partial^2\langle\epsilon\rangle}{\partial x_j\partial x_j}$$
$$-C_{\epsilon_1}\frac{\langle\epsilon\rangle}{\langle k\rangle}\langle u_i'u_j'\rangle\frac{\partial\langle u_i\rangle}{\partial x_j}-C_{\epsilon_2}\frac{\langle\epsilon\rangle^2}{\langle k\rangle}, \tag{6}$$

with $C_{\epsilon_1}=1.4$ and $C_{\epsilon_2}=1.9$. Treatment of the scalar variable requires the solution of additional transport equations for the reactants' covariance $\langle Y_\alpha'Y_\beta'\rangle$, and dissipations $\langle\epsilon_{\alpha\beta}\rangle=\frac{1}{ScRe}\langle\frac{\partial Y_\alpha'}{\partial x_j}\frac{\partial Y_\beta'}{\partial x_j}\rangle$. For the former we have:

$$\frac{\partial\langle Y'_\alpha Y'_\beta\rangle}{\partial t}+\frac{\partial\langle Y'_\alpha Y'_\beta\rangle\langle u_j\rangle}{\partial x_j}=-\frac{\partial\langle u'_j Y'_\alpha Y'_\beta\rangle}{\partial x_j}+\frac{1}{ScRe}\frac{\partial^2\langle Y'_\alpha Y'_\beta\rangle}{\partial x_j\partial x_j}$$
$$-\langle u'_j Y'_\alpha\rangle\frac{\partial\langle Y_\beta\rangle}{\partial x_j}-\langle u'_j Y'_\beta\rangle\frac{\partial\langle Y_\alpha\rangle}{\partial x_j}-\frac{2}{ScRe}\langle\frac{\partial Y'_\alpha}{\partial x_j}\frac{\partial Y'_\beta}{\partial x_j}\rangle$$
$$+\langle\dot{\omega}_\alpha Y'_\beta\rangle+\langle\dot{\omega}_\beta Y'_\alpha\rangle. \tag{7}$$

By neglecting the third-order mass fraction correlations, the chemical source terms in the expanded form read (no summation on greek indexes) $\langle\dot{\omega}_\alpha Y'_\beta\rangle+\langle\dot{\omega}_\beta Y'_\alpha\rangle=-Da[(\langle Y'_\alpha Y'_A\rangle+\langle Y'_\beta Y'_A\rangle)\langle Y_B\rangle+(\langle Y'_\alpha Y'_B\rangle+\langle Y'_\beta Y'_B\rangle)\langle Y_A\rangle]$. Full resolution of the nonlinear interactions in the chemical scalar fields requires significant computational effort in practical applications. The neglect of the higher-order scalar fluctuations is justified by earlier results[28] but cannot be recommended for general applications. In such applications, the single-point probability density function (pdf) or the joint pdf of the scalar variable provides the required information.[29] The inclusion of the pdf is not attempted here.

By using the first order term in the two-scale direct-interaction approximation, Yoshizawa[26] develops a generic model for the scalar dissipation. An equivalent expression is obtained from Yoshizawa's results (by making use of the dissipation time scales ratio $r_\alpha=\epsilon\langle Y'^2_\alpha\rangle/\langle k\rangle\epsilon_\alpha$). The equivalent form of this equation including the effects of chemical reactions is of the form:[30]

$$\frac{\partial\langle\epsilon_{\alpha\beta}\rangle}{\partial t}+\frac{\partial\langle\epsilon_{\alpha\beta}\rangle\langle u_j\rangle}{\partial x_j}=-\frac{\partial}{\partial x_j}\langle u'_j\epsilon_{\alpha\beta}\rangle+\frac{1}{ScRe}\frac{\partial^2\langle\epsilon_{\alpha\beta}\rangle}{\partial x_j\partial x_j}$$
$$-C_{y_1}\frac{\langle\epsilon\rangle}{\langle k\rangle}\frac{1}{2}\left(\langle u'_j Y'_\alpha\rangle\frac{\partial\langle Y_\beta\rangle}{\partial x_j}+\langle u'_j Y'_\beta\rangle\frac{\partial\langle Y_\alpha\rangle}{\partial x_j}\right)-C_{y_2}\frac{\langle\epsilon_{\alpha\beta}\rangle}{\langle k\rangle}\langle u'_i u'_j\rangle\frac{\partial\langle u_i\rangle}{\partial x_j}$$
$$-C_{y_3}\frac{\langle\epsilon_{\alpha\beta}\rangle^2}{\langle Y'_\alpha Y'_\beta\rangle}-C_{y_4}\frac{\langle\epsilon\rangle\langle\epsilon_{\alpha\beta}\rangle}{\langle k\rangle}+\mathcal{S}_{\alpha\beta}. \tag{8}$$

In the limiting case of pure mixing, the magnitudes of the constants are: $C_{y_1}=1.7$, $C_{y_2}=1.4$, $C_{y_3}=2.0$ and $C_{y_4}=0.9$. Similar values are suggested in Ref.[31] In this equation, the chemical source term source is of the form:

$$\mathcal{S}_{\alpha\beta}=-Da\left[(\langle\epsilon_\alpha\rangle+\langle\epsilon_{\alpha\beta}\rangle)\langle Y_\beta\rangle+(\langle\epsilon_\beta\rangle+\langle\epsilon_{\alpha\beta}\rangle)\langle Y_\alpha\rangle\right],\quad\alpha\neq\beta. \tag{9}$$

Each of the reactants' variances obey a similar transport equation with the chemical source:

$$\mathcal{S}_{\alpha\alpha} = -2Da\left(\langle\epsilon_\alpha\rangle\langle Y_\lambda\rangle + \langle\epsilon_{\alpha\lambda}\rangle\rangle\langle Y_\alpha\rangle\right), \tag{10}$$

where $\lambda = B$ if $\alpha = A$ and vice versa. To complete the closure formulation, all the third-order transport terms are described by the gradient diffusion hypothesis. Denoting by Θ any of the second-order scalars, we have:

$$\langle u_i'\Theta\rangle = -C_s\frac{\langle k\rangle}{\langle\epsilon\rangle}\langle u_i'u_j'\rangle\frac{\partial\langle\Theta\rangle}{\partial x_j}, \tag{11}$$

where C_s is taken to be equal to 0.22 for all correlation type of quantities, whereas for the turbulent dissipations, $C_s = 0.18$. Also, the molecular transport terms are neglected under the assumption of high Reynolds-Peclet numbers flow.

III Explicit Algebraic Models

An improved explicit algebraic Reynolds stress model (ARSM) has been derived by Taulbee[2] from the modeled transport equation for the Reynolds stress. This model is based on the general linear pressure-strain closure given by Launder *et al.*[27] The improvement is due to an extended range of validity; the model is valid in both small and large mean strain fields and time scales of the turbulence. In two-dimensional flows, Pope[1] was first to give an explicit solution for the standard ARSM. The analogous improved ARSM as developed by Taulbee[2] reads:

$$\mathbf{a} = -2C_\mu\tau\left[\mathbf{S} + b_1 g\tau\sigma^2(\frac{2}{3}\delta - \delta^{(2)}) + b_2 g\tau(\mathbf{S\Omega} - \mathbf{\Omega S})\right]. \tag{12}$$

Here, $\mathbf{a} = [a_{ij}] = [\langle u_i'u_j'\rangle/\langle k\rangle - 2\delta_{ij}/3]$ designates the anisotropic stress tensor, $\mathbf{S} = [S_{ij}] = [\partial\langle u_i\rangle/\partial x_j + \partial\langle u_j\rangle/\partial x_i]$ and $\mathbf{\Omega} = [\Omega_{ij}] = [\partial\langle u_i\rangle/\partial x_j - \partial\langle u_j\rangle/\partial x_i]$ denote the mean flow strain rate tensor and mean flow rotation rate tensor, respectively. $\delta^{(2)} = [\delta_{ij}^{(2)}] = 1$ for $i = j = 1, 2$ and 0 otherwise, $\tau = \langle k\rangle/\langle\epsilon\rangle$ is the time scale of the turbulence and $\sigma = (S_{ij}S_{ji})^{1/2}$ is a strain rate tensor invariant. The parameters C_μ and g are given by:

$$C_\mu = \frac{4g/15}{1-\frac{2}{3}(b_1 g\tau\sigma)^2 - 2(b_2 g\tau\omega)^2}, \quad g = [C_1 + C_{\epsilon_2} - 2 + (2 - C_{\epsilon_1})P/\langle\epsilon\rangle]^{-1}, \qquad (13)$$

where $P = -\langle k\rangle a_{ij}S_{ji}$ is the production of turbulent kinetic energy, $\omega = (\Omega_{ij}\Omega_{ji})^{1/2}$ is a rotation rate tensor invariant, and C_1, b_1 and b_2 are constants from the pressure-strain correlation model ($b_1 = 0.086$, $b_2 = 0.377$). Lasher & Taulbee (private communication) reffitted the expression for C_1 proposed in Ref.[8] to six return-to-isotropy experiments and four homogeneous shear flow experiments obtaining for the linear model:

$$C_1 = 1.0 + F/18.0\exp(-3.1/\sqrt{Re_l})(29.0\log(1.0 - 17.75(II + 7.15III))$$

where $F = 1 + 27III/8 + 9II/4$ is a parameter involving the second invariant $II = -\frac{1}{2}a_{ij}a_{ji}$ and third invariant $II = -\frac{1}{3}a_{ij}a_{jk}a_{ki}$ of the Reynolds stress anisotropy tensor, and $Re_l = 4\langle k\rangle^2/(9\langle\epsilon\rangle\nu)$, the Reynolds number of the turbulence.

A similar line of reasoning is made to obtain an algebraic closure for the velocity-scalar interactions. The transport equations governing these correlations are transformed into algebraic expressions by making two primary assumptions: (1) Existence of a "near-asymptotic" state, and (2) A negligible difference in the transport terms. The starting equations for the convective scalar fluxes are described by:

$$\begin{aligned}\frac{\partial\langle u_i'Y_\alpha'\rangle}{\partial t} + \frac{\partial\langle u_i'Y_\alpha'\rangle\langle u_j\rangle}{\partial x_j} &= -\frac{\partial(\langle u_j'u_i'Y_\alpha'\rangle + \langle p'Y_\alpha'\rangle/\langle\rho\rangle\delta_{ij})}{\partial x_j} \\ &+\frac{1}{\langle\rho\rangle}\left\langle p'\frac{\partial Y_\alpha'}{\partial x_i}\right\rangle - \left(\langle u_j'u_i'\rangle\frac{\partial\langle Y_\alpha\rangle}{\partial x_j} + \langle u_j'Y_\alpha'\rangle\frac{\partial\langle u_i\rangle}{\partial x_j}\right) \\ &-Da(\langle u_i'Y_\alpha'\rangle\langle Y_\beta\rangle + \langle u_i'Y_\beta'\rangle\langle Y_\alpha\rangle + \langle u_i'Y_\alpha'Y_\beta'\rangle) \\ &+\frac{1}{Re}\left[\frac{\partial}{\partial x_j}\left\langle Y_\alpha'\frac{\partial u_i'}{\partial x_j} + \frac{u_i'}{Sc}\frac{\partial Y_\alpha'}{\partial x_j}\right\rangle\right] - \frac{1+Sc}{ScRe}\left\langle\frac{\partial u_i'}{\partial x_j}\frac{\partial Y_\alpha'}{\partial x_j}\right\rangle. \qquad (14)\end{aligned}$$

In the rhs of this equation, the following terms are identified: turbulent transport, pressure-scalar gradient correlation, production by the mean velocity and the mean scalar gradients, chemical reaction effects, molecular transport (assumed negligible at high Peclet numbers) and viscous dissipation. Based on the Poisson equation satisfied by the pressure fluctuations one can arguably split the pressure-scalar gradient correlation into two parts corresponding to so called rapid and slow terms.[8] The rapid term represents an inner product between the velocity gradient tensor and a third-order tensor, the last one subject to symmetry, continuity and normalization constraints. As suggested by Lumley,[8] since the slow pressure-scalar

gradient term and the viscous dissipation term are functions only of turbulent quantities, they can be incorporated into a single closure. The ensemble of the entire pressure-gradient term and viscous dissipation term enjoys a general relation encompassing some of the formulations proposed in precedent works. This is written consequently:

$$\Phi_{i\alpha} = \frac{1}{\langle\rho\rangle}\left\langle p'\frac{\partial Y'_\alpha}{\partial x_i}\right\rangle - \frac{1+Sc}{ScRe}\left\langle\frac{\partial u'_i}{\partial x_j}\frac{\partial Y'_\alpha}{\partial x_j}\right\rangle = -\frac{\mathcal{C}_{1\alpha}}{2}\frac{\langle\epsilon\rangle}{\langle k\rangle}\langle u'_i Y'_\alpha\rangle$$
$$+\left[c_1\frac{\partial\langle u_i\rangle}{\partial x_j}\langle u'_j Y'_\alpha\rangle + c_2\frac{\partial\langle u_j\rangle}{\partial x_i}\langle u'_j Y'_\alpha\rangle + c_3\frac{\partial\langle u_j\rangle}{\partial x_k}a_{ij}\langle u'_k Y'_\alpha\rangle\right.$$
$$\left.+c_4\frac{\partial\langle u_k\rangle}{\partial x_j}\left(a_{ij}\langle u'_k Y'_\alpha\rangle + a_{kj}\langle u'_i Y'_\alpha\rangle\right) + c_5\frac{\partial\langle u_i\rangle}{\partial x_j}a_{jk}\langle u'_k Y'_\alpha\rangle\right]. \tag{15}$$

The coefficients can take the following values: $\mathcal{C}_{1\alpha} = 6.4,\ c_1 = 0.5,\ c_i = 0,\ i = 2,5$;[18] $\mathcal{C}_{1\alpha} = 18.0(1.0 + 130.0/ScRe)^{0.25}(1.0 + 12.5/Re_t^{0.48})^{-2.08},\ c_i = 0.,\ i = 1,5$, where $Re_t = 4\langle k\rangle^2/(\langle\epsilon\rangle\nu)$;[32] or $c_1 = 4/5,\ c_2 = -1/5,\ c_3 = 1/10,\ c_4 = -3/10,\ c_5 = 1/5$.[33]

To proceed, let us denote the mechanical-chemical correlation coefficient (normalized scalar flux) by:

$$\varphi_{i\alpha} = \frac{\langle u'_i Y'_\alpha\rangle}{\sqrt{\langle k\rangle\langle\Psi\rangle}}, \tag{16}$$

where $\langle\Psi\rangle = (\langle Y'^2_A\rangle + \langle Y'^2_B\rangle)/2$ is the turbulent scalar energy. The results of direct numerical simulations of homogeneous shear flow[32] suggest the existence of an asymptotic state for the normalized correlation coefficient $\varphi_{i\alpha}$, but not for the scalar flux itself. This observation justifies our first assumption. The second approximation is yet to be substantiated. The scalar flux equation can now be represented in terms of the correlation coefficient $\varphi_{i\alpha}$ $(\alpha \neq \beta)$, written symbolically:

$$\frac{D\varphi_{i\alpha}}{Dt} = \frac{1}{\sqrt{\langle k\rangle\langle\Psi\rangle}}\left(\frac{\partial T^\alpha_{ij}}{\partial x_j} - \frac{\varphi_{i\alpha}}{2}\sqrt{\frac{\langle k\rangle}{\langle\Psi\rangle}}\frac{\partial T^\Psi_j}{\partial x_j}\right.$$
$$-\frac{\varphi_{i\alpha}}{2}\sqrt{\frac{\langle\Psi\rangle}{\langle k\rangle}}\frac{\partial T_j}{\partial x_j}\Bigg) - \left[\frac{\varphi_{i\alpha}\langle\epsilon_\Psi\rangle}{2\Psi}\left(\frac{P_\Psi}{\langle\epsilon_\Psi\rangle} - 1 + \frac{\mathcal{S}_\Psi}{\langle\epsilon_\Psi\rangle}\right)\right.$$
$$\left.+\frac{\varphi_{i\alpha}}{2\tau}\left(\frac{P}{\langle\epsilon\rangle} - 1\right)\right] + \overline{P}_{i\alpha} + \overline{\Phi}_{i\alpha} + \overline{\mathcal{S}}_{i\alpha}, \tag{17}$$

where the shorthand notations D/Dt, T_{ij}^{α}, T_j^{Ψ} and T_j stand for convective transport, turbulent transport of scalar flux, scalar energy and kinetic energy, respectively. Moreover $P_\Psi = -\sqrt{\langle k\rangle\langle\Psi\rangle}(\varphi_{jA}\partial\langle Y_A\rangle/\partial x_j + \varphi_{jB}\partial\langle Y_B\rangle/\partial x_j)$ is the production of scalar energy, $\langle\epsilon_\Psi\rangle = \langle\epsilon_A\rangle + \langle\epsilon_B\rangle$ denotes the dissipation of scalar energy, $\mathcal{S}_\Psi = \langle\dot{\omega}_A Y_A'\rangle + \langle\dot{\omega}_B Y_B'\rangle$ is the chemical source term in the Ψ equation, and the remaining quantities are the normalized production, pressure-gradient and the chemical source term:

$$\overline{P}_{i\alpha} = -\sqrt{\frac{\langle k\rangle}{\langle\Psi\rangle}}(a_{ij} + \frac{2}{3}\delta_{ij})\frac{\partial\langle Y_\alpha\rangle}{\partial x_j} - \varphi_{j\alpha}(S_{ij} + \Omega_{ij}) \tag{18}$$

$$\begin{aligned}\overline{\Phi}_{i\alpha} = -\frac{C_{1\alpha}}{2\tau}\varphi_{i\alpha} + [(c_1 + c_2)S_{ij}\varphi_{j\alpha} + (c_1 - c_2)\Omega_{ij}\varphi_{j\alpha} \\ +(c_3 + c_4)a_{ij}S_{jk}\varphi_{k\alpha} + c_5 a_{jk}S_{ij}\varphi_{k\alpha} + (c_3 - c_4)a_{ij}\Omega_{jk}\varphi_{k\alpha} \\ +c_5 a_{jk}\Omega_{ij}\varphi_{k\alpha} + c_4 a_{jk}S_{jk}\varphi_{i\alpha}]\end{aligned} \tag{19}$$

$$\overline{\mathcal{S}}_{i\alpha} = -Da(\varphi_{i\alpha}\langle Y_\beta\rangle + \varphi_{i\beta}\langle Y_\alpha\rangle + \gamma_{i\alpha\beta}\sqrt{\langle\Psi\rangle}). \tag{20}$$

Here $\gamma_{i\alpha\beta} = \langle u_i' Y_\alpha' Y_\beta'\rangle/\sqrt{\langle k\rangle\langle\Psi\rangle^2}$ is the normalized covariance flux vector. Under the stated assumptions, the terms representing the convective transport and the turbulence diffusion difference are set to zero. This procedure leads to an algebraic system of equations for the two unknown vectors $\varphi_{i\alpha}$ and $\varphi_{i\beta}$:

$$\begin{cases} \varphi_\alpha + D_\alpha \mathbf{A}\varphi_\alpha + B_\alpha\varphi_\beta + \mathbf{C}_\alpha &= 0 \\ \varphi_\beta + D_\beta \mathbf{A}\varphi_\beta + B_\beta\varphi_\alpha + \mathbf{C}_\beta &= 0 \end{cases} \tag{21}$$

where the coefficients are

$$D_\alpha = \frac{2\tau h_\alpha}{1 + 2Dah_\alpha\langle Y_\beta\rangle}, \quad D_\beta = \frac{2\tau h_\beta}{1 + 2Dah_\beta\langle Y_\alpha\rangle} \tag{22}$$

$$B_\alpha = Da\langle Y_\alpha\rangle D_\alpha \quad B_\beta = Da\langle Y_\beta\rangle D_\beta, \tag{23}$$

with

$$\begin{aligned}h_\alpha = h_\beta = \Bigg[C_{1\alpha} - 1 + (1 + 2c_4)\frac{P}{\langle\epsilon\rangle} \\ +\frac{\tau\langle\epsilon_\Psi\rangle}{\langle\Psi\rangle}\left(\frac{P_\Psi}{\langle\epsilon_\Psi\rangle} - 1 + \frac{\mathcal{S}_\Psi}{\langle\epsilon_\Psi\rangle}\right)\Bigg]^{-1},\end{aligned} \tag{24}$$

and the free vector terms read:

$$C_{i\alpha} = \frac{2\tau h_\alpha}{1+2Da\tau h_\alpha\langle Y_\beta\rangle}\sqrt{\frac{\langle k\rangle}{\langle\Psi\rangle}}(a_{ki}+\frac{2}{3}\delta_{ki})\frac{\partial\langle Y_\alpha\rangle}{\partial x_k} + \frac{2\tau h_\alpha Da\sqrt{\langle\Psi\rangle}}{1+2Da\tau h_\alpha\langle Y_\beta\rangle}\gamma_{i\alpha\beta}, \tag{25}$$

$$C_{i\beta} = \frac{2\tau h_\beta}{1+2Da\tau h_\beta\langle Y_\alpha\rangle}\sqrt{\frac{\langle k\rangle}{\langle\Psi\rangle}}(a_{ki}+\frac{2}{3}\delta_{ki})\frac{\partial\langle Y_\beta\rangle}{\partial x_k} + \frac{2\tau h_\beta Da\sqrt{\langle\Psi\rangle}}{1+2Da\tau h_\beta\langle Y_\alpha\rangle}\gamma_{i\alpha\beta}. \tag{26}$$

Finally, the anisotropy of the turbulent diffusivity is ensured by the properties of the second order tensor **A**:

$$A_{ik} = [(1-c_1-c_2)S_{ik} + (1-c_1+c_2)\Omega_{ik} - (c_3+c_4)a_{ij}S_{jk} - c_5a_{kj}S_{ji} - (c_3-c_4)a_{ij}\Omega_{jk} + c_5a_{kj}\Omega_{ji}]. \tag{27}$$

This tensor turns out to be traceless ($A_{ii}=0$) as a consequence of incompressibility and of the particular values taken by the constants c_i's. Now, the solution of the system is conveniently represented in the matrix form:

$$\begin{cases} \varphi_\alpha = -\mathbf{M}^{-1}\left[(\delta + D_\beta\mathbf{A})\mathbf{C}_\alpha - B_\alpha\mathbf{C}_\beta\right] \\ \varphi_\beta = -\mathbf{M}^{-1}\left[(\delta + D_\alpha\mathbf{A})\mathbf{C}_\beta - B_\beta\mathbf{C}_\alpha\right] \end{cases} \tag{28}$$

where **M** denotes the matrix $[(1-B_\alpha B_\beta)\delta + (D_\alpha+D_\beta)\mathbf{A} + D_\alpha D_\beta\mathbf{A}^2]$. The new expressions for the turbulent fluxes of reacting scalars exhibits two novel features. First, there is a direct influence of the Damköhler number Da, hence one can expect a higher flexibility of the model with respect to chemistry. Second, the strong coupling existing between the evolution of the reactants is reflected by the nonlinear dependence between the mean scalars and the covariance flux in the closure.

To provide a computationally efficient algorithm, the matrix **M** is inverted analytically. This is achieved via the use of the Cayley-Hamilton theorem and yields a vectorial expansion

defining a natural basis for this problem:

$$\varphi_\alpha = \sum_{n=0}^{2} a_n \mathbf{A}^n C_\alpha + \sum_{n=0}^{2} a'_n \mathbf{A}^n C_\beta. \tag{29}$$

In the Appendix the inversion procedure via the Cayley-Hamilton theorem is outlined and the coefficients a_n and a'_n are listed. The final results provide an explicit solution for the scalar fluxes. In the limit $Da \to \infty$, the coefficients a_n become singular. In this limit, it is recommend to use the mixing solution $Da = 0$ for the transport of a Shvab-Zel'dovich variable.[34]

IV Illustrative Examples

In this section, some sample results are presented of numerical simulations based on the models presented above. There are two primary reasons for conducting these simulations: (1) Model assessments via comparisons with laboratory data, (2) Demonstration of the model capabilities in comparison to traditional closures based on the linear gradient diffusion approximation. The flow configurations considered are those for which abundant laboratory data are available: two-dimensional planar mixing layers under both nonreacting and non-premixed reacting conditions, planar jets and axisymmetric jets. The mean flow motion in all of these shear flows is assumed two-dimensional. The space coordinates are identified by $\underline{x} = [x, y]$, x is the streamwise coordinate denoting the direction of principal evolution of the flow, and y represents the cross-stream direction. The velocity field is identified by $\underline{u} = [u, v]$. In nonreacting flow simulations the mass fraction of one conserved species, Y_A is considered. In the mixing layer configuration, $Y_A = 1, 0$ at the low-speed ($\langle u \rangle = u_L$), and at the high-speed ($\langle u \rangle = u_H$) streams, respectively. The magnitudes of $r = u_H/u_L$ and/or $\Delta u = u_H - u_L$ are set according to each of the experiments considered. In the jet configurations, $Y_A = 1$ is issued from the jet into a surrounding of $Y_A = 0$. In the reactive mixing layer, the two species A and B are introduced into the low- and high-sped sides. These species are assumed thermodynamically identical and there is no trace of one of these species at the feed of the other one, *i.e.* complete initial segregation. The mass fractions of the two species at their respective feeds are set equal to one. In accord with the reacting flow experiments, the heat generated by the reaction is assumed negligible.

The transport equations governing the velocity and the scalar fields are of parabolic type

with the boundary-layer approximation. The numerical algorithm is based on a first-order upwind differencing for the convection terms and a second-order central differencing scheme for all the other terms. Due to the anisotropic character of the algebraic closures, it is possible to evaluate all the components of the Reynolds stress tensor and the scalar flux vectors. The Reynolds stress tensor is predicted by the explicit ARSM solution as developed by Taulbee.[2] The scalar flux vectors are computed with the solution given by Eq. (28). In this equation, several different closures as given in Refs.[18,32,33] are used for the pressure-scalar gradient correlation.

In the evaluation of the Reynolds stress tensor and the scalar flux vectors, the terms appearing as model coefficients (*e.g.* $P/\langle\epsilon\rangle$ in Eq. (24)) are treated as known quantities. Therefore an iterative numerical solution procedure is required. To insure a faster convergence and to avoid numerical instabilities, the initial profiles are set close to those obtained by the similarity solution. The implementation of the boundary conditions is similar to that in many previous simulations of parabolic shear flows (*e.g.* Ref.[28]). In the results presented below, the spatial coordinates are presented by η for hydrodynamic and η^* for the scalar variables. In the mixing layer, $\eta = \frac{y-y(\hat{u}=0.5)}{x-x_0}$, $\eta^* = \frac{y-y(\langle Y_A\rangle=0.5)}{x-x_0}$ where $\hat{u} = \frac{\langle u\rangle - u_L}{\Delta u}$ and x_0 is the virtual origin. In the jet configurations $\eta = \frac{y}{x-x_0}$, and $\eta^* = \frac{y}{y(\langle Y_A\rangle=0.5)}$. In these jets, the subscript CL denotes values at the centerline (*i.e.* $y = 0$). In the reacting mixing layers, the corresponding profiles of Y_A under no chemistry is used in the normalization of the cross-stream coordinate.

In Figs. 1-4, results are presented of nonreacting mixing layer simulations and are compared with data obtained in several laboratory experiments.[35-41] In these and all the figures presented below, the transverse variations of statistical variables are presented. In this particular flow, the model with the coefficients of Ref.[32] yields a constant $C_{1\alpha}$ which is too small for the numerical stability; the closure of Ref.[33] provides the best overall agreement. Figures 1-4 indicate that the agreement between the model predictions and laboratory data is generally good for the mean values of the streamwise velocity and the mass fraction of a conserved scalar. The exception is the behavior near the high-speed stream of Masutani and Bowman's[35] layer where the experimental results are underpredicted by the model. A similar trend has been observed in previous simulations based on a linear gradient diffusion model.[28] A larger skirt of the mean scalar profile is believed to be due dominant influence of large scale structures in this particular experiment.[42,43] The model yields a better agreement with the results of Batt's[36] experiment, in which the flow is less dominated by large scale

structures. For the second order moments, the scatter in reported data does not allow a precise comparison. In general, the trends are in accord with data and the agreement can be potentially improved by modifying the magnitudes of turbulent scales at the boundaries. Associated with the plateau in the measured mean scalar values of Masutani and Bowman,[35] there is a double hump in the experimental scalar variance (Fig. 4(a)). The locations of these humps coincide with regions of localized large mean scalar gradients. This behavior is corroborated by direct simulations[42,43] of two-dimensional, weak turbulent flows but cannot be predicted by the model and is not observed in large Reynolds number experiments.[36]

The anisotropy of the Reynolds stress tensor and the scalar flux vector as predicted by our model, allow a direct comparison of the predicted fluxes with data. Again, the general agreement with laboratory data as witnessed in Figs. 5-7 is satisfactory. Moreover, with these results it is possible to perform *posteriori* appraisal of the closures based on conventional linear gradient diffusion hypothesis. For example, the parameters C_μ and Sc_t as given by:

$$\langle u'v' \rangle = -\mu_t \frac{\partial \langle u \rangle}{\partial y}, \quad \mu_t = C_\mu \frac{\langle k^2 \rangle}{\langle \epsilon \rangle}, \tag{30}$$

$$\langle v' Y'_\alpha \rangle = -\frac{\mu_t}{Sc_t} \frac{\partial \langle Y_\alpha \rangle}{\partial y}, \tag{31}$$

can be directly evaluated. The explicit algebraic relation for C_μ is given by Eq. (13); the relation for the turbulent Schmidt number obtained from the model with coefficients of Ref.[33] is:

$$Sc_t = \frac{2g}{15 h_\alpha} \frac{1 - \left[a_{12}^2 + 3\left(a_{22} + \frac{2}{3}\right)(2 - a_{11} - 2a_{22})\right] \left(\frac{h_\alpha \tau}{5} \frac{d\langle u \rangle}{dy}\right)^2}{\left[1 + (b_2^2 - \frac{b_1^2}{3})(g\tau \frac{d\langle u \rangle}{dy})^2\right] \left(1 - \frac{2}{5}\tau h_\alpha a_{12} \frac{d\langle u \rangle}{dy}\right) \left(a_{22} + \frac{2}{3}\right)}. \tag{32}$$

Figures 8-9 show the streamwise variations of these parameters. A somewhat similar qualitative behavior is observed in the jet flows. These results can be compared with $C_\mu = 0.09$ and $Sc_t = 0.7$ typically employed in the linear gradient diffusion approximations.[44,6] Also, the ratio of the scalar to velocity time scales (r_α) as shown in Fig. 10 indicates that an approximate constant value can be used for the central region of the layer. This is in accord with the results in Refs.[45,46] However, there are large peaks near the free-streams. The amplitude of the peaks can be somewhat controlled by modifications of the boundary conditions. An exact specification of these conditions requires inputs from the laboratory measurements.

The results for the reacting mixing layer are presented in Figs. 11-12, where comparisons are made with experimental results.[35] Figure 11 indicates that the predicted mean mass fraction of reactant A is in accord with data. Because of the consumption of the reactant by the chemical reaction, the discrepancy near the free-stream as noted in Fig. 3 is not observed here. Naturally, the second hump in the experimental profiles of the reactant's variance vanishes as the species is consumed. The variance amplitude is, nevertheless, still underpredicted by the model as shown in Fig. 12. The cross-stream variation of the reactants' covariance (the unmixedness) as predicted by the model is shown in Fig. 13. In accord with the physics of turbulent flows with segregated reactants, the unmixedness is negative throughout the layer. The same is true in the limit of zero chemistry (mixing only) as shown in this figure. However, in this case the amplitude of the unmixedness is slightly larger. This is not in agreement with Toor's[47,48] hypothesis which suggests an independency of unmixedness to the Damköhler number, but is consistent with the more rigorous theories of nonpremixed turbulent reacting systems[49–52] which indicate dependence on the Damköhler number. The results in Figs. 8-10 also suggest that chemistry induces a profound influence on the amplitude of the model constants.

The measurement results pertaining to planar jet hydrodynamics as reported in Refs.[53–55] are compared with the model predictions in Figs. 14 through 20. The agreement is reasonable for the mean streamwise velocity and also the components of the Reynolds stress tensor. The same level of agreement is witnessed in the profiles of the conserved scalar mean and variance as compared with the experimental results of Refs.[56–60] In this case, it seems that the model with the coefficients of Ref.[33] provides the closest prediction of the scalar mean and variance values. However, the predicted values of the amplitude of scalar-velocity correlation is larger than some of the experimentally reported data.

The comparative assessment of the models for the prediction of axisymmetric jet flows is provided in Figs. 21-27 where the experimental data in Refs.[61–63] are used for hydrodynamics variables and those in Refs.[64–66] for scalar variables. Again, all the mean values are reasonably well-predicted. The same is true for the Reynolds stresses and the scalar variance as the model results are within the scatter of the data. In this configuration also the experimental results for the scalar fluxes are overpredicted. However, the experiments of Ref.[64] are not conducted in the self-preserving regions of the jet. Therefore a definite verdict cannot be reached without comparisons with further data.

From the preceding comparisons, it can be concluded that the algebraic model developed

here provides an effective means of predicting the second-order moments in reacting turbulent flows. Because of their anisotropic feature, these algebraic schemes are more flexible than the conventional linear gradient diffusion schemes. The explicit nature of the relations, facilitated by the Cayley-Hamilton theorem, is particularly convenient for simulating complex flows. Additional improvement of these models is possible by fine-tuning of the pressure-gradient correlation models, and also the higher order moments of scalar-scalar fluctuations in reacting flows. Further extension of the model is recommended to account for the effects of exothermicity in nonequilibrium chemically reacting systems.

Appendix

The procedure leading to explicit solutions for the scalar-flux vector, as governed by Eq. (21) is described here.

Consider an arbitrary three-dimensional second-order tensor $\mathbf{Q} = [Q_{ij}]$ and the corresponding Kronecker tensor $\delta = [\delta_{ij}]$. According to the Cayley-Hamilton theorem, this matrix satisfies its own characteristic polynomial:

$$\mathbf{Q}^3 - I_Q\mathbf{Q}^2 + II_Q\mathbf{Q} - III_Q\delta = \mathbf{0} \tag{33}$$

where $I_Q = \{\mathbf{Q}\} = Q_{ii}$, $II_Q = \frac{1}{2}[\{\mathbf{Q}\}^2 - \{\mathbf{Q}^2\}] = \frac{1}{2}[Q_{ii}Q_{jj} - Q_{ij}Q_{ji}]$, $III_Q = \frac{1}{6}[\{\mathbf{Q}\}^3 - 3\{\mathbf{Q}\}\{\mathbf{Q}^2\} + 2\{\mathbf{Q}^3\}] = \frac{1}{6}[Q_{ii}Q_{jj}Q_{kk} - 3Q_{ii}Q_{jk}Q_{kj} + 2Q_{ij}Q_{jk}Q_{ki}]$ are the three tensorial invariants. Multiplying the characteristic polynomial with $\mathbf{Q}^{-1}$ and solving for the inverse we obtain:

$$\mathbf{Q}^{-1} = \frac{1}{III_Q}(\mathbf{Q}^2 - I_Q\mathbf{Q} + II_Q\delta). \tag{34}$$

This relation can be used now to find explicit solutions to the problem considered here. For example, for the case with $Da = 0$ (pur mixing) we can write:

$$\varphi_\alpha = -(\delta + \mathbf{G})^{-1}\mathbf{C}, \tag{35}$$

where $\mathbf{G} = D_\alpha\mathbf{A}$. Hence:

$$(\delta + \mathbf{G})^{-1} = \frac{1}{III_{\delta+\mathbf{G}}}[\mathbf{G}^2 + (2 - I_{\delta+\mathbf{G}})\mathbf{G} + (1 - I_{\delta+\mathbf{G}} + II_{\delta+\mathbf{G}})\delta]. \tag{36}$$

It is easy to show that $I_{\delta+\mathbf{G}} = I_{\mathbf{G}} + \{\delta\}$, $II_{\delta+\mathbf{G}} = 2I_{\mathbf{G}} + II_{\mathbf{G}} + \{\delta\}$, $III_{\delta+\mathbf{G}} = I_{\mathbf{G}} + II_{\mathbf{G}} + III_{\mathbf{G}} + \frac{\{\delta\}}{3}$. Therefore the normalized scalar flux vector takes the form:

$$\varphi_\alpha = a_0\mathbf{C} + a_1\mathbf{GC} + a_2\mathbf{G}^2\mathbf{C} \tag{37}$$

with the coefficients:

$$a_0 = -\frac{1 + I_{\mathbf{G}} + II_{\mathbf{G}}}{1 + I_{\mathbf{G}} + II_{\mathbf{G}} + III_{\mathbf{G}}} \tag{38}$$

$$a_1 = \frac{1 + I_{\mathbf{G}}}{1 + I_{\mathbf{G}} + II_{\mathbf{G}} + III_{\mathbf{G}}} \tag{39}$$

$$a_2 = -\frac{1}{1 + I_{\mathbf{G}} + II_{\mathbf{G}} + III_{\mathbf{G}}}. \tag{40}$$

In a homogeneous solenoidal field the pressure-gradient correlations are described by traceless rapid parts. This further translates into $\{\mathbf{A}\} = 0$, and thus:

$$a_0 = -\frac{1 - \frac{1}{2}\{\mathbf{G}^2\}}{1 - \frac{1}{2}\{\mathbf{G}^2\} + \frac{1}{3}\{\mathbf{G}^3\}} \tag{41}$$

$$a_1 = \frac{1}{1 - \frac{1}{2}\{\mathbf{G}^2\} + \frac{1}{3}\{\mathbf{G}^3\}} \tag{42}$$

$$a_2 = -\frac{1}{1 - \frac{1}{2}\{\mathbf{G}^2\} + \frac{1}{3}\{\mathbf{G}^3\}}. \tag{43}$$

The reacting case is somewhat more complex. Nevertheless, by following the same procedure explicit solutions are obtained:

$$\varphi_\alpha = a_0\mathbf{C}_\alpha + a_0'\mathbf{C}_\beta + a_1\mathbf{AC}_\alpha + a_1'\mathbf{AC}_\beta + a_2\mathbf{A}^2\mathbf{C}_\alpha + a_2'\mathbf{A}^2\mathbf{C}_\beta \tag{44}$$

$$\varphi_\beta = b_0\mathbf{C}_\alpha + b_0'\mathbf{C}_\beta + b_1\mathbf{AC}_\alpha + b_1'\mathbf{AC}_\beta + b_2\mathbf{A}^2\mathbf{C}_\alpha + b_2'\mathbf{A}^2\mathbf{C}_\beta, \tag{45}$$

with the coefficients:

$$a_0 = -\frac{F_\beta(F_\alpha + D_\alpha^2\frac{\{\mathbf{A}^3\}}{3}) + B_\alpha B_\beta\left[\frac{\{\mathbf{A}^3\}}{3}(D_\beta F_\alpha - ED_\alpha)D_\beta - E(E + \frac{\{\mathbf{A}^3\}}{3}D_\alpha D_\beta)\right]}{(1 - B_\alpha B_\beta)(F_\alpha F_\beta - E^2 B_\alpha B_\beta)}, \tag{46}$$

$$a_0' = B_\alpha\frac{F_\alpha(F_\beta + D_\beta^2\frac{\{\mathbf{A}^3\}}{3}) + D_\alpha\frac{\{\mathbf{A}^3\}}{3}(D_\alpha F_\beta - ED_\beta) - EB_\alpha B_\beta(E + \frac{\{\mathbf{A}^3\}}{3}D_\alpha D_\beta)}{(1 - B_\alpha B_\beta)(F_\alpha F_\beta - E^2 B_\alpha B_\beta)}, \tag{47}$$

$$a_1 = \frac{B_\alpha B_\beta\left[E(D_\beta - D_\alpha) + F_\alpha D_\beta\right] - D_\alpha F_\beta}{D_\alpha(F_\alpha F_\beta - E^2 B_\alpha B_\beta)} \tag{48}$$

$$a_1' = \frac{B_\alpha}{D_\alpha} \frac{D_\alpha F_\beta - D_\beta F_\alpha - E(D_\beta - D_\alpha B_\alpha B_\beta)}{F_\alpha F_\beta - E^2 B_\alpha B_\beta} \tag{49}$$

$$a_2 = \frac{D_\alpha F_\beta - E D_\beta B_\alpha B_\beta}{F_\alpha F_\beta - E^2 B_\alpha B_\beta} \tag{50}$$

$$a_2' = -B_\alpha \frac{D_\alpha F_\beta - E D_\beta}{F_\alpha F_\beta - E^2 B_\alpha B_\beta}, \tag{51}$$

with the shorthand notations:

$$F_\alpha = (1 - B_\alpha B_\beta)(D_\alpha \frac{\{\mathbf{A}^2\}}{2} - \frac{1}{D_\alpha} - \frac{B_\alpha B_\beta}{D_\beta}) - D_\alpha^2 \frac{\{\mathbf{A}^3\}}{3} \tag{52}$$

$$F_\beta = (1 - B_\alpha B_\beta)(D_\beta \frac{\{\mathbf{A}^2\}}{2} - \frac{1}{D_\beta} - \frac{B_\alpha B_\beta}{D_\alpha}) - D_\beta^2 \frac{\{\mathbf{A}^3\}}{3} \tag{53}$$

$$E = (\frac{1}{D_\alpha} + \frac{1}{D_\beta})(1 - B_\alpha B_\beta) - D_\alpha D_\beta \frac{\{\mathbf{A}^3\}}{3}. \tag{54}$$

The coefficients b_i are obtained from the a_i's through the permutations $\alpha \rightarrow \beta$, $\beta \rightarrow \alpha$, $a_0 \rightarrow b_0'$, $a_0' \rightarrow b_0$, $a_1 \rightarrow b_1'$, $a_1' \rightarrow b_1$, $a_2 \rightarrow b_2'$ and $a_2' \rightarrow b_2$.

References

[1] Pope, S. B., A More General Effective-Viscosity Hypothesis, *J. Fluid Mech.*, **72**:331–340 (1975).

[2] Taulbee, D. B., An Improved Algebraic Reynolds Stress Model and Corresponding Nonlinear Stress Model, *Phys. Fluids A*, **4**(11):2555–2561 (1992).

[3] Libby, P. A. and Williams, F. A., editors, *Turbulent Reacting Flows*, Academic Press, London, UK, 1994.

[4] Galperin, B. and Orszag, S. A., editors, *Large Eddy Simulations of Complex Engineering and Geophysical Flows*, Cambridge University Press, Cambridge, U.K., 1993.

[5] Givi, P., Spectral and Random Vortex Methods in Turbulent Reacting Flows, In Libby and Williams,[3] chapter 8, pp. 475–572.

[6] Launder, B. E. and Spalding, D. B., The Numerical Computation of Turbulent Flows, *Comput. Methods Appl. Mech. Engng*, **3**:269–289 (1974).

[7] Reynolds, W. C., Computation of Turbulent Flows, *Annu. Rev. Fluid Mech.*, **8**:183–208 (1976).

[8] Lumley, J. L., Computational Modeling of Turbulent Flows, *Adv. Appl. Mech.*, **18**:123–176 (1978).

[9] Taulbee, D. B., Engineering Turbulence Models, in George, W. K. and Arndt, R., editors, *Advances in Turbulence*, pp. 75–125, Hemisphere Publishing Co., New York, NY., 1989.

[10] Launder, B. E., Current Capabilities for Modelling Turbulence in Industrial Flows, *Applied Scientific Research*, **48**:247–269 (1991).

[11] Libby, P. A. and Williams, F. A., editors, *Turbulent Reacting Flows*, *Topics in Applied Physics*, Vol. 44, Springer-Verlag, Heidelberg, 1980.

[12] Jones, W. P., Models for Turbulent Flows with Variable Density and Combustion, in Kollmann, W., editor, *Prediction Methods for Turbulent Flows*, pp. 380–421, Hemisphere Publishing Co., New York, NY, 1980.

[13] Jones, W. P. and Whitelaw, J. H., Calculation Methods for Reacting Turbulent Flows: A Review, *Combust. Flame*, **48**:1–26 (1982).

[14] Jones, W. P. and Whitelaw, J. H., Modelling and Measurements in Turbulent Combustion, in *20th Symp. (Int.) on Combustion*, pp. 233–249, The Combustion Institute, Pittsburgh, PA, 1984.

[15] Borghi, R. and Murthy, S. N. B., editors, *Turbulent Reacting Flows*, *Lecture Notes in Engineering*, Vol. 40, Springer-Verlag, New York, NY, 1989.

[16] Jones, W. P., Turbulence Modelling and Numerical Solution Methods for Variable Density and Combusting Flows, In Libby and Williams,[3] chapter 6, pp. 309–374.

[17] Rodi, W., A New Algebraic Relation for Calculating the Reynolds Stresses, *ZAMM*, **56**:T219–T221 (1976).

[18] Launder, B. E., On the Effects of a Gravitational Field on the Turbulent Transport of Heat and Momentum, *J. Fluid Mech.*, **67**:569–581 (1975).

[19] Rodi, W., Turbulence Models for Environmental Problems, in Kollmann, W., editor, *Prediction Methods for Turbulent Flows*, pp. 260–349, Hemisphere Publishing Co., New York, NY, 1980.

[20] Speziale, C. G., Analytical Methods for the Development of Reynolds Stress Closures in Turbulence, *Ann. Rev. Fluid Mech.*, **23**:107–157 (1991).

[21] Gatski, T. B. and Speziale, C. G., On Explicit Algebraic Stress Models for Complex Turbulent Flows, *J. Fluid Mech.*, **254**:59–78 (1993).

[22] Taulbee, D. B., Sonnenmeier, J. R., and Wall, K. W., Stress Relation for Three-Dimensional Turbulent Flows, *Phys. Fluids*, **6**(3):1399–1401 (1993).

[23] Yakhot, V. and Orszag, S. A., Renormalization Group Analysis of Turbulence. I. Basic Theory, *J. Sci. Comput.*, **1**(1):3–52 (1986).

[24] Horiuti, K., Higher Order Terms in the Anisotropic Representation of Reynolds Stresses, *Phys. Fluids*, **2**(10):1708–1711 (1969).

[25] Yoshizawa, A., Statistical Analysis of the Deviation of the Reynolds Stress from its Eddy-Viscosity Representation, *Phys. Fluids*, **27**:1377–1387 (1984).

[26] Yoshizawa, A., Statistical Modelling of Passive-Scalar Diffusion in Turbulent Shear Flows, *J. Fluid Mech.*, **195**:541–555 (1988).

[27] Launder, B. E., Reece, G. J., and Rodi, W., Progress in the Development of a Reynolds-Stress Turbulence Closure, *J. Fluid Mech.*, **68**:537–566 (1975).

[28] Givi, P., Turbulent Reacting Flows, Ph.D. Thesis, Carnegie Tech., Pittsburgh, PA., 1984.

[29] Pope, S. B., PDF Methods for Turbulent Reactive Flows, *Prog. Energy Combust. Sci.*, **11**:119–192 (1985).

[30] Adumitroaie, V., Ph.D. Thesis, Department of Mechanical and Aerospace Engineering, State University of New York at Buffalo, Buffalo, NY, 1994, In preparation.

[31] Jones, W. P. and Musonge, P., Closure of the Reynolds Stress and Scalar Flux Equations, *Phys. Fluids*, **31**(12):3589–3604 (1988).

[32] Rogers, M. M., Mansour, N. N., and Reynolds, W. C., An Algebraic Model for the Turbulent Flux of a Passive Scalar, *J. Fluid Mech.*, **203**:77–101 (1989).

[33] Shih, T.-H. and Lumley, J. L., Modeling of Pressure Correlation Terms in Reynolds-Stress and Scalar Flux Equations, Technical Report FDA-85-3, Sibley School of Mechanical and Aerospace Engineering, Cornell University, Ithaca, New York, 1985.

[34] Williams, F. A., *Combustion Theory*, The Benjamin/Cummings Publishing Company, Menlo Park, CA, 2nd edition, 1985.

[35] Masutani, S. M. and Bowman, C. T., The Structure of a Chemically Reacting Plane Mixing Layer, *J. Fluid Mech.*, **72**:93–126 (1986).

[36] Batt, R. G., Turbulent Mixing of Passive and Chemically Reacting Species in a Low-Speed Shear Layer, *J. Fluid Mech.*, **82**:53 (1977).

[37] Sunyach, M., Contribution à l'étude des frontières d'écoulements turbulents libres, Sc.D. Thesis, Université Claude Bernard de Lyon, Lyon, France, 1971.

[38] Patel, R. P., An Experimental Study of Plane Mixing Layer, *AIAA J.*, **11**:67–71 (1973).

[39] Liepmann, H. W. and Laufer, J., Investigation of Free Turbulent Mixing, Technical Report 1257, NACA, 1946.

[40] Bradshaw, P., The Effect of Initial Conditions on the Development of a Free Shear Layer, *J. Fluid Mech.*, **26**:225–236 (1966).

[41] Wygnanski, I. and Fiedler, H. E., The Two-Dimensional Mixing Region, *J. Fluid Mech.*, **41**:327–361 (1970).

[42] Givi, P. and Jou, W.-H., Mixing and Chemical Reaction in a Spatially Developing Mixing Layer, *J. Nonequil. Thermodyn.*, **13**(4):355–372 (1988).

[43] Battaglia, F. and Givi, P., Direct Lagrangian Simulations of a Mixing Layer by the Transport-Element Method, *J. Nonequil. Thermodyn.*, **18**:173–194.

[44] Givi, P., Model Free Simulations of Turbulent Reactive Flows, *Prog. Energy Combust. Sci.*, **15**:1–107 (1989).

[45] Beguier, C., Dekeyser, I., and Launder, B. E., Ratio of Scalar and Velocity Dissipation Time Scales in Shear Flow Turbulence, *Phys. Fluids*, **21**(3):307–310 (1978).

[46] Tavoularis, S. and Corrsin, S., Experiments in Nearly Homogenous Turbulent Shear Flow with a Uniform Mean Temperature Gradient. Part 1, *J. Fluid Mech.*, **104**:311–347 (1981).

[47] Toor, H. L., Mass Transfer in Dilute Turbulent and Nonturbulent Systems with Rapid Irreversible Reactions and Equal Diffusivities, *AIChE J.*, **8**:70–78 (1962).

[48] Toor, H. L., The Non-Premixed Reaction: $A + B \rightarrow Products$, in Brodkey, R. S., editor, *Turbulence in Mixing Operations*, pp. 123–166, Academic Press, New York, NY, 1975.

[49] Givi, P. and McMurtry, P. A., Non-Premixed Reaction in Homogeneous Turbulence: Direct Numerical Simulations, *AIChE J.*, **34**(6):1039–1042 (1988).

[50] McMurtry, P. A. and Givi, P., Direct Numerical Simulations of Mixing and Reaction in a Nonpremixed Homogeneous Turbulent Flow, *Combust. Flame*, **77**:171–185 (1989).

[51] Frankel, S. H., Madnia, C. K., and Givi, P., Comparative Assessment of Closures for Turbulent Reacting Flows, *AIChE J.*, **39**(5):899–903 (1993).

[52] Madnia, C. K., Frankel, S. H., and Givi, P., Reactant Conversion in Homogeneous Turbulence: Mathematical Modeling, Computational Validations and Practical Applications, *Theoret. Comput. Fluid Dynamics*, **4**:79–93 (1992).

[53] Gutmark, E. and Wygnanski, I., The Planar Turbulent Jet, *J. Fluid Mech.*, **73**:465–495 (1976).

[54] Bradbury, L. J. S., The Structure of Self-Preserving Turbulent Plane Jet, *J. Fluid Mech.*, **23**:31–64 (1965).

[55] Heskestad, G., Hot Wire Measurements in a Plane Turbulent Jet, *J. Appl. Mech.*, **32**:721–734 (1965).

[56] Browne, L. W. B., Antonia, A. R., and Chambers, A. J., The Interaction Region of a Turbulent Plane Jet, *J. Fluid Mech.*, pp. 355–373 (1984).

[57] Bashir, J. and Uberoi, M. S., Experiments on Turbulent Structure and Heat Transfer in a Two Dimensional Jet, *Phys. Fluids*, **18**(4):405–410 (1975).

[58] Uberoi, M. S. and Singh, P. I., Turbulent Mixing in a Two Dimensional Jet, *Phys. Fluids*, **18**(7):764–769 (1975).

[59] Jenkins, P. E. and Goldscmidt, V. W., Mean Temperature and Velocity in a Plane Turbulent Jet, *ASME Journal of Fluids Engineering*, **95**:581–584 (1973).

[60] Antonia, R. A., Browne, L. W., Chambers, A. J., and Rajagopalan, S., Budget of Temperature Variance in a Turbulent Plane Jet, *Int. J. Heat Mass Transfer*, **26**(1):41–48 (1983).

[61] Hussein, H. J., Capp, S. P., and George, W. K., Velocity Measurements in a High-Reynolds-Number, Momentum-Conserving, Axisymmetric, Turbulent Jet, *J. Fluid Mech.*, **258**:31–75 (1994).

[62] Abbiss, J. B., Bradbury, L. J. S., and Wright, M. P., Measurements in an Axisymmetric Jet Using a Photon Correlator, in *Proceedings of the LDA Symposium*, Copenhagen, Denmark, 1975.

[63] Wygnanski, I. and Fiedler, H., Some Measurements in the Self-Preserving Jet, *J. Fluid Mech.*, **38**:577–612 (1969).

[64] Chevray, R. and Tutu, N. K., Intermittency and Preferential Transport of Heat in a Round Jet, *J. Fluid Mech.*, **88**(1):133–160 (1978).

[65] Becker, H. A., Hottel, H. C., and Williams, G. C., The Nozzle Fluid Concentration Field of the Round Turbulent Free Jet, *J. Fluid Mech.*, **30**(2):285–303 (1976).

[66] Lockwood, F. C. and Moneib, H. A., Fluctuating Temperature Measurement in a Heated Round Free Jet, *Combust. Sci. and Tech.*, **22**:63–81 (1980).

Figure Captions

Figure 1. Cross-stream variation of $\hat{u}$ for the mixing layer.

Figure 2. Cross-stream variation of $\langle u'^2 \rangle^{1/2}$ for the mixing layer.

Figure 3. Cross-stream variation of $\langle Y_A \rangle$ for the nonreacting mixing layer.

Figure 4. Cross-stream variation of $\langle Y_A'^2 \rangle^{1/2}$ for the nonreacting mixing layer.

Figure 5. Cross-stream variation of $\langle u'v' \rangle / \Delta u \times 100$ for the mixing layer.

Figure 6. Cross-stream variation of $\langle v'^2 \rangle^{1/2} / \Delta u$ for the mixing layer.

Figure 7. Cross-stream variation of $\langle v' Y_A' \rangle / \Delta u$ for the nonreacting mixing layer.

Figure 8. Cross-stream variation of C_μ for the mixing layer.

Figure 9. Cross-stream variation of Sc_t for the nonreacting and reacting mixing layers.

Figure 10. Cross-stream variation of r_A for the nonreacting and reacting mixing layers.

Figure 11. Cross-stream variation of $\langle Y_A \rangle$ for the reacting mixing layer.

Figure 12. Cross-stream variation of $\langle Y_A'^2 \rangle^{1/2}$ for the reacting mixing layer.

Figure 13. Cross-stream variation of $\langle Y_A' Y_B' \rangle$ for the nonreacting and reacting mixing layer.

Figure 14. Cross-stream variation of $\langle u \rangle / \langle u \rangle_{CL}$ for the planar jet.

Figure 15. Cross-stream variation of $\langle u'^2 \rangle / \langle u \rangle_{CL}^2$ for the planar jet.

Figure 16. Cross-stream variation of $\langle u'v' \rangle / \langle u \rangle_{CL}^2$ for the planar jet.

Figure 17. Cross-stream variation of $\langle v'^2 \rangle / \langle u \rangle_{CL}^2$ for the planar jet.

Figure 18. Cross-stream variation of $\langle Y_A \rangle / \langle Y_A \rangle_{CL}$ for the planar jet.

Figure 19. Cross-stream variation of $\langle Y_A'^2 \rangle^{1/2} / \langle Y_A \rangle_{CL}$ for the planar jet.

Figure 20. Cross-stream variation of $\langle v' Y_A' \rangle / \langle u \rangle_{CL} \langle Y_A \rangle_{CL}$ for the planar jet.

Figure 21. Cross-stream variation of $\langle u \rangle / \langle u \rangle_{CL}$ for the round jet.

Figure 22. Cross-stream variation of $\langle u'^2 \rangle / \langle u \rangle_{CL}^2$ for the round jet.

Figure 23. Cross-stream variation of $\langle u'v' \rangle / \langle u \rangle_{CL}^2$ for the round jet.

Figure 24. Cross-stream variation of $\langle v'^2 \rangle / \langle u \rangle_{CL}^2$ for the the round jet.

Figure 25. Cross-stream variation of $\langle Y_A \rangle / \langle Y_A \rangle_{CL}$ for the round jet.

Figure 26. Cross-stream variation of $\langle Y_A'^2 \rangle^{1/2} / \langle Y_A \rangle_{CL}$ for the round jet.

Figure 27. Cross-stream variation of $\langle v' Y_A' \rangle / \langle u \rangle_{CL} \langle Y_A \rangle_{CL}$ for the round jet.

Figure 1

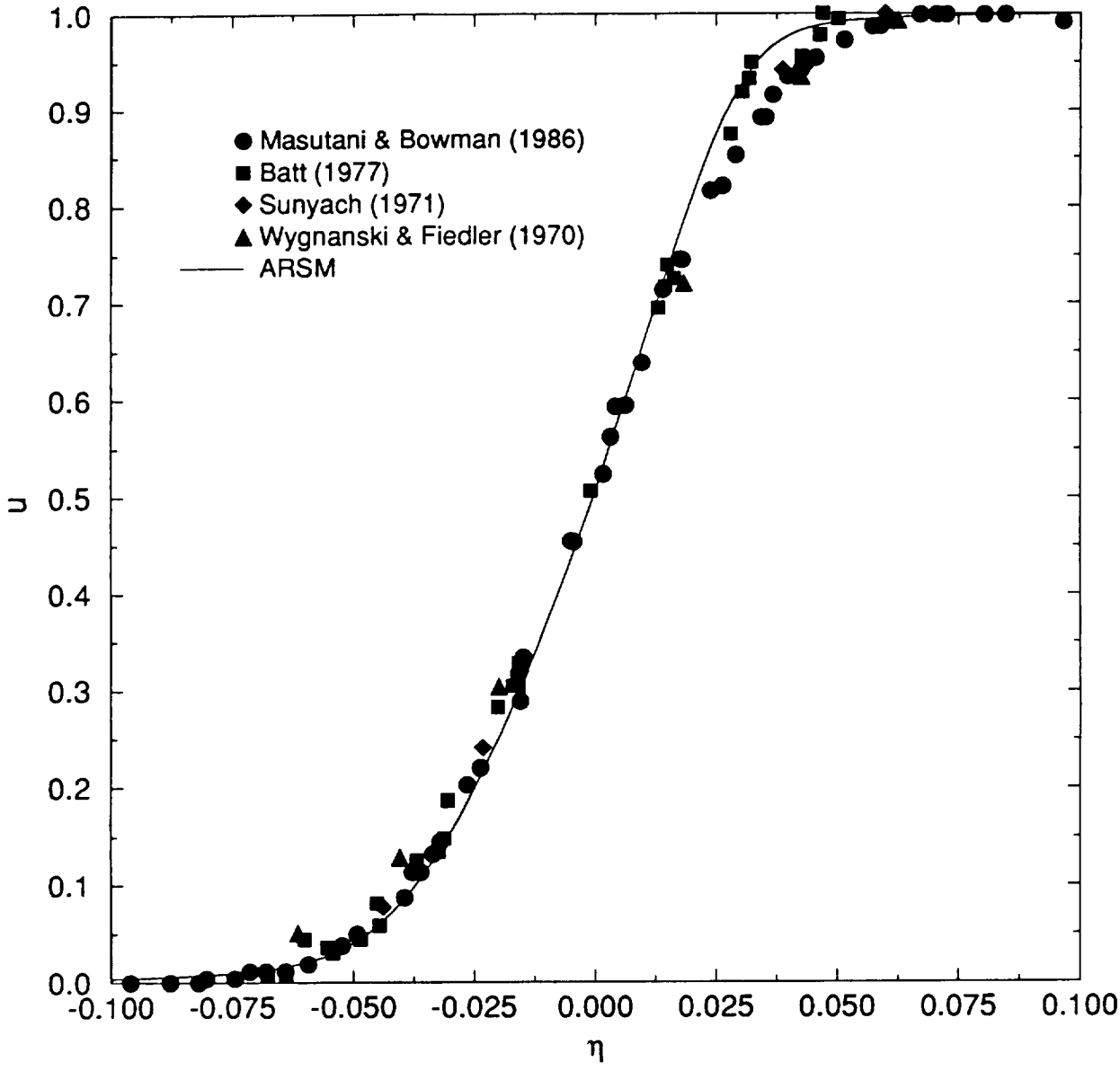
1.0
0.9
0.8
0.7
0.6
0.5
0.4
0.3
0.2
0.1
0.0
u
-0.100
-0.075
-0.050
-0.025
0.000
0.025
0.050
0.075
0.100
η
Masutani & Bowman (1986)
Batt (1977)
Sunyach (1971)
Wygnanski & Fiedler (1970)
ARSM

Figure 2 (a)

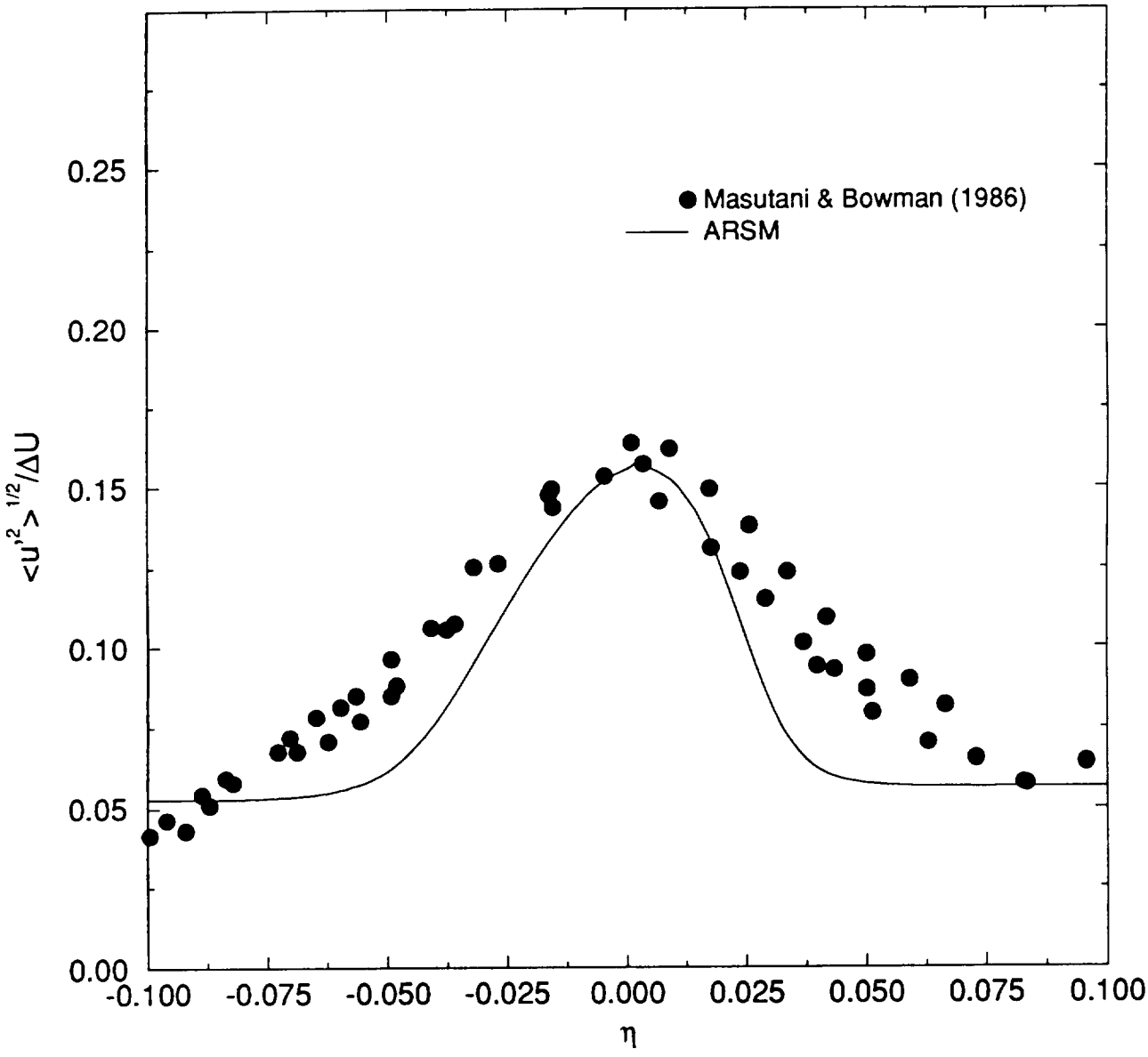
Masutani & Bowman (1986)
ARSM
0.25
0.20
0.15
0.10
0.05
0.00
-0.100
-0.075
-0.050
-0.025
0.000
0.025
0.050
0.075
0.100
η
<u'^2>^1/2/ΔU

Figure 2 (b)

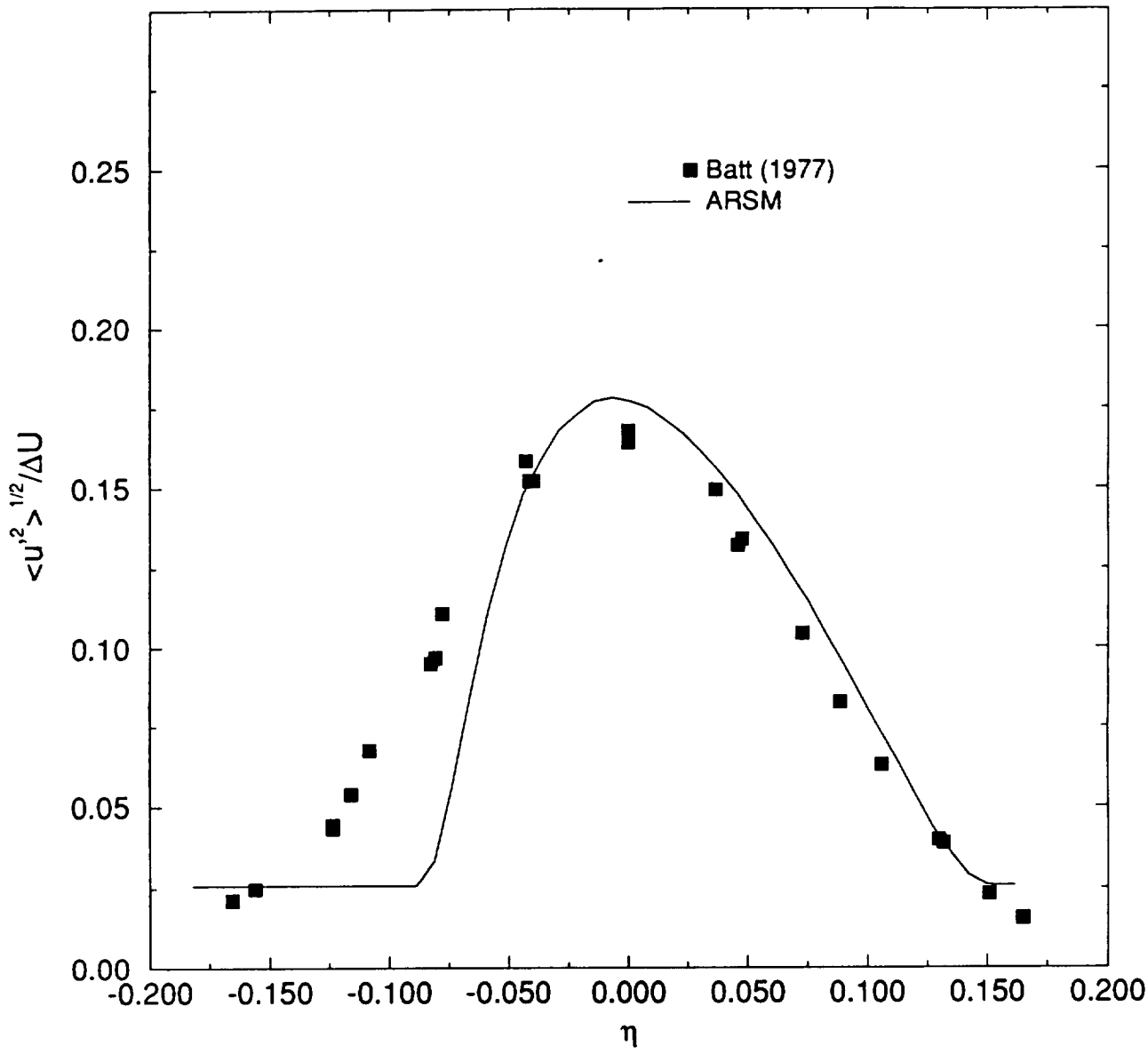
Batt (1977)
ARSM
0.25
0.20
0.15
0.10
0.05
0.00
-0.200
-0.150
-0.100
-0.050
0.000
0.050
0.100
0.150
0.200
η
<u'^2>^1/2/ΔU

Figure 3

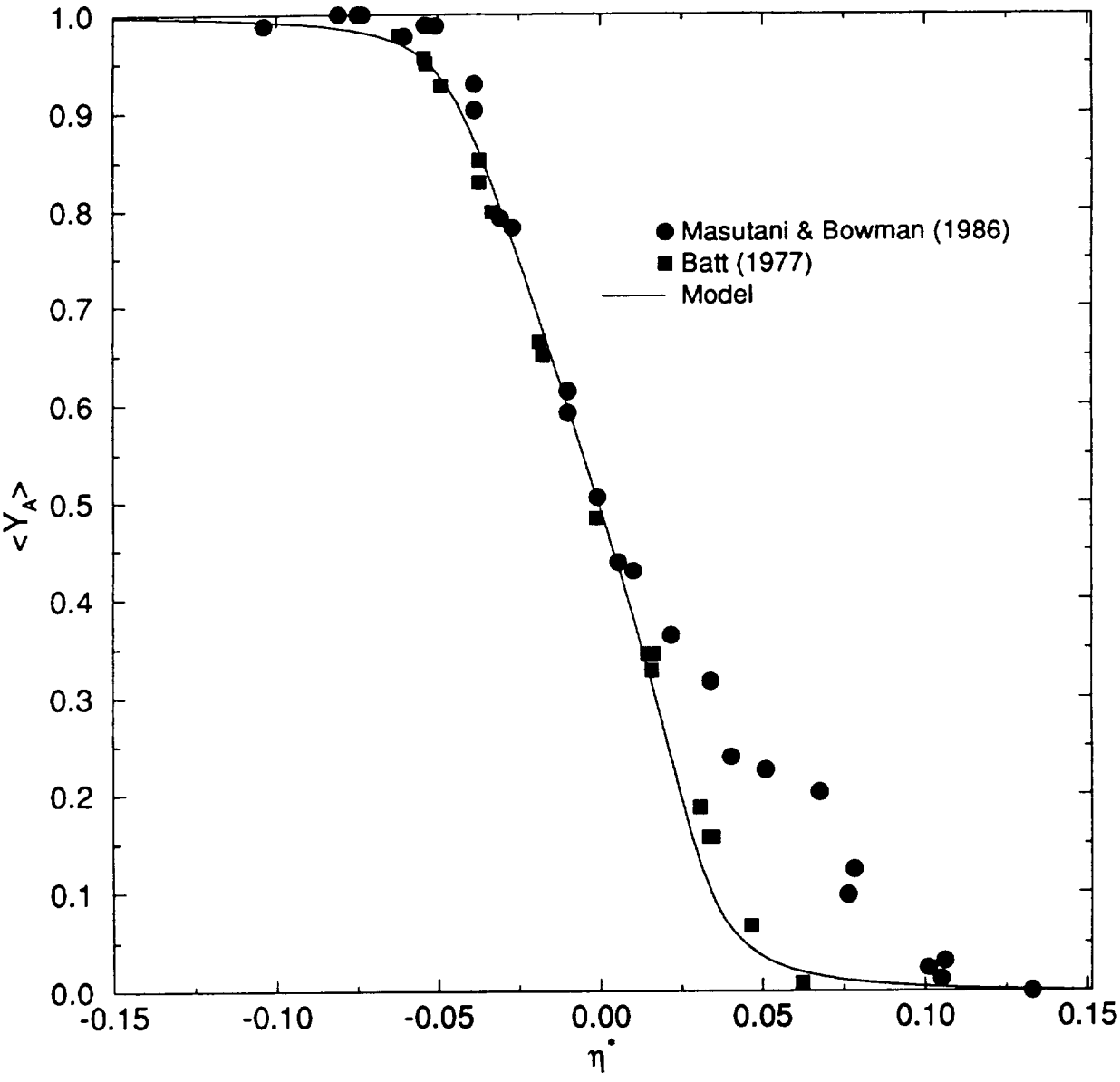
1.0
0.9
0.8
0.7
0.6
0.5
0.4
0.3
0.2
0.1
0.0
<Y_A>
-0.15
-0.10
-0.05
0.00
0.05
0.10
0.15
η*
Masutani & Bowman (1986)
Batt (1977)
Model

Figure 4 (a)

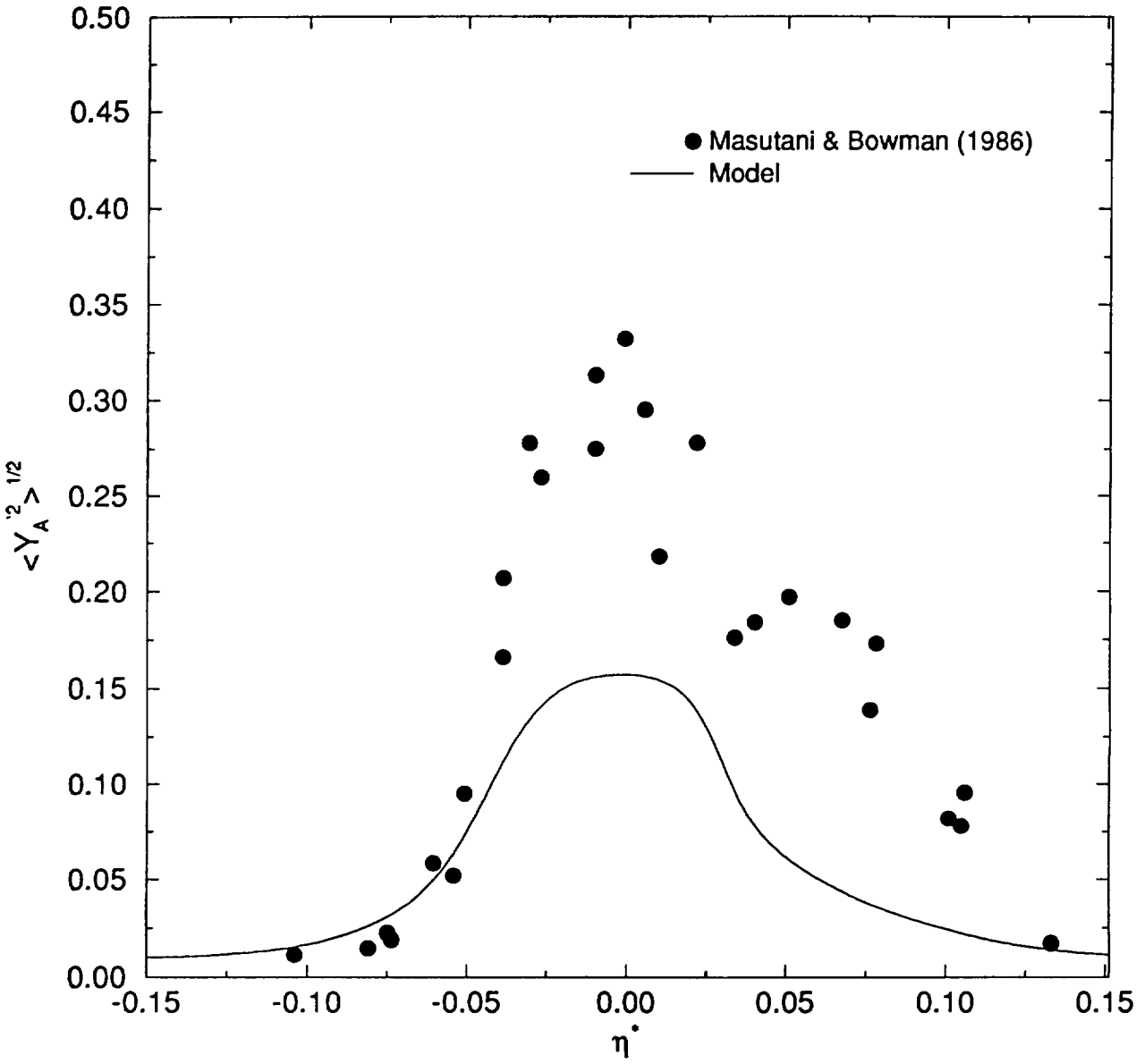
0.50
0.45
0.40
0.35
0.30
0.25
0.20
0.15
0.10
0.05
0.00
-0.15
-0.10
-0.05
0.00
0.05
0.10
0.15
η*
<Y_A'^2>^1/2
Masutani & Bowman (1986)
Model

Figure 4 (b)

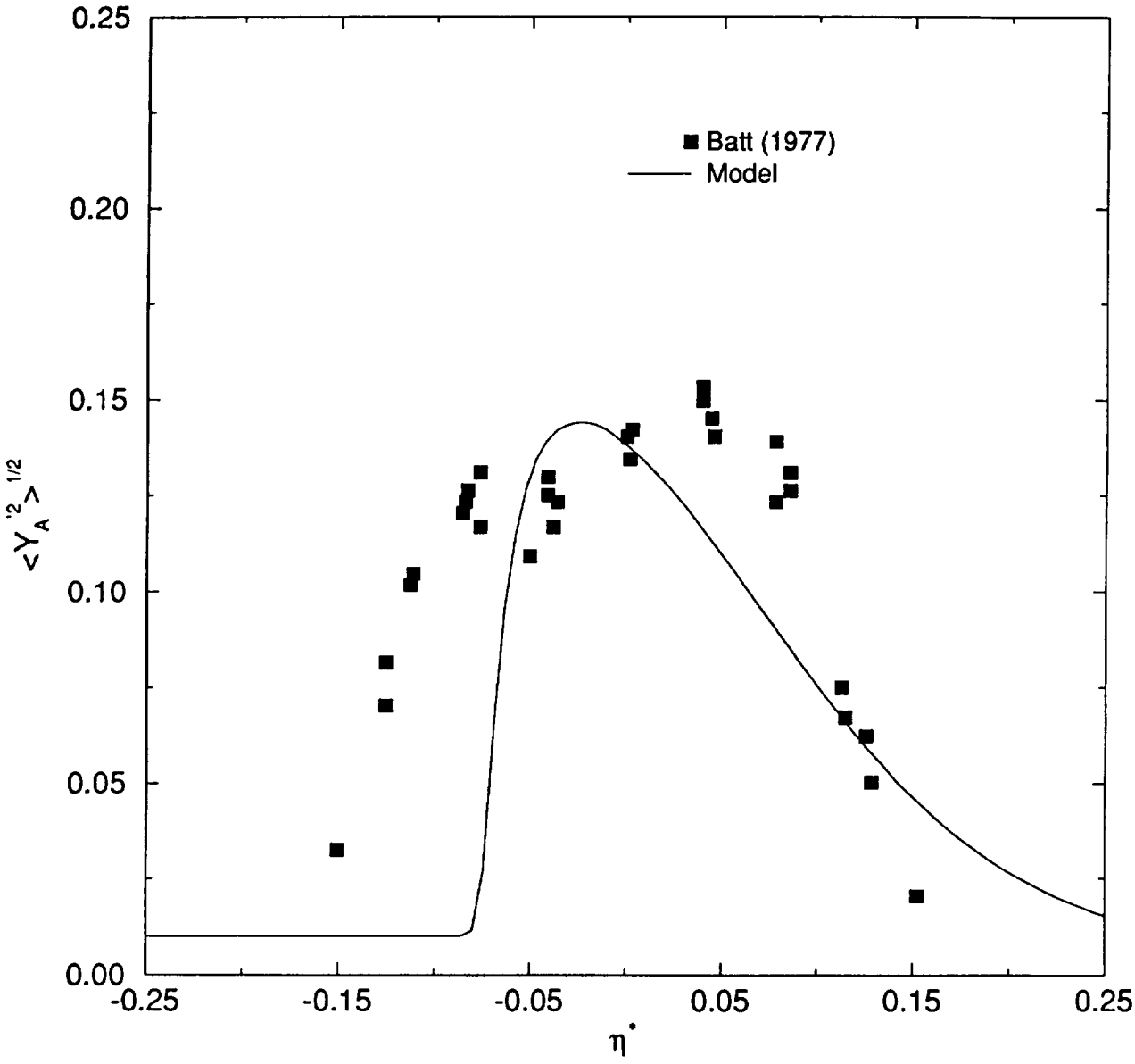
0.25
0.20
0.15
0.10
0.05
0.00
-0.25
-0.15
-0.05
0.05
0.15
0.25
η*
<Y'2A>1/2
Batt (1977)
Model

Figure 5

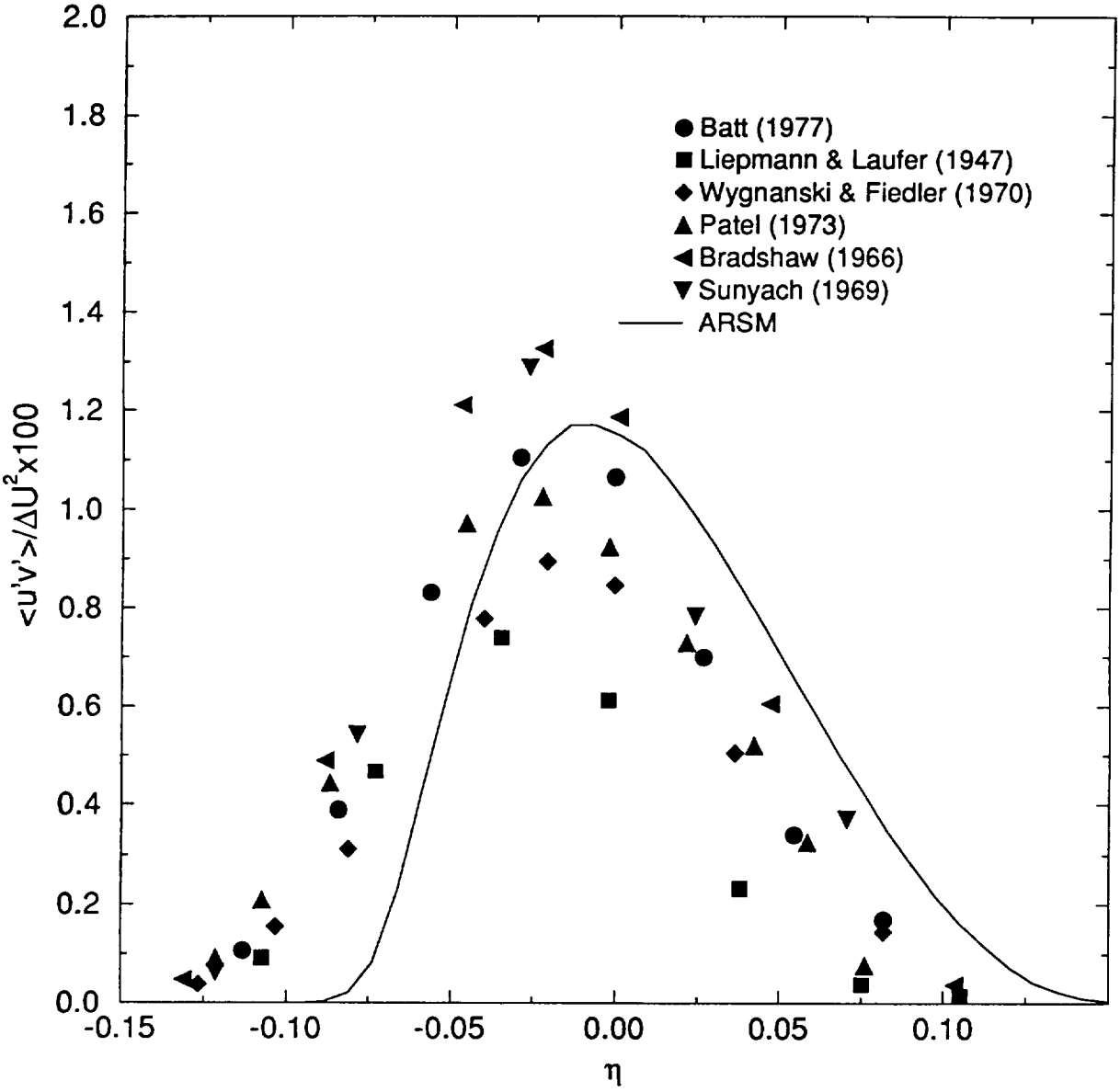
2.0
1.8
1.6
1.4
1.2
1.0
0.8
0.6
0.4
0.2
0.0
-0.15
-0.10
-0.05
0.00
0.05
0.10
η
<u'v'>/ΔU²x100
Batt (1977)
Liepmann & Laufer (1947)
Wygnanski & Fiedler (1970)
Patel (1973)
Bradshaw (1966)
Sunyach (1969)
ARSM

Figure 6

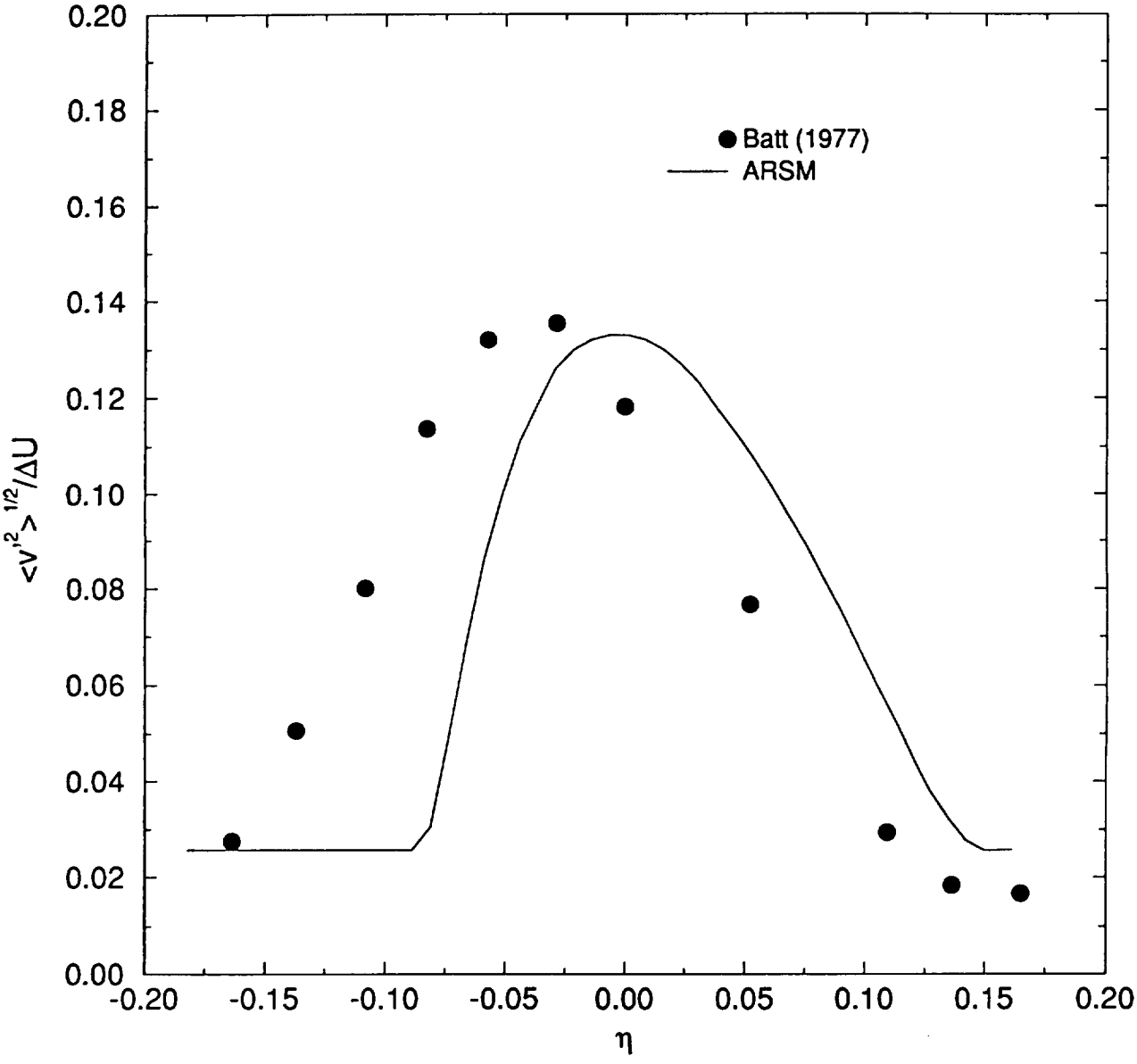
0.20
0.18
0.16
0.14
0.12
0.10
0.08
0.06
0.04
0.02
0.00
-0.20
-0.15
-0.10
-0.05
0.00
0.05
0.10
0.15
0.20
η
<v'^2>^1/2/ΔU
Batt (1977)
ARSM

Figure 7

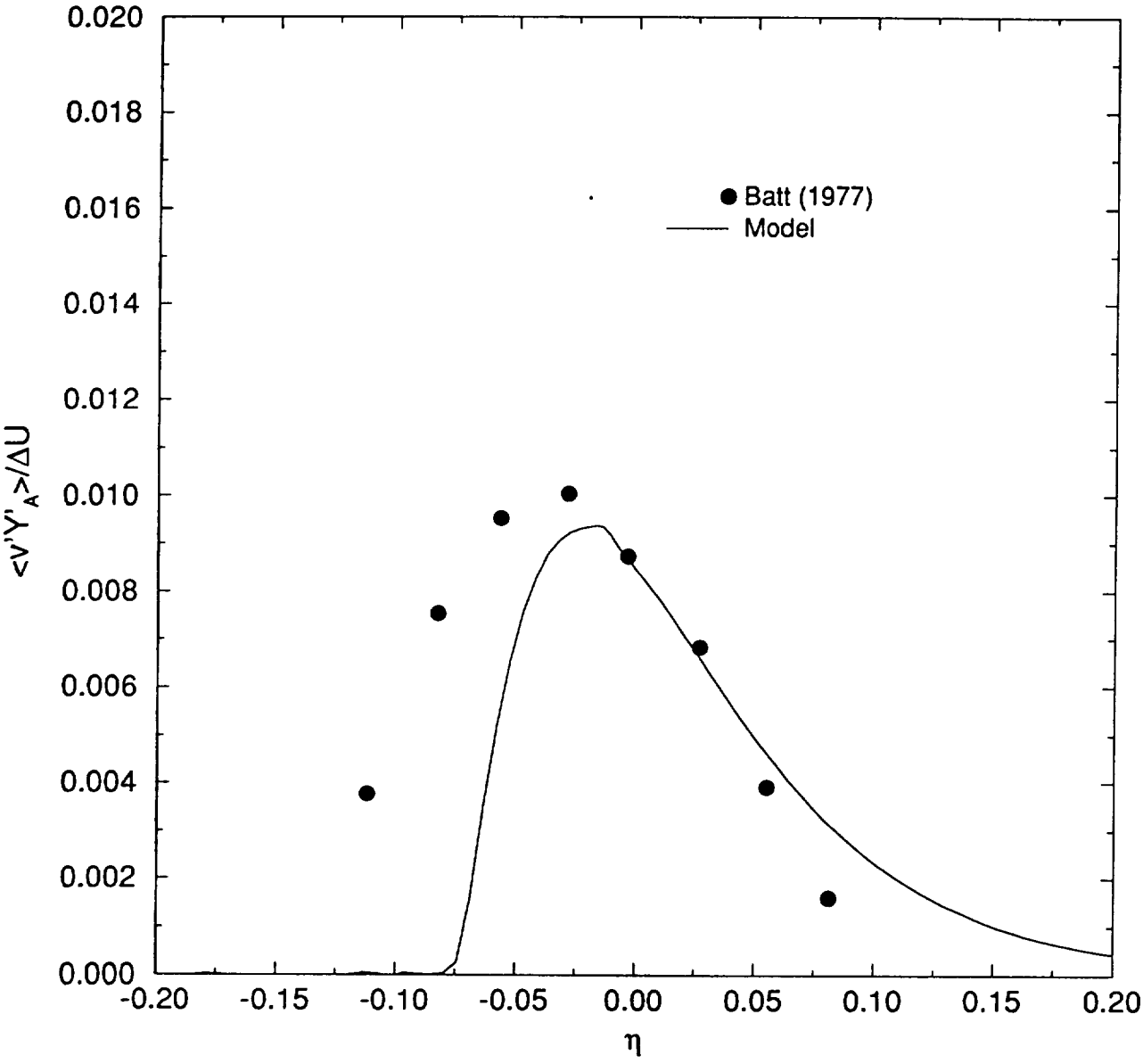
0.020
0.018
0.016
0.014
0.012
0.010
0.008
0.006
0.004
0.002
0.000
<v'Y'A>/ΔU
-0.20
-0.15
-0.10
-0.05
0.00
0.05
0.10
0.15
0.20
η
Batt (1977)
Model

Figure 8

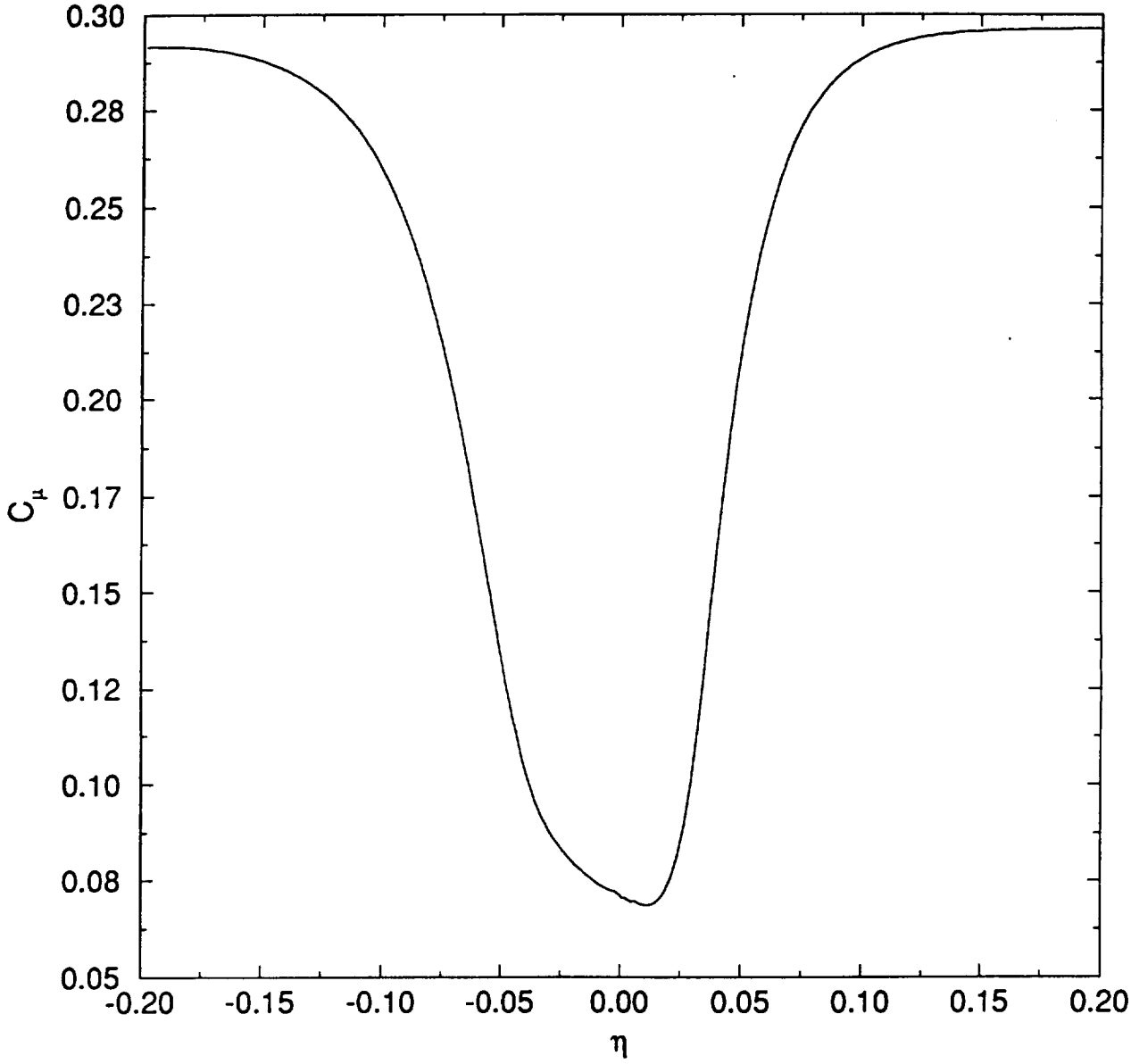
0.30
0.28
0.25
0.23
0.20
0.17
0.15
0.12
0.10
0.08
0.05
C_μ
-0.20
-0.15
-0.10
-0.05
0.00
0.05
0.10
0.15
0.20
η

Figure 9

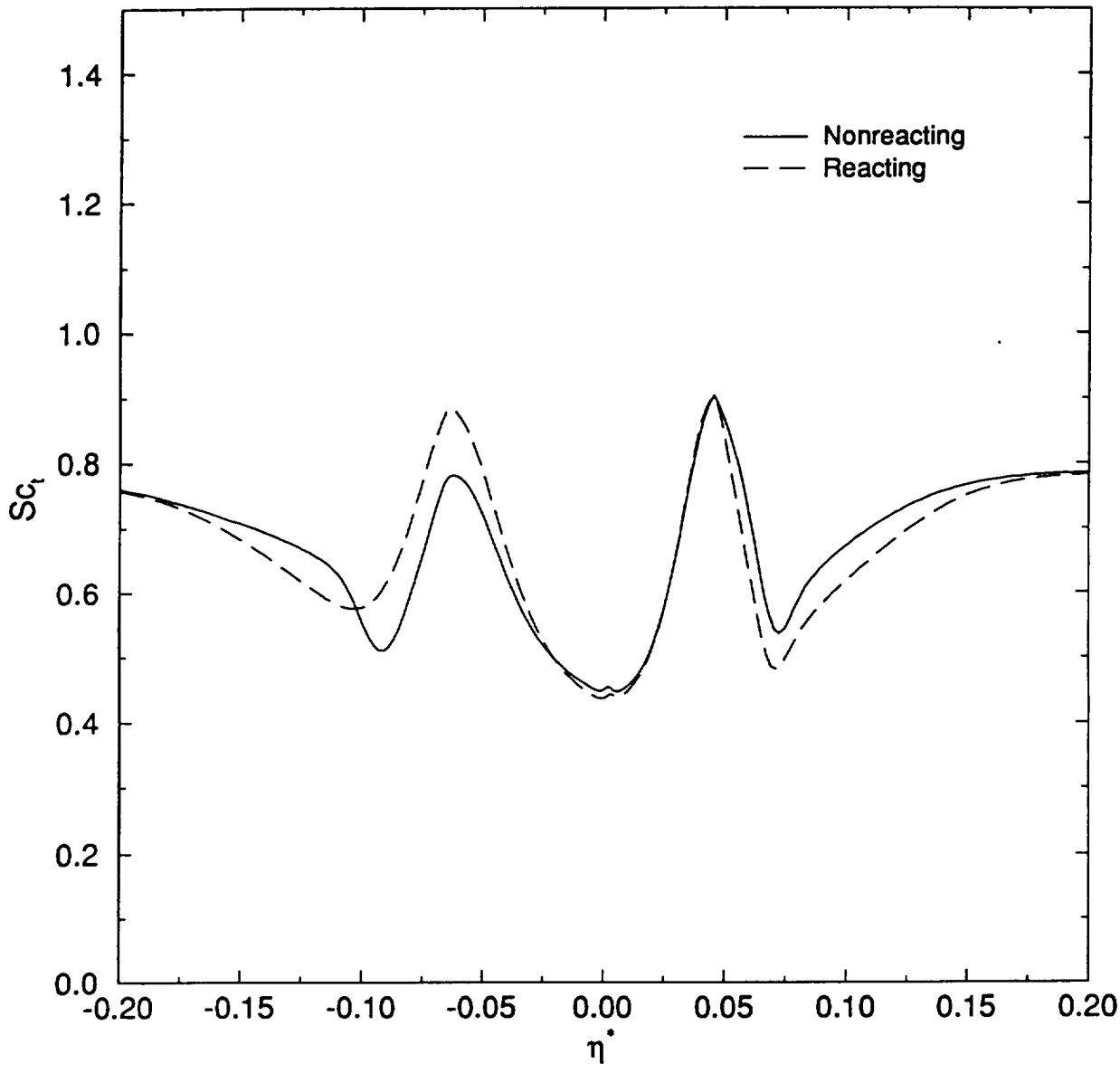
1.4
1.2
1.0
0.8
0.6
0.4
0.2
0.0
Sc_t
-0.20
-0.15
-0.10
-0.05
0.00
0.05
0.10
0.15
0.20
η^*
Nonreacting
Reacting

Figure 10

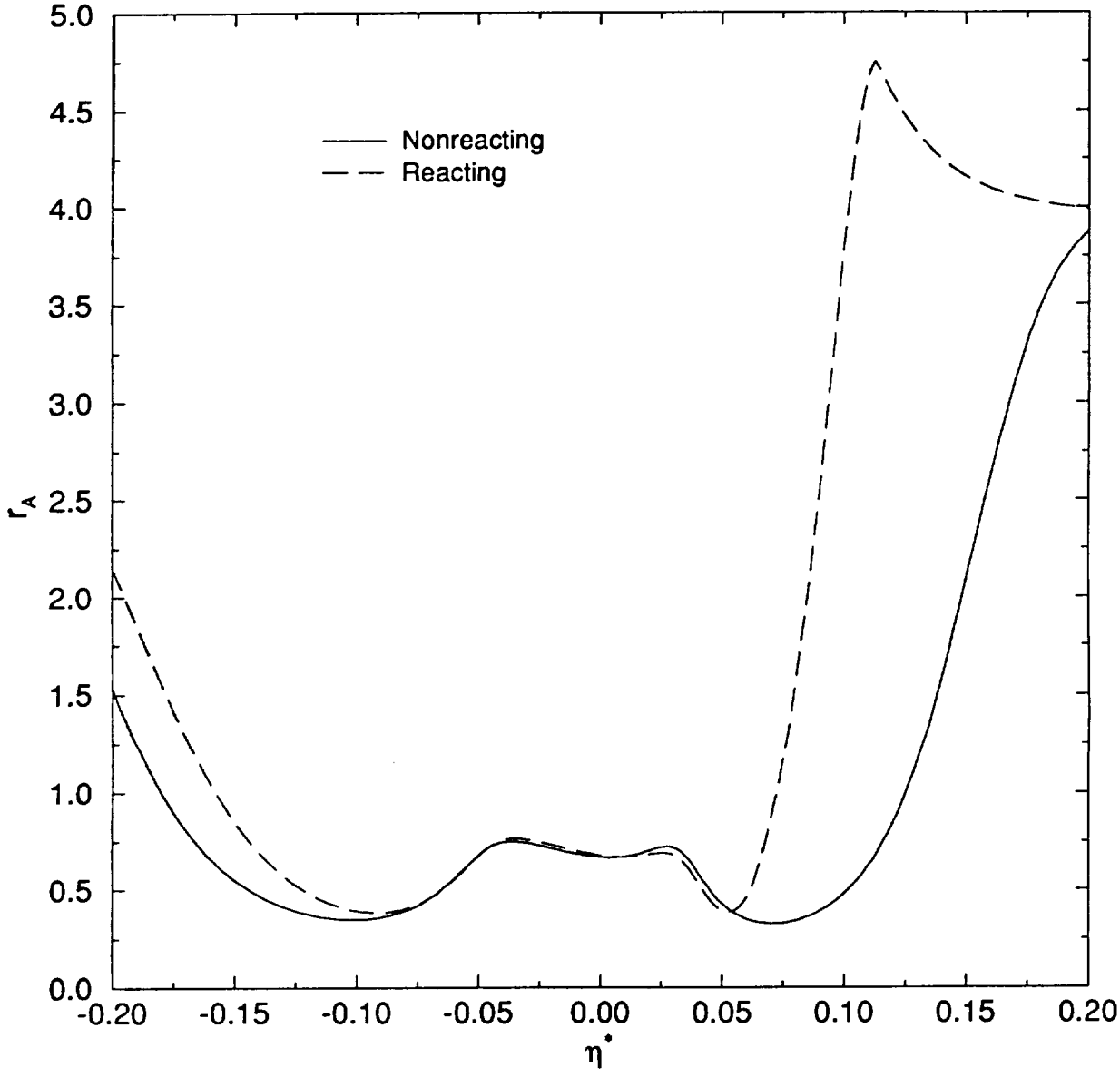
5.0
4.5
4.0
3.5
3.0
2.5
2.0
1.5
1.0
0.5
0.0
r_A
Nonreacting
Reacting
-0.20
-0.15
-0.10
-0.05
0.00
0.05
0.10
0.15
0.20
η^*

Figure 11

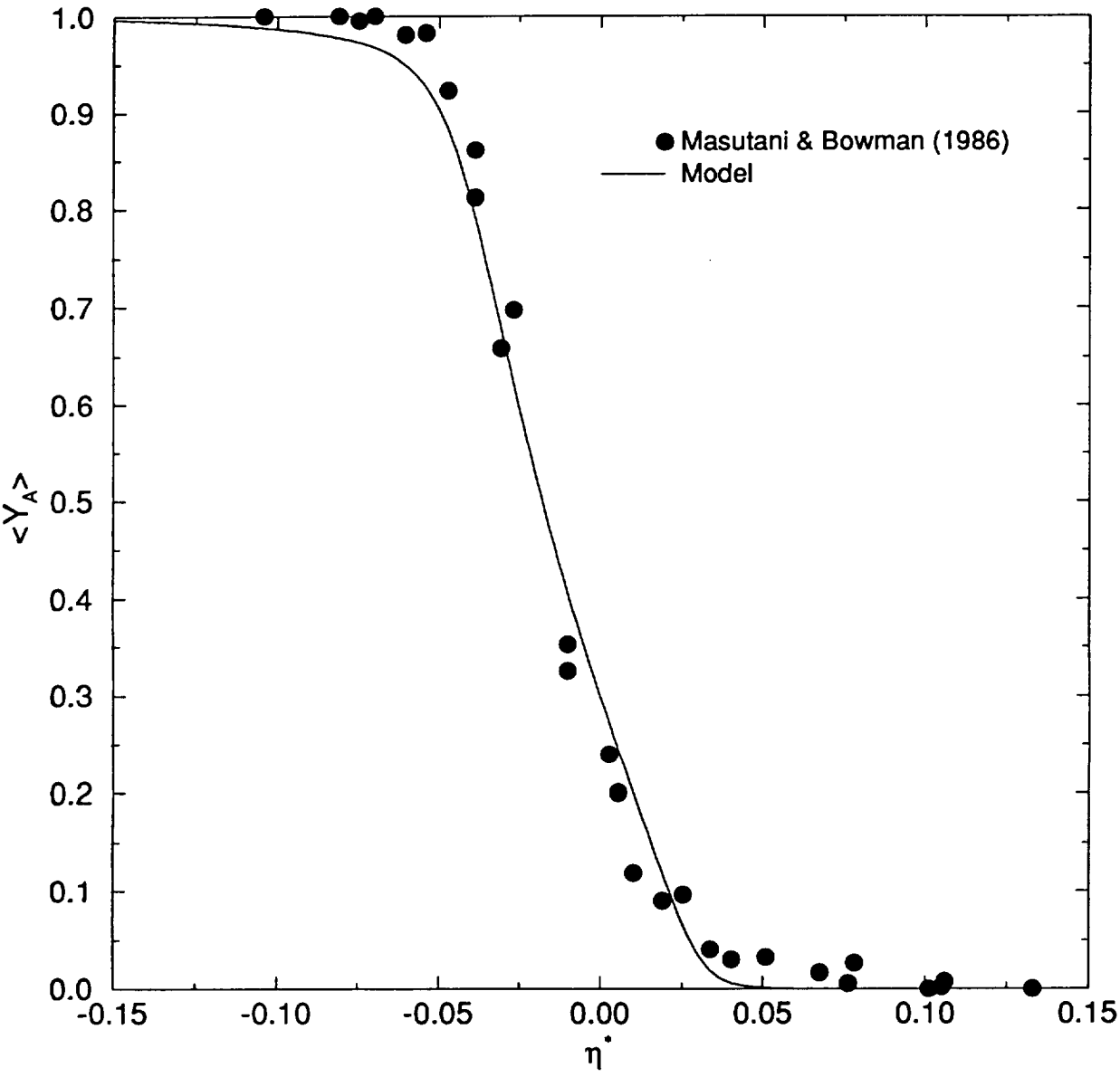
1.0
0.9
0.8
0.7
0.6
0.5
0.4
0.3
0.2
0.1
0.0
<Y_A>
-0.15
-0.10
-0.05
0.00
0.05
0.10
0.15
η*
Masutani & Bowman (1986)
Model

Figure 12

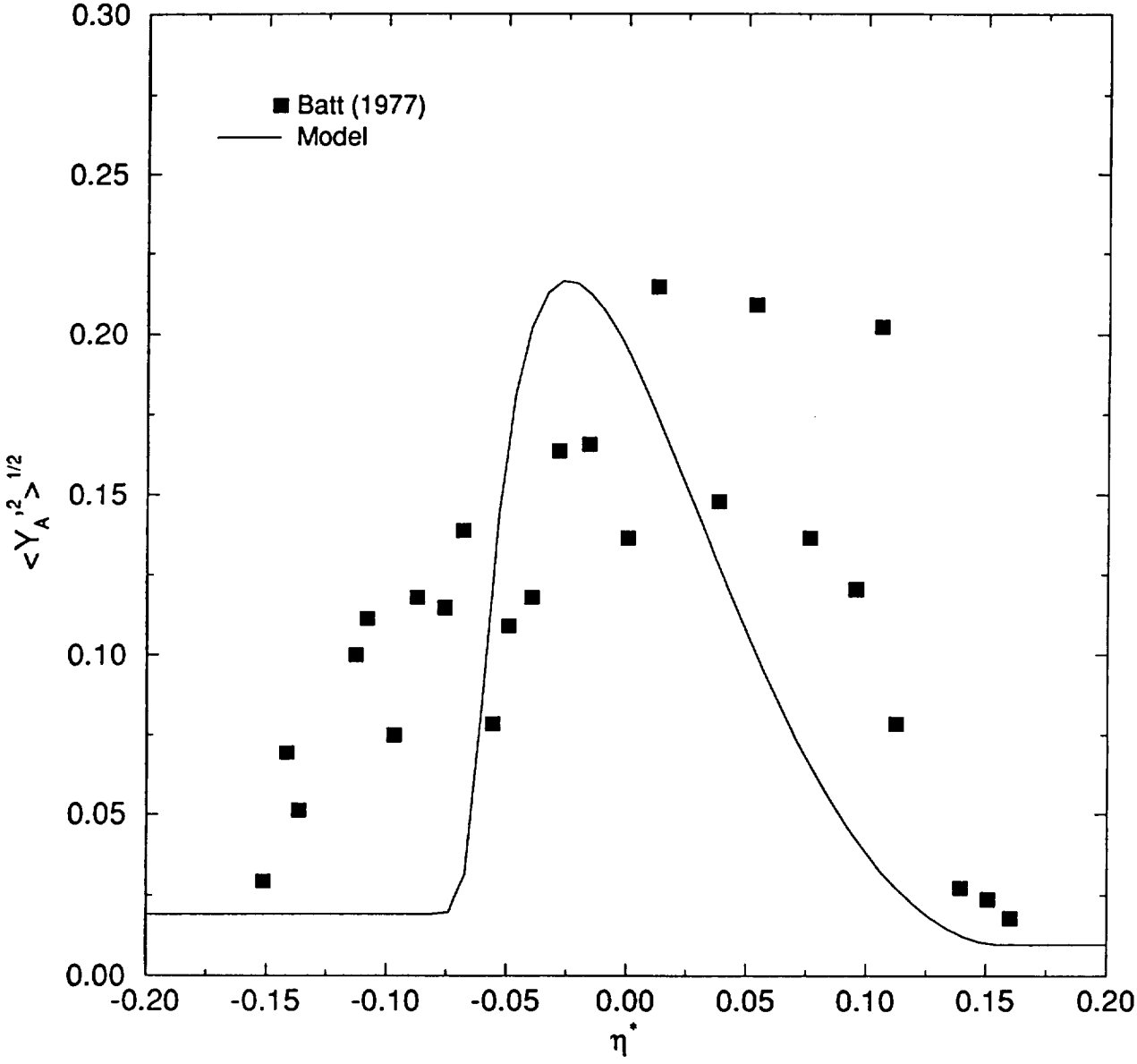
Batt (1977)
Model
0.30
0.25
0.20
0.15
0.10
0.05
0.00
-0.20
-0.15
-0.10
-0.05
0.00
0.05
0.10
0.15
0.20
η^*
$\langle Y_A'^2 \rangle^{1/2}$

Figure 13

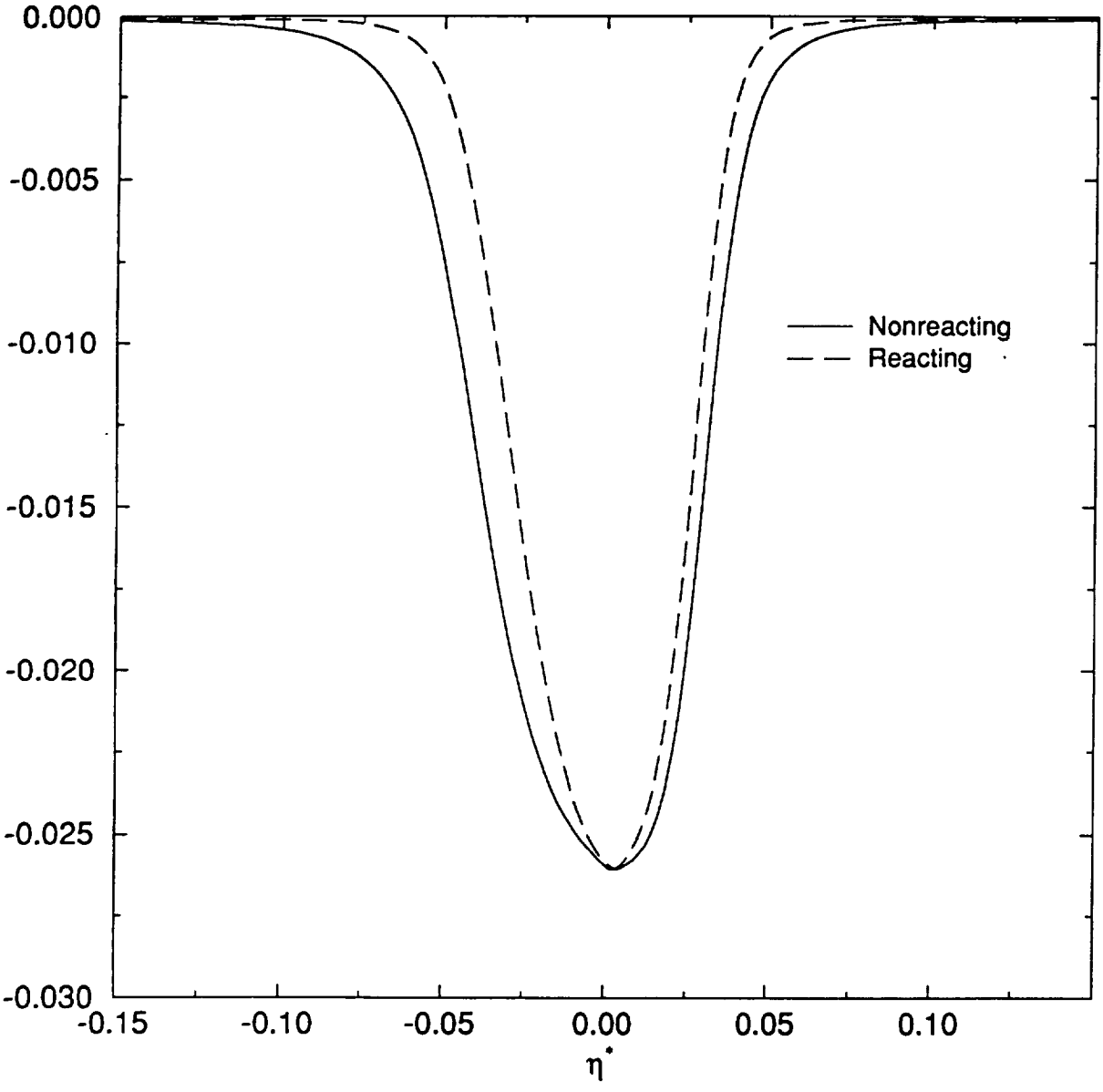
0.000
-0.005
-0.010
-0.015
-0.020
-0.025
-0.030
-0.15
-0.10
-0.05
0.00
0.05
0.10
η*
<Y'A'B>
Nonreacting
Reacting

Figure 14

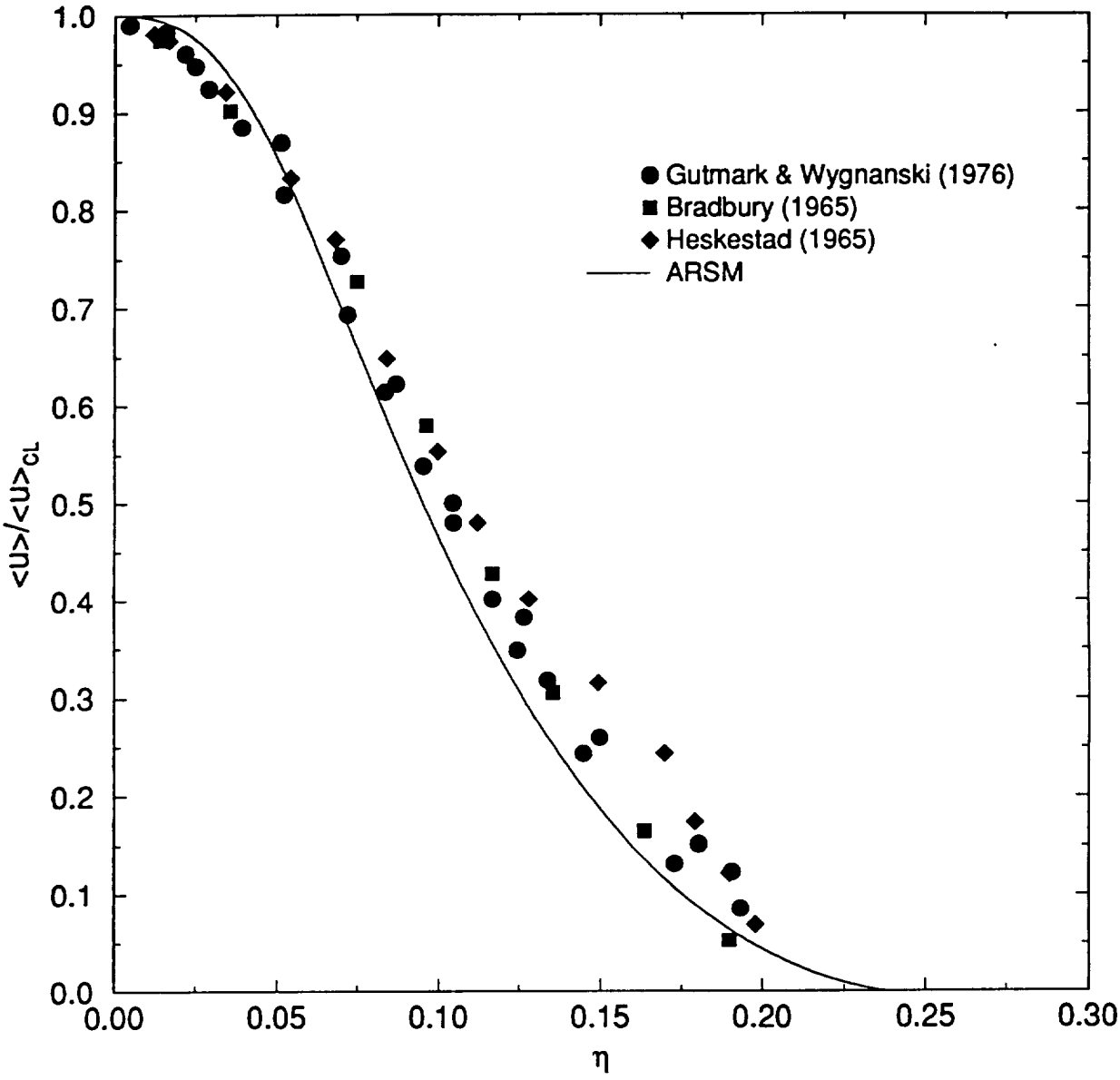
1.0
0.9
0.8
0.7
0.6
0.5
0.4
0.3
0.2
0.1
0.0
<U>/<U>CL
0.00
0.05
0.10
0.15
0.20
0.25
0.30
η
Gutmark & Wygnanski (1976)
Bradbury (1965)
Heskestad (1965)
ARSM

Figure 15

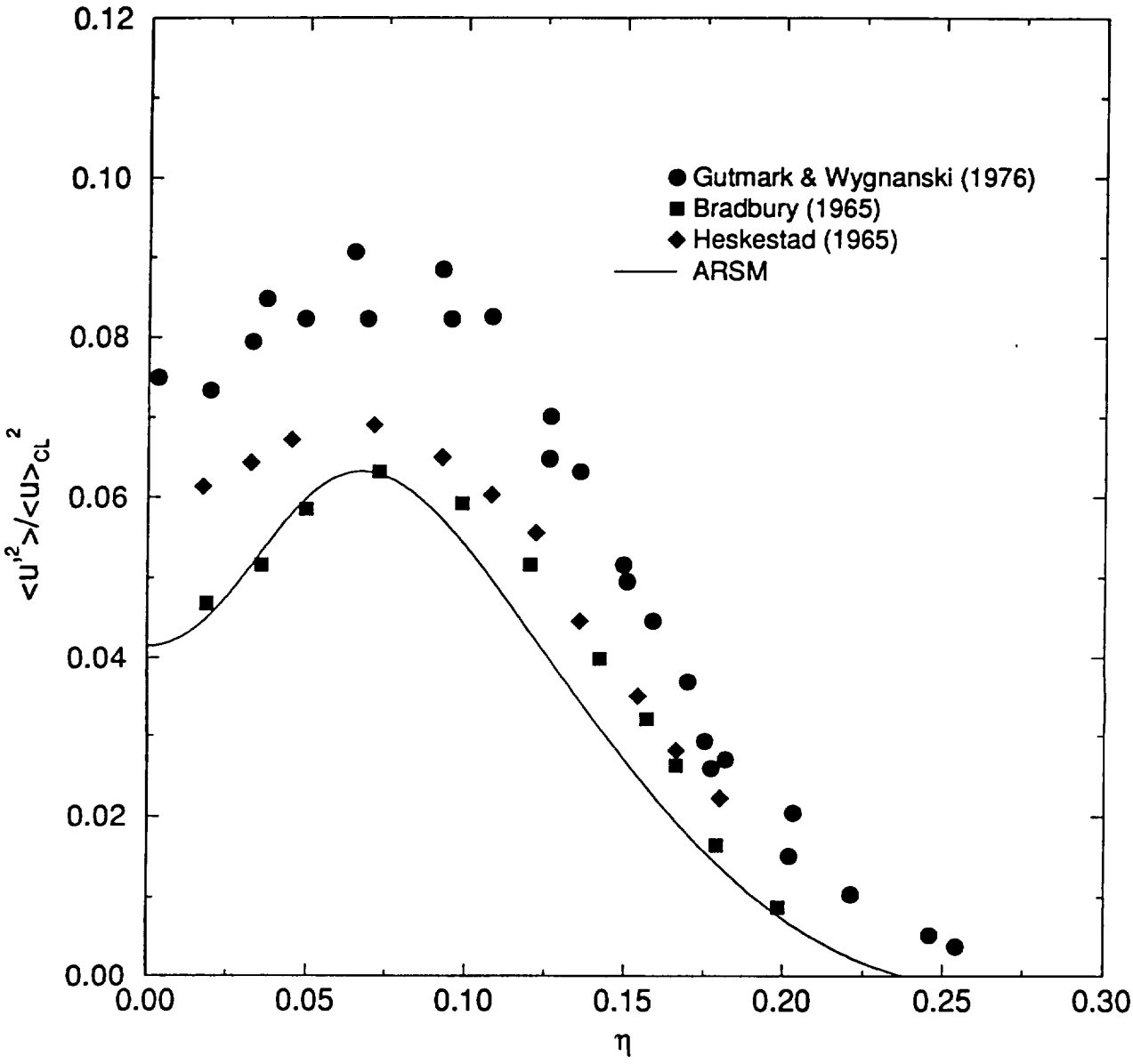
0.12
0.10
0.08
0.06
0.04
0.02
0.00
0.00
0.05
0.10
0.15
0.20
0.25
0.30
η
<u'²>/<u>CL²
Gutmark & Wygnanski (1976)
Bradbury (1965)
Heskestad (1965)
ARSM

Figure 16

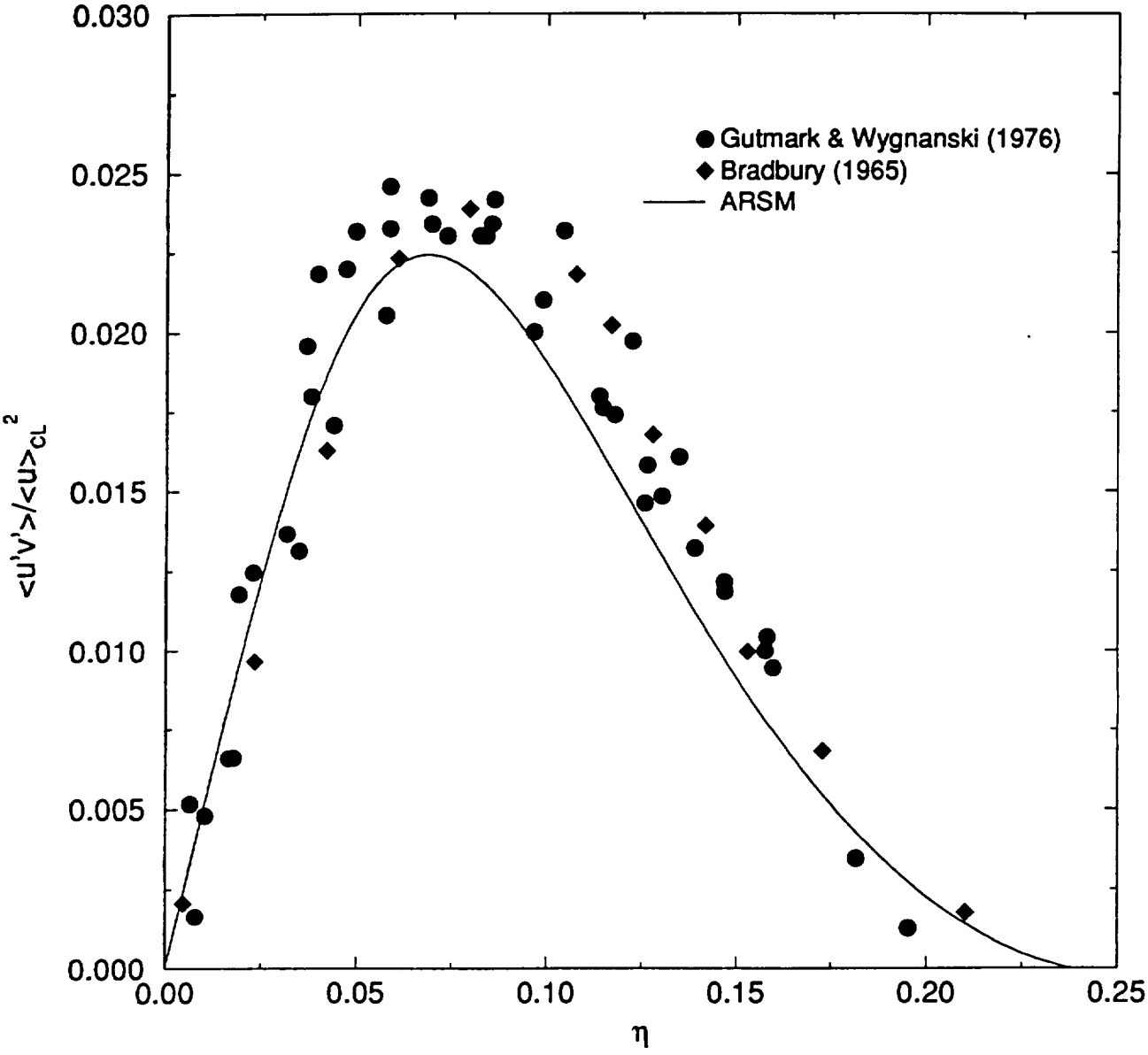
0.030
0.025
0.020
0.015
0.010
0.005
0.000
0.00
0.05
0.10
0.15
0.20
0.25
η
<u'v'>/<u>cL2
Gutmark & Wygnanski (1976)
Bradbury (1965)
ARSM

Figure 17

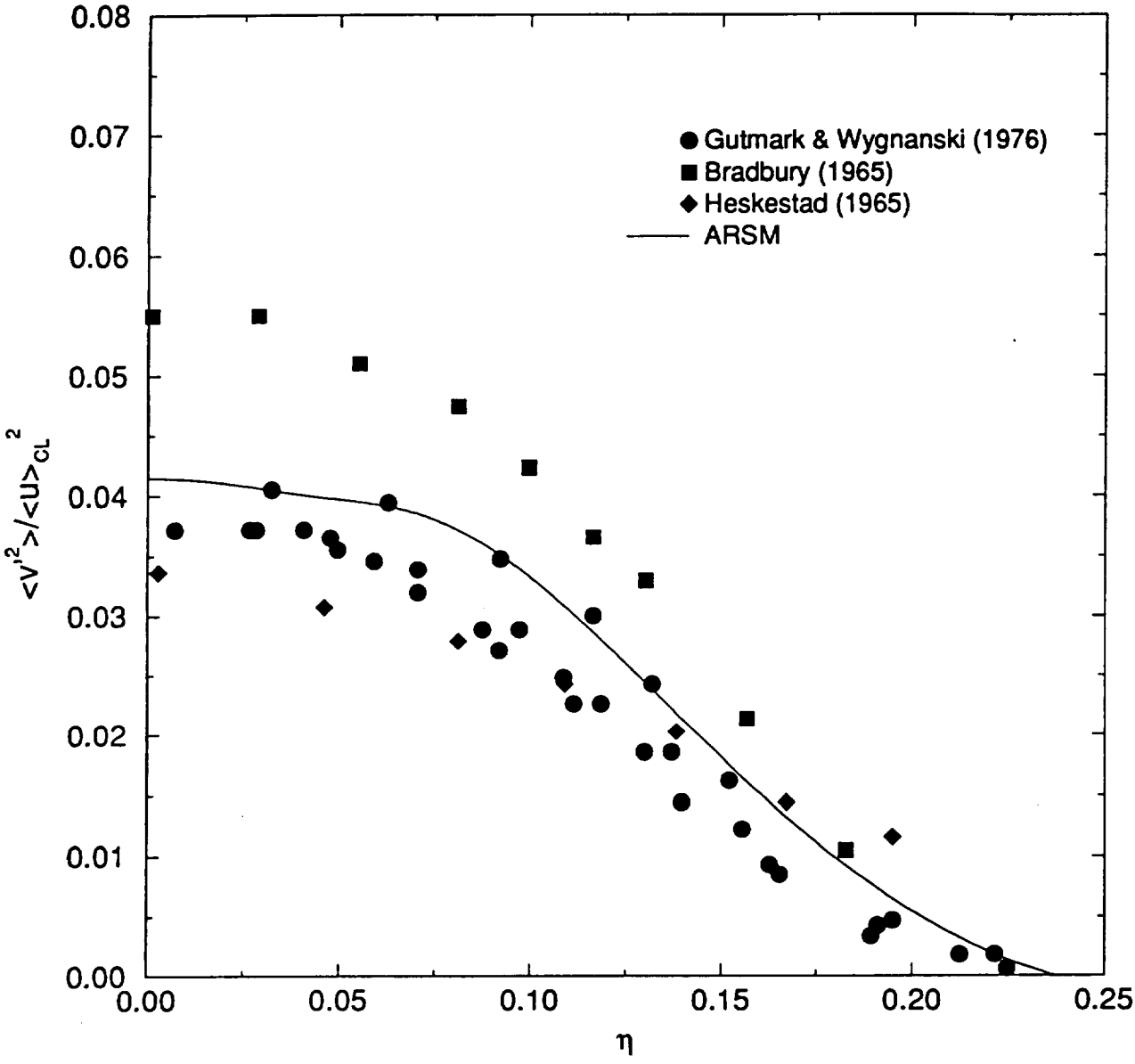
0.08
0.07
0.06
0.05
0.04
0.03
0.02
0.01
0.00
0.00
0.05
0.10
0.15
0.20
0.25
η
$<v'^2>/<U>_{CL}^2$
Gutmark & Wygnanski (1976)
Bradbury (1965)
Heskestad (1965)
ARSM

Figure 18

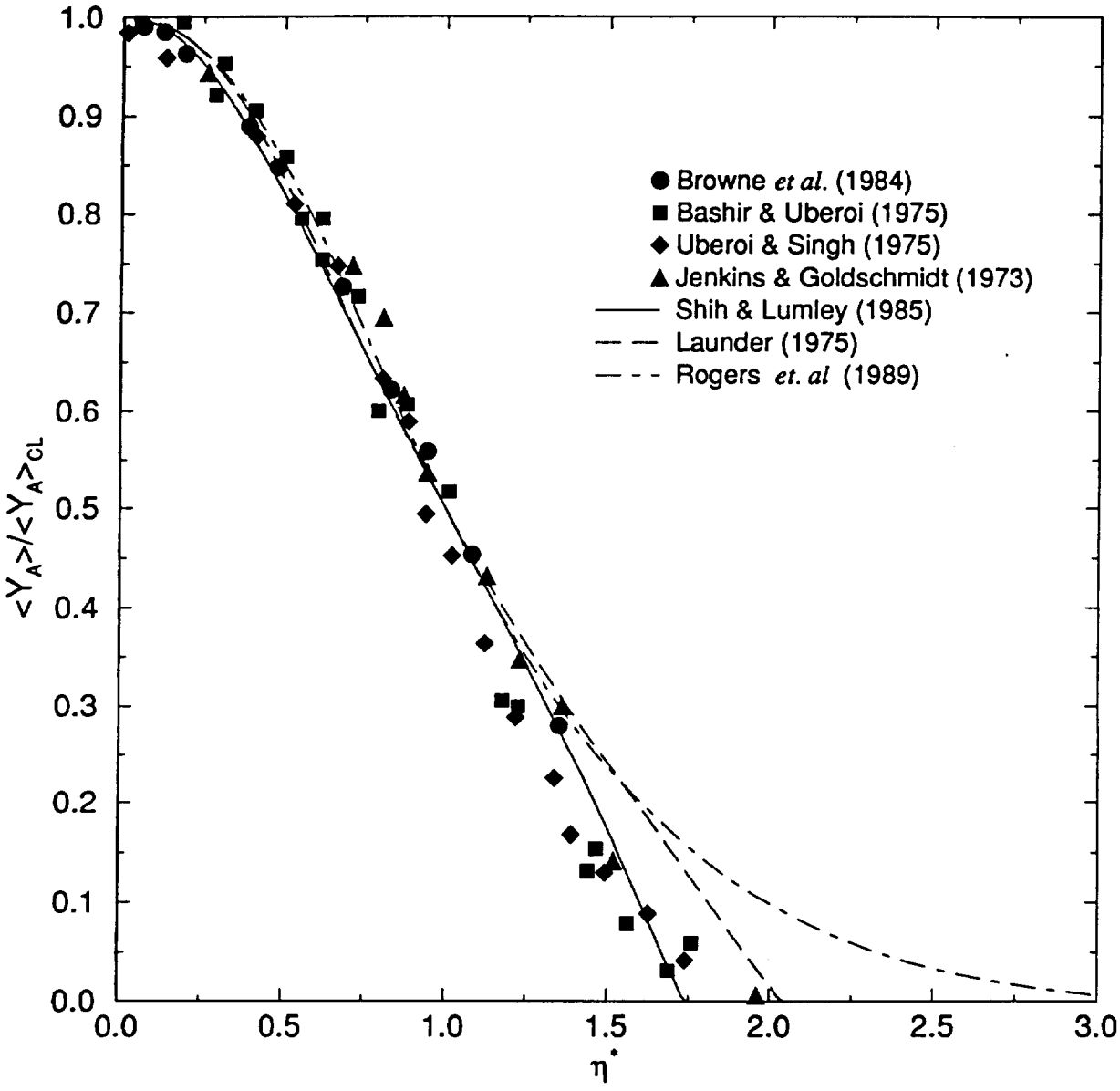
1.0
0.9
0.8
0.7
0.6
0.5
0.4
0.3
0.2
0.1
0.0
0.0
0.5
1.0
1.5
2.0
2.5
3.0
η^*
$<Y_A>/<Y_A>_{CL}$
Browne *et al.* (1984)
Bashir & Uberoi (1975)
Uberoi & Singh (1975)
Jenkins & Goldschmidt (1973)
Shih & Lumley (1985)
Launder (1975)
Rogers *et. al* (1989)

Figure 19

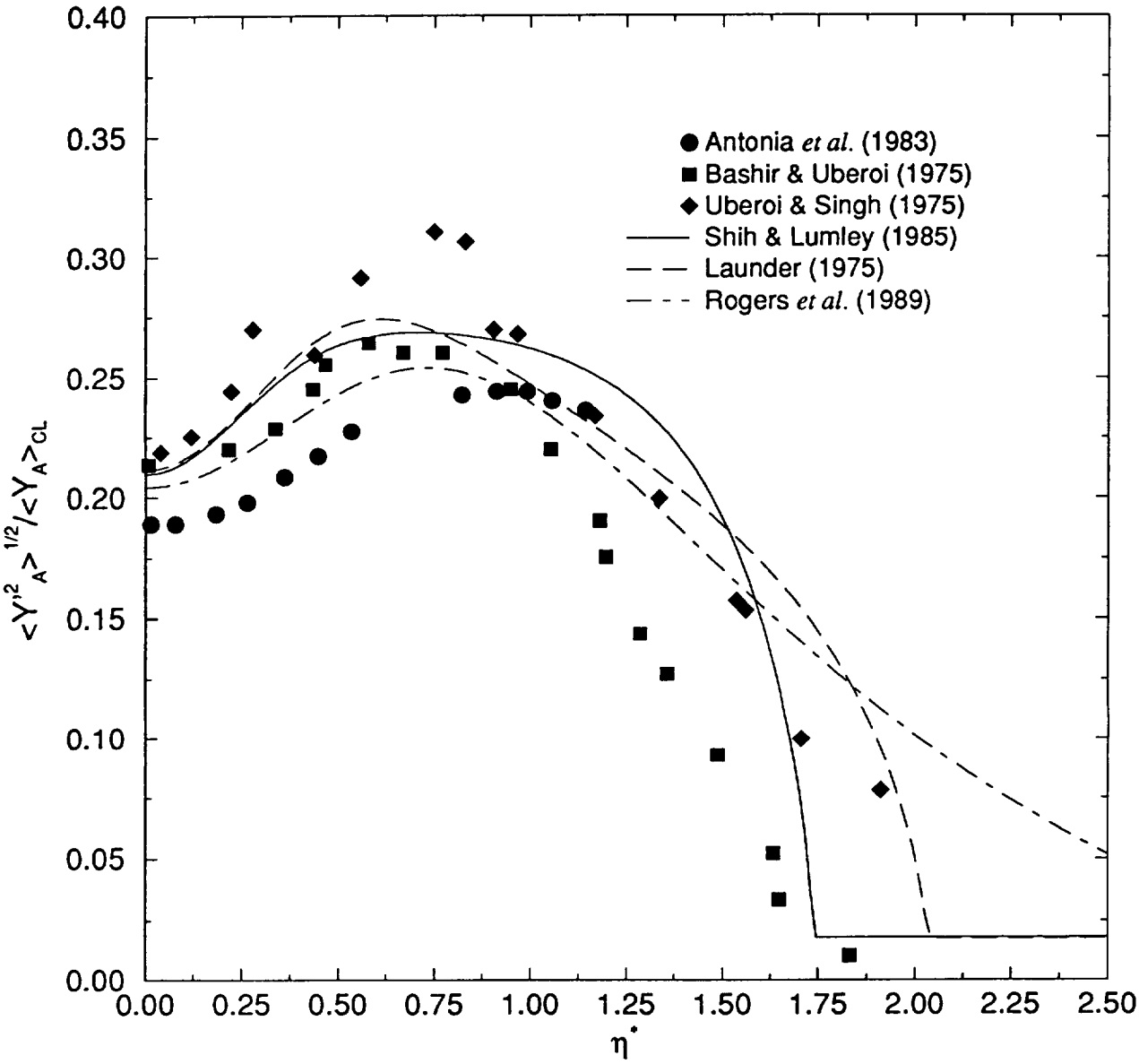
0.40
0.35
0.30
0.25
0.20
0.15
0.10
0.05
0.00
0.00
0.25
0.50
0.75
1.00
1.25
1.50
1.75
2.00
2.25
2.50
η*
<Y'2A>1/2/<YA>CL
Antonia et al. (1983)
Bashir & Uberoi (1975)
Uberoi & Singh (1975)
Shih & Lumley (1985)
Launder (1975)
Rogers et al. (1989)

Figure 20

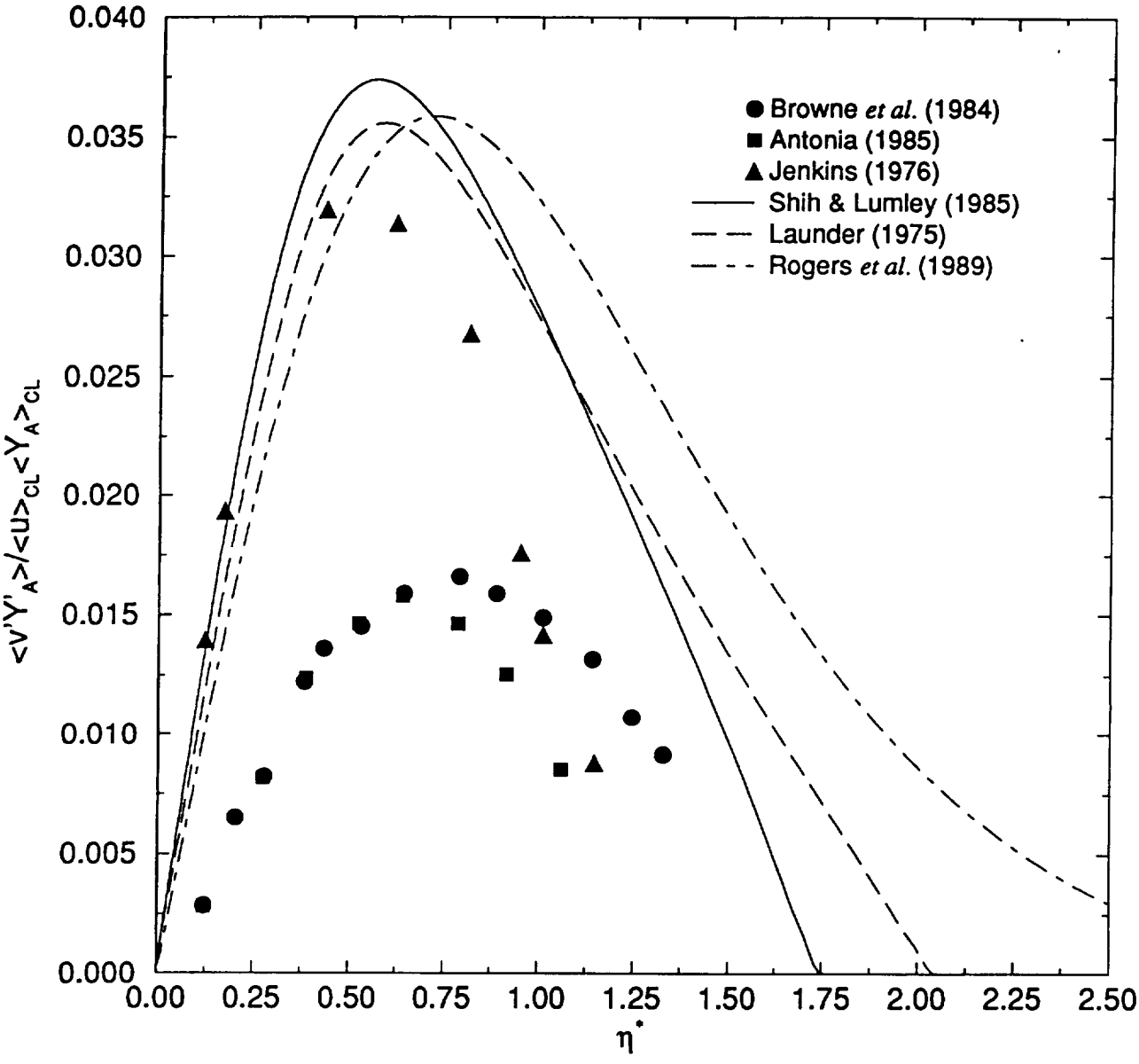
0.040
0.035
0.030
0.025
0.020
0.015
0.010
0.005
0.000
0.00
0.25
0.50
0.75
1.00
1.25
1.50
1.75
2.00
2.25
2.50
η*
<v'Y'A>/<u>CL<YA>CL
Browne et al. (1984)
Antonia (1985)
Jenkins (1976)
Shih & Lumley (1985)
Launder (1975)
Rogers et al. (1989)

Figure 21

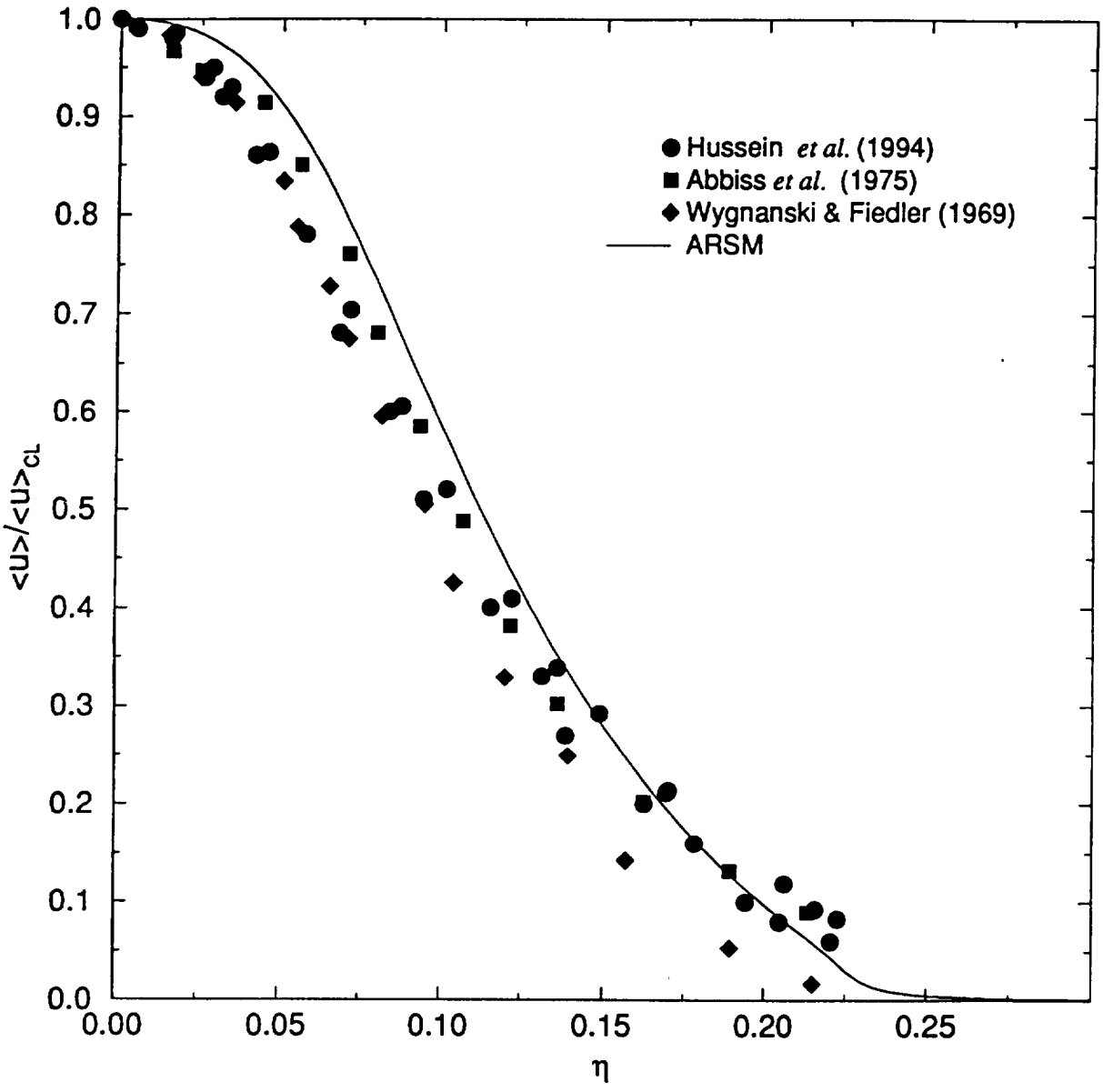
1.0
0.9
0.8
0.7
0.6
0.5
0.4
0.3
0.2
0.1
0.0
0.00
0.05
0.10
0.15
0.20
0.25
η
<u>/<u>CL
Hussein et al. (1994)
Abbiss et al. (1975)
Wygnanski & Fiedler (1969)
ARSM

Figure 22

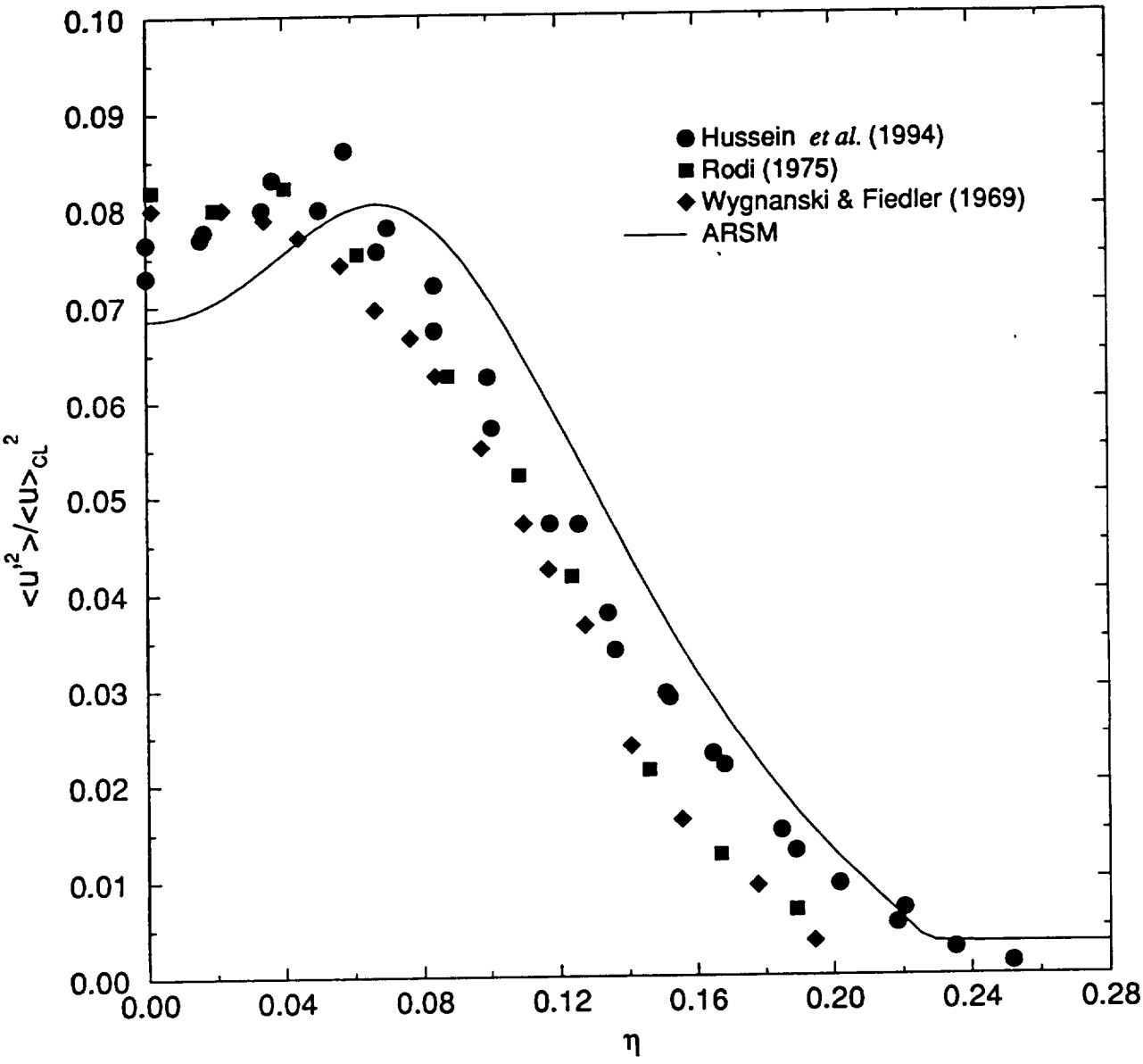
0.10
0.09
0.08
0.07
0.06
0.05
0.04
0.03
0.02
0.01
0.00
0.00
0.04
0.08
0.12
0.16
0.20
0.24
0.28
η
<u'²>/<U>CL²
Hussein et al. (1994)
Rodi (1975)
Wygnanski & Fiedler (1969)
ARSM

Figure 23

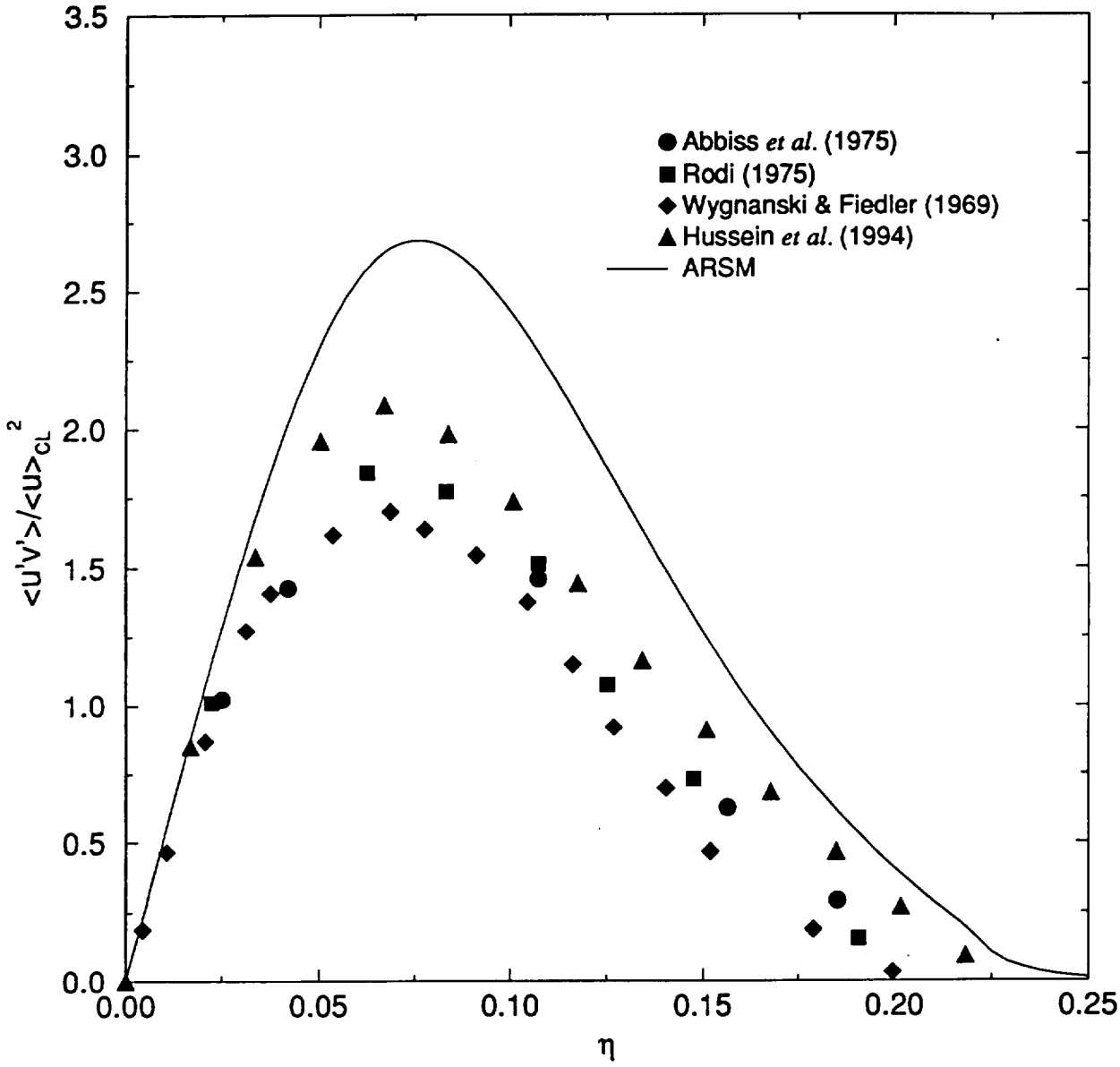
3.5
3.0
2.5
2.0
1.5
1.0
0.5
0.0
0.00
0.05
0.10
0.15
0.20
0.25
η
<u'v'>/<u>cL 2
Abbiss et al. (1975)
Rodi (1975)
Wygnanski & Fiedler (1969)
Hussein et al. (1994)
ARSM

Figure 24

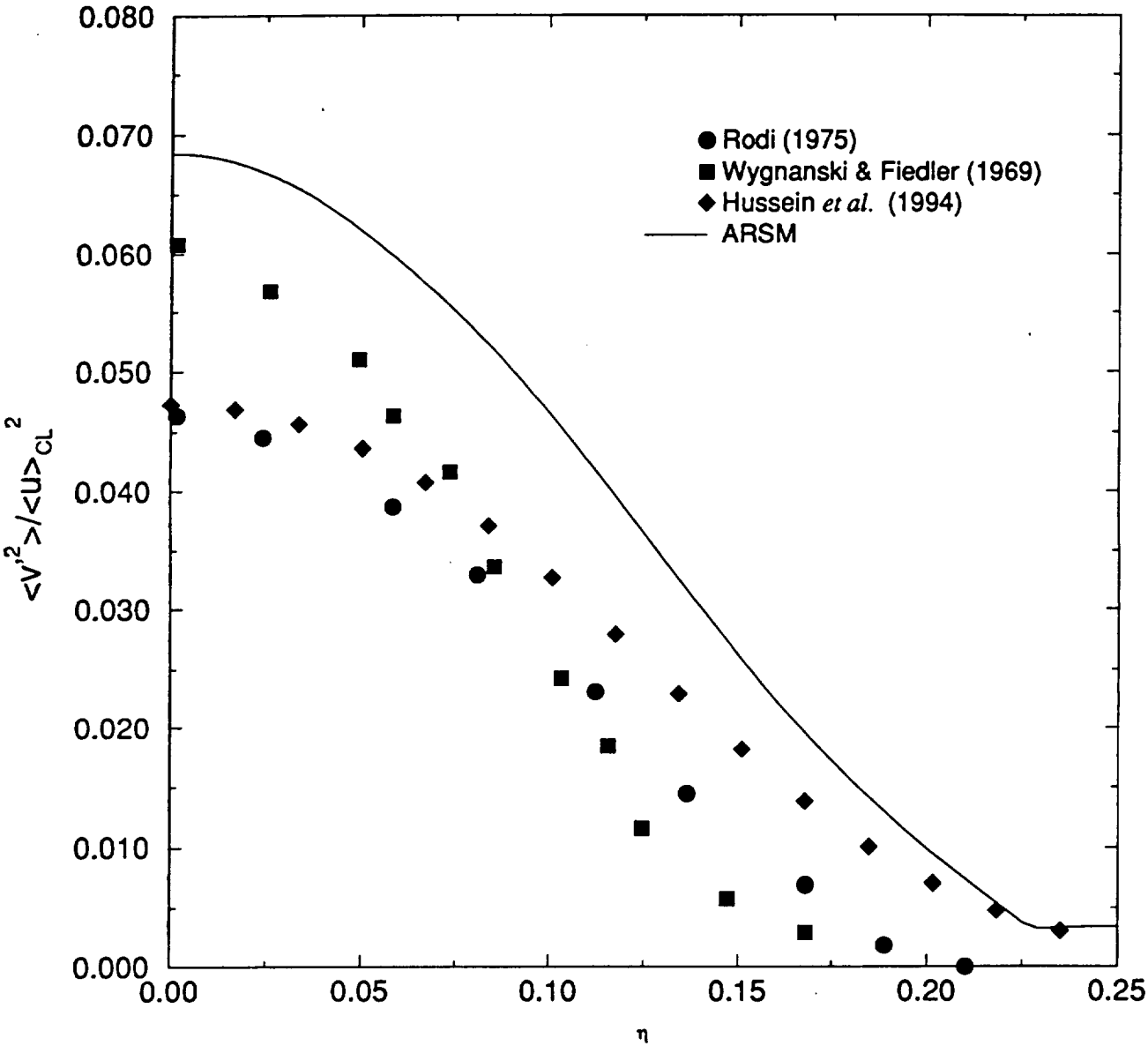
0.080
0.070
0.060
0.050
0.040
0.030
0.020
0.010
0.000
0.00
0.05
0.10
0.15
0.20
0.25
η
<v'2>/<U>CL2
Rodi (1975)
Wygnanski & Fiedler (1969)
Hussein et al. (1994)
ARSM

Figure 25

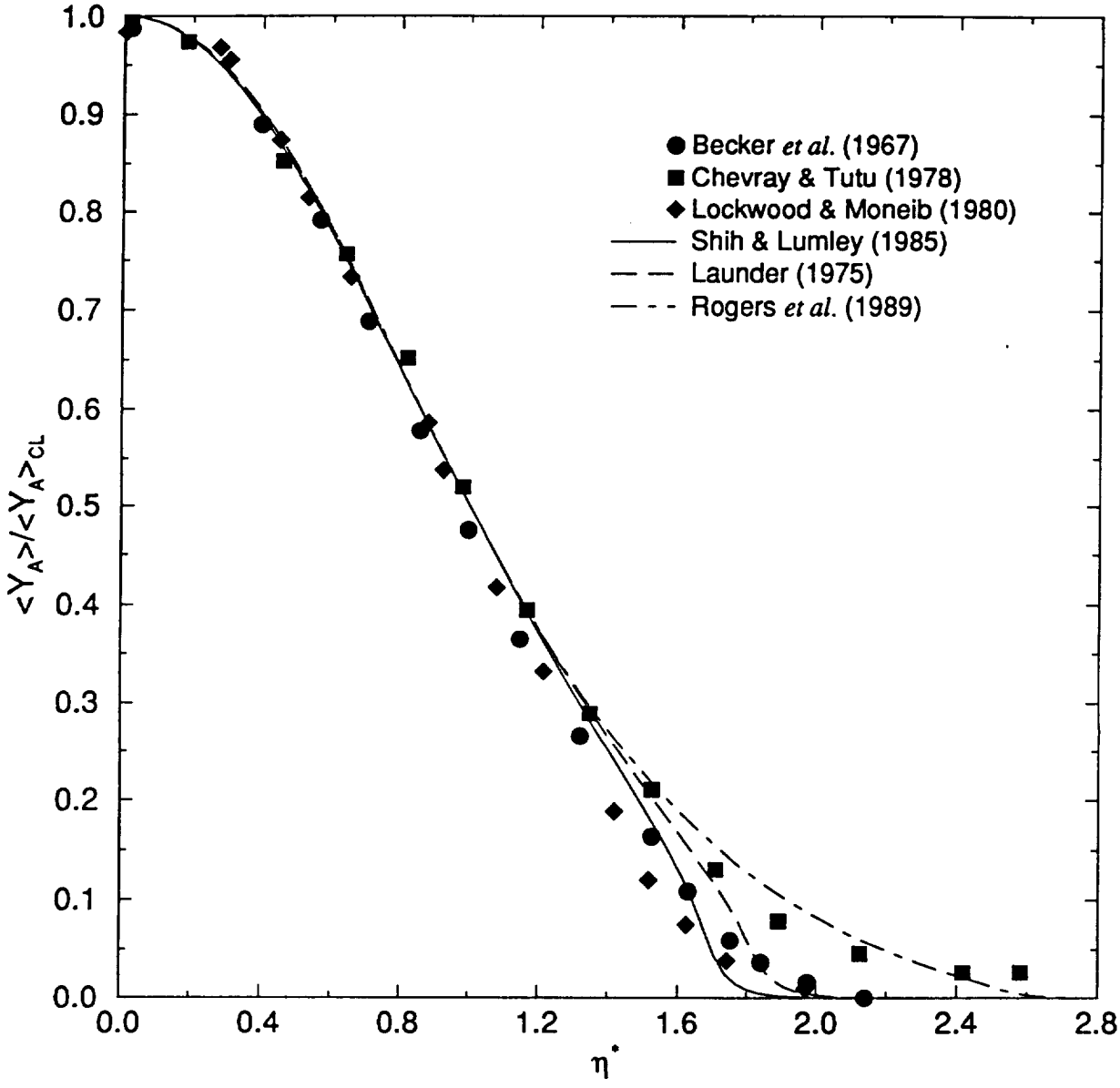
1.0
0.9
0.8
0.7
0.6
0.5
0.4
0.3
0.2
0.1
0.0
0.0
0.4
0.8
1.2
1.6
2.0
2.4
2.8
η^*
$\langle Y_A \rangle / \langle Y_A \rangle_{CL}$
Becker *et al.* (1967)
Chevray & Tutu (1978)
Lockwood & Moneib (1980)
Shih & Lumley (1985)
Launder (1975)
Rogers *et al.* (1989)

Figure 26

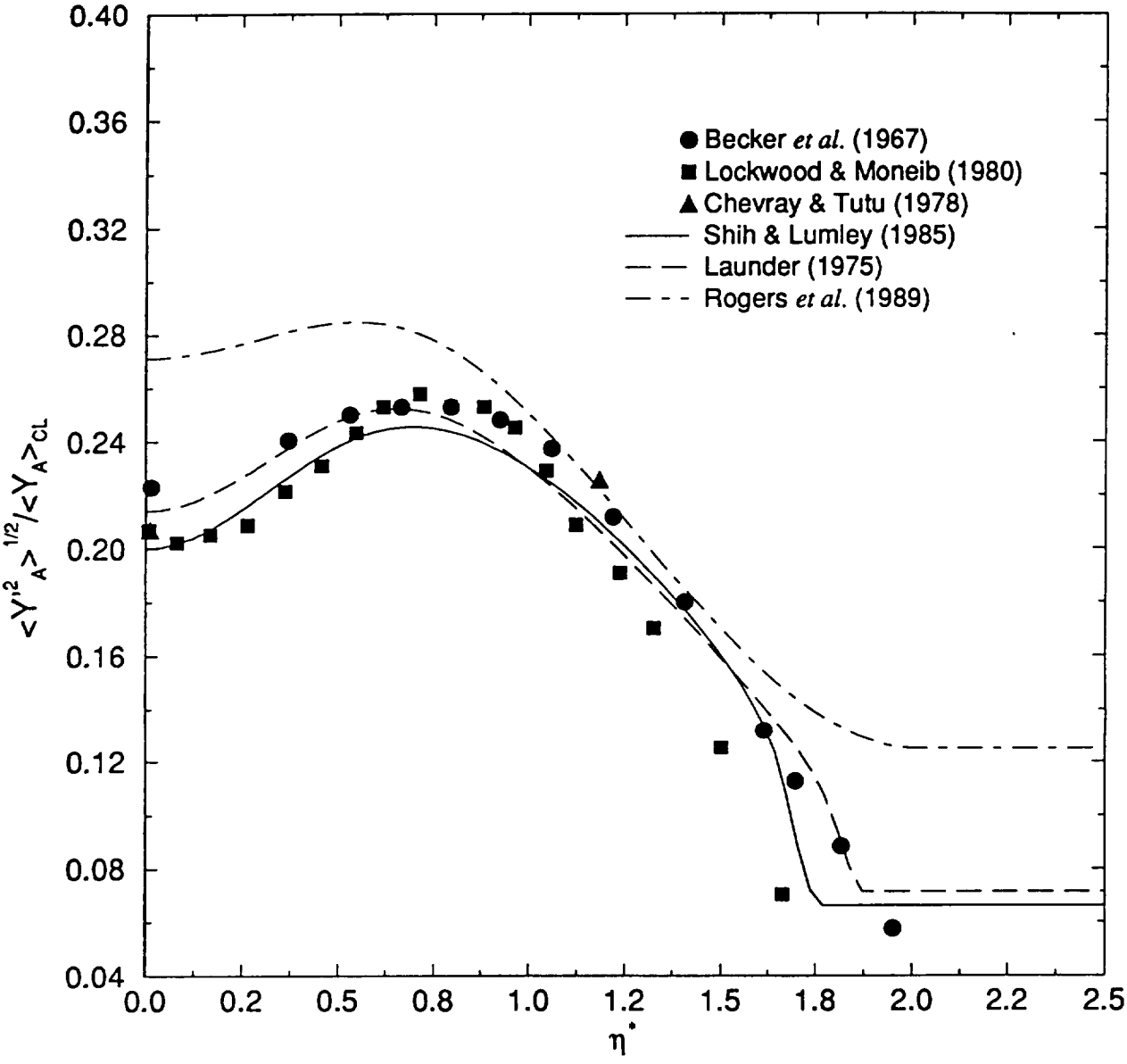
0.40
0.36
0.32
0.28
0.24
0.20
0.16
0.12
0.08
0.04
0.0
0.2
0.5
0.8
1.0
1.2
1.5
1.8
2.0
2.2
2.5
η*
<Y'2A>1/2/<YA>CL
Becker et al. (1967)
Lockwood & Moneib (1980)
Chevray & Tutu (1978)
Shih & Lumley (1985)
Launder (1975)
Rogers et al. (1989)

Figure 27

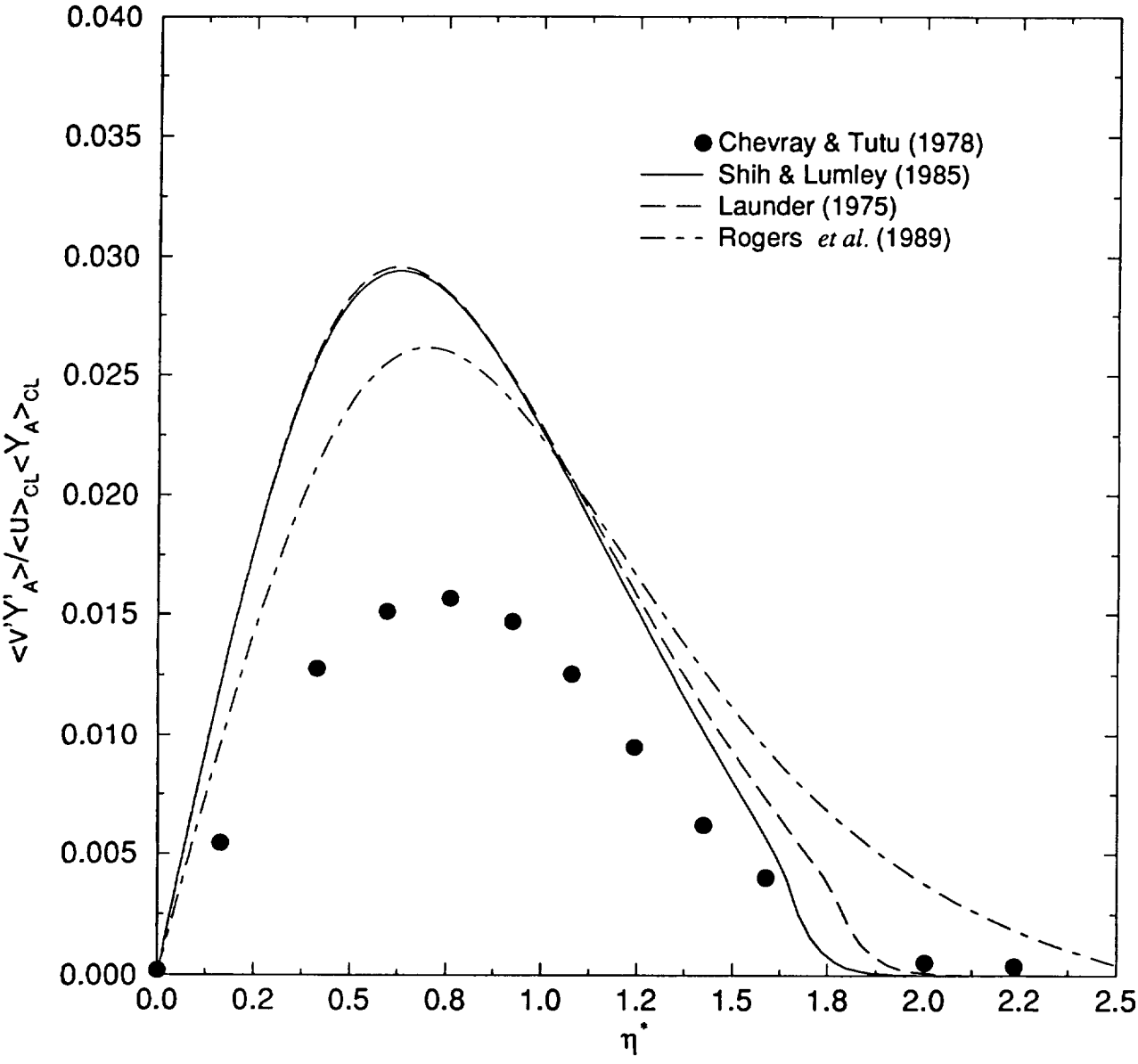
0.040
0.035
0.030
0.025
0.020
0.015
0.010
0.005
0.000
0.0
0.2
0.5
0.8
1.0
1.2
1.5
1.8
2.0
2.2
2.5
η*
<v'Y'A>/<u>CL<YA>CL
Chevray & Tutu (1978)
Shih & Lumley (1985)
Launder (1975)
Rogers et al. (1989)

APPENDIX II

Modeling of the Fluctuations and the Frequency-Spectra of Reactants in Turbulent Scalar Mixing Layers

G.J. Sabini, G.S. Shieh and P. Givi
Department of Mechanical and Aerospace Engineering
State University of New York at Buffalo
Buffalo, New York 14260-4400

Abstract

Experimental data of Bilger *et al.* (1991) pertaining to the compositional structure of a turbulent reactive scalar mixing layer are reproduced by a mathematical-computational procedure utilizing the *Pearson* family (PF) of univariate and multivariate scalar probability density functions (pdfs). Aided by comparisons against these data and some additional data generated here by direct numerical simulation (DNS) of a spatially developing reacting mixing layer, an appraisal is made of the applicability and the extent of validity of the PF for the statistical description of the reactant fluctuations. In accord with the experiment, a chemical reaction of the type $A + B \rightarrow$ *Products* is simulated in isothermal, incompressible flows. A wide range of the Damköhler number is considered including both frozen and equilibrium chemistry flows. The comparison of the predicted results with laboratory data indicates that the PF generated pdfs are very convenient, in the absence of better alternatives, for modeling the influence of turbulence on the mean reactant conversion rate. In particular, the *Dirichlet* frequency parameterized with the "scalar-energy" provides the most reasonable means of portraying the multivariate scalar pdf. A more detailed comparative assessment of the model predictions against the DNS data confirms the relative superiority of the Dirichlet pdf even though it is mathematically shown that this frequency cannot be justified for modeling of equilibrium flows.

With the use of the PF generated pdf, the autospectral density function and the cross-spectral density function of the reacting scalars under equilibrium chemistry are related to the frequency spectrum of the mixture fraction. This relation is very convenient and is favored over previous models for predicting the spectral characteristics of reacting scalars in the central region of the laboratory mixing layer and in any other homogeneous flow configuration which yields an asymptotic gaussian pdf for the mixture fraction. The correction to these spectral relations for asymptotic exponential pdfs is provided, and the influence of the Damköhler number on both the auto- and the cross-spectral density functions is assessed by the analysis of the DNS data.

1 Introduction

In a recent article, Bilger *et al.* (1991) (hereinafter referred to as BSK) report the results of extensive laboratory measurements on the compositional structure of a turbulent reactive scalar mixing layer. The objective of these measurements is to portray the behavior of the reacting scalar field in both "single-point spatial" and "two-time" statistical levels. In the format presented, the data are very useful for assessing the influence of scalar fluctuations on the rate of mean reactant conversion and also for examining the spectral characteristics of reactive scalars in a chemical reaction of the type $A + B \rightarrow Products$. A wide range of chemistry parameters is considered including both frozen and equilibrium flows. The extent of the measured data together with the relative simplicity of the flow configuration provide an excellent setting for appraising the performance of turbulence closures in accounting for the role of scalar fluctuations (Komori *et al.*, 1991), and for predicting the spectra of reacting scalars. The conclusion of this work advocates the need for mathematical models for depicting the stochastic and the spectral character of reacting scalars for general applications.

Mathematical modeling of scalar fluctuations in stochastic treatment of turbulent reacting flows has been the subject of broad investigations since the pioneering work of Toor (1962). One approach which has proven particularly useful is based on the probability density function (pdf) or joint pdf of scalar quantities (Libby and Williams, 1980; O'Brien, 1980; Bilger, 1980; Pope, 1985; Givi, 1989; Kollmann, 1990; Pope, 1990). This approach offers the advantage that all the statistical information pertaining to the scalar field is embedded within the pdf. Therefore, once the pdf is known the effects of scalar fluctuations are easily determined. Because of their capabilities, pdf methods have been widely utilized for a variety of reacting systems (see Libby and Williams (1994); Pope (1994) for recent reviews). A systematic approach for determining the pdf is by means of solving the transport equation governing its evolution (Lundgren, 1967; Lundgren, 1969; Pope, 1985). In this equation the effects of chemical reactions appear in a closed form, but modeling is needed to account for the transport of the pdf in the composition domain of the random variables. This transport describes the role of the molecular action. In addition, there are extra dimensions associated with the

composition domain which must be treated. These problems have constituted a stumbling block in utilizing pdf methods in practical applications; developments of turbulence closures and numerical schemes which can effectively deal with these difficulties have been the subject of numerous investigations within the past two decades (Libby and Williams, 1980; Libby and Williams, 1994).

An alternative approach in pdf modeling is based on *"field-parameterization"* methods. In these methods the pdf is not determined by solving a transport equation. Rather, its shape is *"assumed"* in terms of the low order moments of the random variable(s). Obviously, this method is *ad hoc* but it offers more flexibility than the first approach. Presently, the use of parameterized methods is justified in cases where there is strong evidence that the pdf adopts a particular distribution (Bilger, 1980; Pope, 1994).

Between these two approaches, obviously the first is preferable if an appropriate closure is available to account for the effects of molecular action. In its application in turbulent combustion, traditionally the family of models based on the coalescence/dispersion (C/D) closures (Curl, 1963; Janicka *et al.*, 1979; Pope, 1982; Kosály and Givi, 1987; Norris and Pope, 1991), or linear mean square estimation methods (Dopazo and O'Brien, 1976; O'Brien, 1980) have been employed. These closures are plausible from a computational standpoint and can be effectively simulated via Monte Carlo numerical methods (Pope, 1981). However, there are several drawbacks associated with these closures which restrict their use for reliable predictions (Pope, 1982; Kosály and Givi, 1987). Some of these drawbacks are overcome in the newly developed *Amplitude Mapping Closure* (AMC) (Kraichnan, 1989; Chen *et al.*, 1989). This has been established in a number of recent validation assessments of the AMC by means of comparison of its predicted results with those of DNS (Pope, 1991; Madnia *et al.*, 1992; Jiang *et al.*, 1992; Frankel *et al.*, 1993), and experimental (Frankel *et al.*, 1992) data.

Despite its demonstrated properties, there are some deficiencies associated with the AMC which require further investigation. These are discussed in detail by Miller *et al.* (1993); the most serious of these are: (1) the "single-point" nature of the closure, (2) the difficulties

associated with its numerical implementation especially in multivariate statistical analyses, and (3) its inability to account for the migration of scalar bounds as mixing proceeds. The first problem is shared with C/D models and indicates the deficiency of the approach in accounting for the variation of turbulent length and time scales. The other problems are exclusive to the AMC and can cause difficulties in its applications.

Considering the current state of progress in pdf modeling, it can be cautiously argued that parameterized pdf methods are somewhat more "feasible" than the transport equation approach for practical applications. This is not to suggest the superiority of assumed methods. Rather, it is to encourage further research on the first scheme before it can be implemented routinely. In this regard, Miller *et al.* (1993) and Frankel *et al.* (1993) have conducted detailed investigations based on the two approaches. The general conclusion drawn from these studies is that in cases where the AMC has proven useful, other approaches based on parameterized pdfs are equally effective. In the cases considered by Miller *et al.* (1993), it is shown that in simple flows where the AMC can be employed, the family of pdfs based on the *Johnson Edgeworth Translation* (JET) (Johnson, 1949b; Edgeworth, 1907) can also be used. In fact, for the simple problem of binary mixing in isotropic turbulence - a standard test case - the solution generated by the AMC (Pope, 1991; Gao, 1991) can be viewed as a member of the JET family. Furthermore, due to established similarities of the JET with simpler distributions belonging to the *Pearson Family* (PF) of pdfs (Pearson, 1895), it can be argued that the PF can also be considered as a viable alternative (Frankel *et al.*, 1993).

There is a long history of the use of the PF pdfs in turbulent combustion, *e.g.* Rhodes (1975); Jones and Priddin (1978); Lockwood and Moneib (1980); Peters (1984); Janicka and Peters (1982); for recent reviews see Williams (1985); Givi (1989); Priddin (1991). In most applications to date, this family has been used in the form of the Beta density of the first kind (Pearson Type I and Type II distributions). This is due to the flexibility of this density in portraying bimodal distributions. The properties of this density have been examined in detail by Madnia *et al.* (1992); Miller *et al.* (1993) and Frankel *et al.* (1993). According to these studies there are some similarities between the PF and the AMC,

as well as some distinct differences. As indicated before, both these methods are utilized in the context of a single-point closure. Therefore, in both cases the magnitudes of the moments up to second order must be provided externally. Also, both methods suffer from an inability to account for the shrinking bounds of the scalar domain as mixing proceeds. This is manifested by the failure of both closures in producing a correct evolution for the conditional statistics of the scalar; namely, the conditional expected dissipation and the conditional expected diffusion. This can be troublesome and may produce significant errors, especially in modeling of non-equilibrium flames. In modeling of equilibrium reacting homogeneous flows, both closures are satisfactory regardless of the equivalence ratio (Madnia *et al.*, 1992; Frankel *et al.*, 1993). However, the actual implementation of the AMC is very difficult, if not impossible, for applications in non-homogeneous flows regardless of the chemistry model. In such systems the mapping transfer function must be evaluated numerically, and in non-equilibrium flows the multivariate form of the pdf must be considered. These require serious investigations before they can be implemented routinely (Pope, 1991). In these cases the application of the PF is much more straightforward but obviously cannot be justified rigorously. The corresponding multivariate pdf is the *Dirichlet* frequency (Narumi, 1923; Johnson, 1987; Johnson and Kotz, 1972; Wilks, 1962), and its mathematical implementation is straightforward.

Description of the spectral characteristics of turbulent flows has also been a challenging issue since the early contribution of Taylor (1938). This is again due to the system non-linearities; and development of closures to account for the influence of convection in the spectral transport equations continues to be an active area of research (Stanisić, 1988; Lesieur, 1990; Orszag, 1977). Naturally, the degree of difficulty is escalated when modeling of the spectral density function of reactive scalars is attempted (Corrsin, 1961). In such modeling, in addition to the influence of convective fluctuations the role of the chemical effects must also be considered. The challenge in developing reliable spectral closures for this purpose has also been long-recognized (O'Brien, 1960; Corrsin, 1981). Recent efforts are devoted on developing closures by which the spectral transport equations are coupled with the single-point pdf evolution equation (O'Brien, 1985; Jiang, 1992; Frankel *et al.*, 1992). In these approaches,

the spectral closures include two-point statistical information, and the pdf provides the closure to account for the influence of chemistry.

The objective of this work is to develop mathematical turbulence closures for modeling of the fluctuations and the frequency spectra of reactive scalars in the context considered in the BSK experiments (and also in Saetran *et al.* (1989)). The goal is to analyze the influence of the scalar fluctuations on the rate of mean reactant conversion and to determine the auto- and the cross-spectral density functions of the reactant fluctuations. In accord with the experiments, a homogeneous mixing layer is considered and the models are appraised by detailed comparisons against these laboratory data. Comparisons are also made with additional data generated here by Direct Numerical Simulation (DNS) of a spatially developing planar mixing layer. The hope is to provide simple working relations for general applications.

2 Flow Configurations

A scalar mixing layer is formed when a traditional "grid-generated turbulent flow" is augmented with a scalar gradient (Libby, 1975; LaRue and Libby, 1981; LaRue *et al.*, 1981; Saetran *et al.*, 1989). This can be facilitated by either a temperature gradient, *i.e.* by heating half of the grids (Libby, 1975), or by introducing two different chemical species (BSK). The schematic of the homogeneous reacting scalar mixing layer is shown in Fig. 1(a). This configuration consists of a unform mean streamwise velocity carrier inert gas contaminate by two reacting scalars, A and B. In the BSK experiments, doping gases are injected and are uniformly mixed in a carrier air stream. For the passive scalar experiments, nitric oxide (NO) is injected into one stream; in the reacting layer experiments, NO and O_3 are introduced in separate feeds into the air. The concentrations of the reactive species are sufficiently small (of order of parts per million), allowing the assumption of constant density and isothermal flow.

In the spatially developing mixing layer, in addition to scalar gradients there is also a cross-stream variation of the mean velocities. The schematic diagram of this configuration is

shown in Fig. 1(b). Two co-flowing streams traveling at different velocities are merged at the trailing edge of a partition plate. The reactants A and B are introduced into the high- and the low-speed streams, respectively. In this flow, in addition to small scale turbulent transport, the formation of large scale coherent vortical structures also plays a significant role on the rate of chemical reactant conversion. Therefore, the spatial inhomogeneity of the flow in the transverse direction makes the statistical analysis more challenging in comparison to that in homogeneous flows.

There is a wealth of recent experimental data available pertaining to transport of reacting chemical species in spatially developing mixing layer, *e.g.* Koochesfahani and Dimotakis (1986); Masutani and Bowman (1986). However, the statistical results reported are not as detailed as those furnished by BSK. Therefore, alternatively, data are produced here by means of direct numerical simulation. DNS has proven very useful in capturing many features of turbulent transport (Givi, 1994) and provides a powerful complement to laboratory measurements for the analyses of turbulent reacting flows. The configuration considered here is similar to that treated by Givi and Jou (1988); McMurtry and Givi (1992), but the statistical analyses are conducted in a format similar to those in the BSK experiment.

3 Formulation, Modeling and the Computational Procedure

3.1 Modeling of the Reactant Conversion

In both flows, all the chemical species are assumed thermodynamically identical and the fluid is assumed to be calorically perfect. The value of the molecular Schmidt number is set to unity and it is assumed that the two reactants are completely segregated at the inflow. With unity normalized mass fractions of the two species at their respective feeds, a mixture fraction denoted by f is defined (Williams, 1985; Bilger, 1980; Bilger, 1989) to have

normalized values of 1 and 0 in the streams containing A and B respectively. Under chemical equilibrium, the statistics of the reacting field are directly related to those of the mixture fraction. Therefore, univariate statistical analyses are sufficient. In non-equilibrium flows, the joint statistics of the reacting variables are required. The coordinates x and y denote, respectively, the streamwise and the cross-stream direction in both configurations (Fig. 1). Due to the single-point nature of the statistical treatment, all the moments up to second order serve as "inputs" for the pdf parameterization. In modeling of the homogeneous flow, the procedure developed by Libby (1975) is followed. Turbulent convective fluxes are modeled by the gradient diffusion closure with a constant turbulent viscosity ν. The "self-similar" behavior of the layer is predicted within the domain of the transformed cross-stream direction, $\eta = Y/\sqrt{\nu^* X}$, where $Y = y/M$, $X = x/M$ (M is the mesh spacing) and $\nu^* = \nu/\tilde{U}M$ (U is the streamwise velocity, and tilde denotes ensemble-averaging). With this framework, the modeled transport equations governing the ensemble mean value of the mixture fraction, $\tilde{f}$, and its variance, $\widetilde{f'^2}$ (prime denotes fluctuations from the mean value) are given, in order, by:

$$\frac{d^2\tilde{f}}{d\eta^2} + \frac{\eta}{2}\frac{d\tilde{f}}{d\eta} = 0, \tag{1}$$

$$C_1\frac{d^2\widetilde{f'^2}}{d\eta^2} + \frac{\eta}{2}\frac{d\widetilde{f'^2}}{d\eta} + 2\left(\frac{d\tilde{f}}{d\eta}\right)^2 - C_2\widetilde{f'^2} = 0, \tag{2}$$

where C_1, C_2 are empirical constants. In the limit of infinitely fast chemistry, the pdf of the mixture fraction is sufficient to determine all the statistical information pertaining to mass fractions of the species. The most convenient of the PF is the Pearson (1895) Type I in the form of the Beta density of the first kind:

$$P_f(\psi) = \frac{1}{B(\alpha,\beta)}\psi^{\alpha-1}(1-\psi)^{\beta-1}. \tag{3}$$

Here, $B(\alpha,\beta)$ is the Beta function: $B(\alpha,\beta) = \Gamma(\alpha)\Gamma(\beta)/\Gamma(\alpha+\beta)$, Γ is the Gamma function,

and the parameters α, β are uniquely determined by $\tilde{f}$ and $\widetilde{f'^2}$ (Abramowitz and Stegun, 1972). With this density, all the moments of the mass fractions of the reactants are expressed in a closed analytical form:

$$\begin{aligned}\widetilde{Y_A^n} &= \frac{1}{B(\alpha,\beta)}\frac{1}{(1-f_s)^n}\int_{f_s}^{1}(f_s-f)^n f^{\alpha-1}(1-f)^{\beta-1}\,df \\ &= \frac{1}{B(\alpha,\beta)}\frac{1}{(1-f_s)^n}\sum_{r=1}^{n}\binom{n}{r}(-f_s)^r\int_{f_s}^{1} f^{(\alpha-1)+(n-r)}(1-f)^{\beta-1}\,df,\end{aligned}$$

$$\widetilde{Y_A^n Y_B^m} = 0, \tag{4}$$

provided that $n, m \neq 0$. Here, Y_i indicates the mass fraction of i-th species, and f_s denotes the stoichiometric value of the mixture fraction. For unity normalized mass fractions at free streams, $f_s = 1/2$. Analytic forms of these integrals are easily attainable and can be expressed in terms of the incomplete Beta density function (Madnia *et al.*, 1992):

$$\mathcal{I}_{f_s}(\alpha,\beta) = \frac{1}{B(\alpha,\beta)}\int_0^{f_s} f^{\alpha-1}(1-f)^{\beta-1}df. \tag{5}$$

In non-equilibrium flows, the transport equations for the first two moments (and/or cross moments) are coupled with the pdf. The transport equation for the ensemble-average of the mass fractions of the reactants, say species A is given by:

$$\frac{d^2\widetilde{Y_A}}{d\eta^2} + \frac{\eta}{2}\frac{d\widetilde{Y_A}}{d\eta} - X\widetilde{\dot{\omega}_A} = 0 \tag{6}$$

where $\dot{\omega}_A$ denotes the reaction rate of species A. The normalized form of this rate is given by $\dot{\omega}_A = DaY_AY_B$; Da is the Damköhler number (BSK). The closure for the evaluation of the mean reaction rate is provided by the pdf. Here, the *Dirichlet* frequency (Johnson, 1987)

is proposed for this purpose:

$$P(\psi_1, \psi_2, \ldots, \psi_n) = \frac{\Gamma(\xi_1 + \xi_2 + \ldots + \xi_{n+1})}{\Gamma(\xi_1)\Gamma(\xi_2)\ldots\Gamma(\xi_{n+1})}(\psi_1)^{\xi_1 - 1}(\psi_2)^{\xi_2 - 1}(1 - \psi_1 - \psi_2 - \ldots - \psi_n)^{\xi_{n+1} - 1} \tag{7}$$

where $\psi_j > 0$, $j = 1, n$; $\sum_{j=1}^{n} \psi_j \leq 1$; and $\xi_k > 0$, $k = 1, n+1$. The $n+1$ parameters (ξ_k's) can be evaluated if the values of an equal number of moments are supplied. Therefore the knowledge of at least one second order moment is necessary, a recognizable feature of single-point closures. It is straightforward to show that the product moments of order $r = \sum_{j=1}^{n} r_j$ with respect to the origin are:

$$\begin{aligned} \mu'_{r_1 r_2 \cdots r_n} &= \int_{S_n} \psi_1^{r_1}\psi_2^{r_2}\cdots\psi_n^{r_n} P(\psi_1, \psi_2, \cdots, \psi_n) d\psi_1 d\psi_2 \cdots d\psi_n \\ &= \frac{\Gamma(\xi_1 + \xi_2 + \cdots + \xi_{n+1})\Gamma(\xi_1 + r_1)\Gamma(\xi_2 + r_2)\cdots\Gamma(\xi_n + r_n)}{\Gamma(\xi_1)\Gamma(\xi_2)\cdots\Gamma(\xi_n)\Gamma(\xi_1 + \xi_2 + \cdots + \xi_{n+1} + r_1 + r_2 + \cdots + r_n)}, \end{aligned} \tag{8}$$

where S_n is the support of $P(\psi)$ in the composition space. With this, the ensemble mean value of the mass fraction of the i-th species is:

$$\widetilde{\psi_i} = \frac{\xi_i}{\sum_{k=1}^{n+1} \xi_k}, \tag{9}$$

and the $r_i + r_j$th order correlation (product moment with respect to the mean values) between species ψ_i and ψ_j is:

$$\mu_{r_i r_j} = \sum_{l=1}^{r_i}\sum_{k=1}^{r_j}(-1)^{l+k}\binom{r_i}{l}\binom{r_j}{k}(\widetilde{\psi_i})^l(\widetilde{\psi_j})^k \frac{\xi_i(\xi_i+1)\cdots(\xi_i + r_i - l - 1)\xi_j(\xi_j+1)\cdots(\xi_j + r_j - k - 1)}{(\sum_{m=1}^{n+1}\xi_m + 1)\cdots(\sum_{m=1}^{n+1}\xi_m + r_i - l + r_j - k - 1)}. \tag{10}$$

Therefore, the variance of species i and the covariance of species i and j are, in order:

$$\widetilde{\psi_i''^2} = \frac{\xi_i(\sum_{k=1}^{n+1}\xi_k - \xi_i)}{(\sum_{k=1}^{n+1}\xi_k)^2(\sum_{k=1}^{n+1}\xi_k + 1)}; \quad \widetilde{\psi_i'\psi_j'} = \frac{\xi_i\xi_j}{(\sum_{k=1}^{n+1}\xi_k)^2(\sum_{k=1}^{n+1}\xi_k + 1)}. \tag{11}$$

A particularly pleasing feature of the Dirichlet density is the condition $\sum_{j=1}^{n}\psi_j \leq 1$. This constraint is in accord with the law of conservation of species. However, the parameterization of the pdf is somewhat "overdetermined" in that it is not clear which combination of the moments is to be used to specify the parameters of the pdf (values of ξ_j). In the reaction scheme considered by BSK, $n = 2$; thus the parameterization requires the knowledge of three moments. The mean values of the two reactants, $\widetilde{Y_A}, \widetilde{Y_B}$ are obvious choices; but the specification of the third moment is not clear. Here, we consider two options: (1) the scalar-energy $Q = \widetilde{Y_A''^2} + \widetilde{Y_B''^2}$, and (2) the covariance (unmixedness) $C = \widetilde{Y_A''Y_B''}$. These schemes are enacted with the relations:

$$\xi_1 = \widetilde{Y_A}\lambda; \ \xi_2 = \widetilde{Y_B}\lambda; \ \xi_3 = (1 - \widetilde{Y_A} - \widetilde{Y_B})\lambda; \ \lambda = \xi_1 + \xi_2 + \xi_3, \tag{12}$$

where:

$$\lambda = \frac{\widetilde{Y_A}(1 - \widetilde{Y_A}) + \widetilde{Y_B}(1 - \widetilde{Y_B})}{\widetilde{Y_A''^2} + \widetilde{Y_B''^2}} - 1 \tag{13}$$

with the first option, and

$$\lambda = -(\frac{\widetilde{Y_A}\widetilde{Y_B}}{\widetilde{Y_A''Y_B''}} + 1) \tag{14}$$

for the second one. This overdetermination is not encountered with the use of the multivariate gaussian pdf, typically used in combustion modeling *e.g.* Bockhorn (1988a); Bockhorn (1988b). However this frequency has serious drawbacks in requiring an infinite support (Leemis, 1986) and not satisfying the law of conservation of species. The transport equations for the second order moments (and cross moments) are of a similar nature. For example, for

the unmixedness:

$$C_1 \frac{d^2 \widetilde{Y_A'' Y_B''}}{d\eta^2} + \frac{\eta}{2} \frac{d\widetilde{Y_A'' Y_B''}}{d\eta} + 2 \frac{d\widetilde{Y_A}}{d\eta} \frac{d\widetilde{Y_B}}{d\eta} - C_2 \widetilde{Y_A'' Y_B''} + X(\widetilde{\dot{\omega}_A Y_B''} + \widetilde{\dot{\omega}_B Y_A''}) = 0. \qquad (15)$$

The only additional modeling requirement is the specification of the empirical constants C_1 and C_2. Here, the constants are determined in such a way as to yield the best agreement with the laboratory data for the first two moments, as will be discussed in Section 4. The resulting system of nonlinear coupled differential equations is solved by means of the Newton-Raphson iterative scheme. The derivatives are approximated via a second order accurate finite-difference scheme utilizing 51 grid points within the domain $-4 \leq \eta \leq 4$. The independency of the results to the selected number of grids and the size of the domain was confirmed.

The procedure followed for model assessment in the spatially developing mixing layer is essentially the same, but the input moments are obtained by DNS. The computational procedure is based on a hybrid finite difference-pseudospectral scheme. A fifth-order compact parameter difference scheme (Carpenter, 1990) is used for discretization in the streamwise direction and a spectral collocation method (Givi and Madnia, 1993) employing Fourier expansions for the cross-stream discretization. Time discretization is achieved by the Adams-Bashforth scheme. The computational domain is bounded by $0 \leq x \leq 64\delta_w, -16\delta_w \leq y \leq 16\delta_w$, where δ_w is the vorticity thickness at the inflow. The resolution consists of 256 finite difference points and 128 collocation nodes. With this resolution, reliable DNS with a Reynolds number $Re = 200$ and Damköhler numbers up to $Da = 10$ (based on the mean streamwise velocity difference and the vorticity thickness at the inlet) is possible. The inflow condition for the streamwise mean velocity profile is given by a hyperbolic tangent function. The free stream velocity ratio is set arbitrarily equal to $\frac{\widetilde{U}_1}{\widetilde{U}_2} = 3$. The flow is forced randomly at the inflow to expedite the formation of large scale structures within the domain considered. The maximum amplitude of the perturbations is set equal to 5% of the mean flow. For a detail description of the numerical procedure we refer to Givi and Jou (1988); McMurtry and Givi (1992).

3.2 Frequency-Spectra of Reacting Scalars

With the assumption of ergodic flow, the temporal correlations of the scalar mass fractions are defined (Bendat and Piersol, 1986).

$$R_{AA}(\tau) = \widetilde{Y_A(t)Y_A(t+\tau)} \tag{16}$$

is the autocorrelation of the mass fraction of species A, and

$$R_{AB}(\tau) = \widetilde{Y_A(t)Y_B(t+\tau)} \tag{17}$$

is the cross correlation of the mass fractions of the two species A and B. Associated with these correlations are the autocovariance function and the cross-variance function, defined respectively as:

$$C_{AA}(\tau) = R_{AA}(\tau) - \widetilde{Y_A}^2, \quad C_{AB}(\tau) = R_{AB}(\tau) - \widetilde{Y_A}\widetilde{Y_B}. \tag{18}$$

The autospectral density function of scalar A is the Fourier transform of its autocorrelation:

$$S_{AA}(\Omega) = \int_{-\infty}^{\infty} R_{AA}(\tau)\exp(-2\pi\Omega\tau\jmath)d\tau, \quad \jmath = \sqrt{-1}, \tag{19}$$

Ω is the frequency. Similarly the cross-spectral density function for scalars A and B is:

$$S_{AB}(\Omega) = \int_{-\infty}^{\infty} R_{AB}(\tau)\exp(-2\pi\Omega\tau\jmath)d\tau. \tag{20}$$

It is customary to express the cross-spectrum as:

$$S_{AB}(\Omega) = |S_{AB}(\Omega)| \exp\left[-\jmath\Theta_{AB}(\Omega)\right] \tag{21}$$

where $\Theta(\Omega)$ is the "phase," and the "coherence function" is defined by:

$$\gamma^2_{AB}(\Omega) = \frac{|S_{AB}(\Omega)|^2}{S_{AA}(\Omega)S_{BB}(\Omega)}. \tag{22}$$

It is desirable to relate the time-correlations and the frequency spectral densities of the reacting scalars to the frequency-spectrum of the mixture fraction. This, in general, is a formidable task as the relation (if it could be obtained) is dependent on the chemistry. Since the primary influence of chemical reaction is at diffusion scales, it is impossible to provide simple mathematical relations amongst the various spectral density functions. In the limit of equilibrium chemistry, the situation simplifies considerably as shown by Kosály (1993). However, an exact determination still requires multi- (in this case, two-) time level stochastic analyses. In the presence of spatial symmetry, it is possible to simplify the relations further. For example, at the center of the scalar mixing layer in the BSK experiments ($\eta = 0, \widetilde{f} = \frac{1}{2}$), all the statistical properties of the two reactants are identical. Based on this symmetry it is easy to show for $Da \to \infty$ (Kosály, 1993):

$$R_{AA}(\tau)|_{\eta=0,Da\to\infty} = R_{BB}(\tau)|_{\eta=0,Da\to\infty} = \frac{1}{4}\left[R_{FF}(\tau) + R_{F^*F^*}(\tau)\right]_{\eta=0}, \tag{23}$$

$$R_{AB}(\tau)|_{\eta=0,Da\to\infty} = R_{BA}(\tau)|_{\eta=0,Da\to\infty} = \frac{1}{4}\left[-R_{FF}(\tau) + R_{F^*F^*}(\tau)\right]_{\eta=0}. \tag{24}$$

where $F = 2f - 1$ and $F^* \equiv |F|$. Similar relations hold for the spectral densities of A and B in terms of those of F and F^*. Therefore, for the spectral densities normalized by their respective variances, it is straightforward to show (from here on, the subscript $\eta = 0, Da \to \infty$ is dropped):

$$\hat{S}_{AA}(\Omega) = \frac{S_{AA}(\Omega)}{\widetilde{Y_A'^2}} = \hat{S}_{BB}(\Omega) = \frac{1}{4\widetilde{Y_A'^2}}\left[\hat{S}_{FF}(\Omega)\widetilde{F'^2} + \hat{S}_{F^*F^*}(\Omega)\widetilde{F^{*\prime 2}}\right] \tag{25}$$

$$\frac{S_{AB}(\Omega)}{S_{AA}(\Omega)} = 1 - \frac{1}{2}\left(\frac{\hat{S}_{FF}(\Omega)\widetilde{F'^2}}{\hat{S}_{AA}(\Omega)\widetilde{Y_A'^2}}\right) \tag{26}$$

To complete the formulation, the statistics of F, $|F|$, A and B are required. Kosály (1993) assumes a gaussian pdf for F from which all the statistics are subsequently determined. This pdf is justified only at regions far away from the inlet. In this particular experiment this assumption is reasonable as the data show an approximate gaussian pdf (not considering the discrepancy associated with the infinite support). In other homogenous flows, however, this approximation can yield significant errors (Frankel *et al.*, 1993) since at the initial stages of mixing the pdf is composed of two approximate delta functions, *i.e.* complete segregation. At such stages, the use of the PF generated pdfs is more reasonable. In particular, the Pearson Type II is justified at all the locations along the center of the layer. With this frequency, Eqs. (3)-(4) with $\alpha = \beta$ yield:

$$\widetilde{F^2} = \widetilde{F'^2} = \widetilde{F^{*2}} = \frac{1}{2\alpha + 1} \equiv \Sigma^2. \tag{27}$$

Therefore:

$$\widetilde{Y_A'^2} = \frac{\Sigma^2}{2} - \left(\frac{G}{2}\right)^2, \quad \widetilde{F^{*\prime 2}} = \Sigma^2 - G^2, \quad G(\Sigma) = \frac{\Gamma(\frac{1}{2\Sigma^2})}{\sqrt{\pi}\Gamma(\frac{1}{2\Sigma^2} + \frac{1}{2})}. \tag{28}$$

Substituting Eqs. (27)-(28) into Eqs. (25)-(26) yields:

$$\hat{S}_{AA}(\Omega) = \hat{S}_{BB}(\Omega) = \frac{\Sigma^2}{2\Sigma^2 - G^2}\hat{S}_{FF}(\Omega) + \frac{\Sigma^2 - G^2}{2\Sigma^2 - G^2}\hat{S}_{F^*F^*}(\Omega), \tag{29}$$

$$\frac{S_{AB}(\Omega)}{S_{AA}(\Omega)} = 1 - \frac{2}{1 + \frac{\Sigma^2 - G^2}{\Sigma^2} \frac{\hat{S}_{F^*F^*}(\Omega)}{\hat{S}_{FF}(\Omega)}}. \tag{30}$$

These equations would be identical to those suggested by Kosály (1993) only when $\Sigma \rightarrow 0$. In this limit, the Beta density approaches a gaussian pdf (Leemis, 1986); therefore:

$$\lim_{\Sigma \rightarrow 0} \left(\frac{\Sigma^2 - G^2}{\Sigma^2} \right) = \frac{\pi - 2}{\pi} \tag{31}$$

which is valid only at final stages of mixing in homogeneous flows. For the other limiting conditions near the inlet of the BSK's mixing layer, or the initial stages of mixing in homogeneous flows (Madnia *et al.*, 1992) we have $\Sigma^2 = G = 1$. Therefore, the physical requirement:

$$\hat{S}_{AA}(\Omega)|_{x=0} = \hat{S}_{FF}(\Omega)|_{x=0}, \quad \frac{S_{AB}(\Omega)}{S_{AA}(\Omega)}|_{x=0} = -1, \tag{32}$$

can be *only* realized via the relations provided by Eqs. (30)-(31). To demonstrate this point more clearly, the variations of the parameters appearing in Eqs. (29)-(30) are shown in Fig. 2 in terms of Σ. In the form presented $\Sigma = 1, 0$ denote the initial and the final stage of mixing, respectively. Note that only the values at $\Sigma \rightarrow 0$ are in accord with Kosàly's results.

All the results presented here are based on the assumption of an asymptotic gaussian pdf for the variable F. However, the results of numerous recent laboratory measurements (Castaing *et al.*, 1989; Sano *et al.*, 1989; Castaing *et al.*, 1990; Jayesh and Warhaft, 1991; Jayesh and Warhaft, 1992; Gollub *et al.*, 1991; Lane *et al.*, 1993) and numerical simulations (Metais and Lesieur, 1992; Kimura and Kraichnan, 1993; Kerstein, 1991; Pumir *et al.*, 1991) suggest that the exponential distribution may provide a more reasonable representation of the pdf in high Reynolds number flows. The family of exponential pdfs is represented by:

$$P_F(\psi, q) = C(K, q) \exp\left(-\frac{|\psi|^q}{K(q,\sigma)}\right), \tag{33}$$

where σ is the standard deviation and $C = [2K^{\frac{1}{q}}\Gamma(\frac{q+1}{q})]^{-1}$. The value $q = 2$ corresponds to a gaussian pdf and $q = 1$ implies a Laplace (double exponential) density. To use this density for the evaluation of the spectral density functions, Eqs. (25)-(26) are represented in the simpler form:

$$\hat{S}_{AA}(\Omega) = \hat{S}_{BB}(\Omega) = \frac{\hat{S}_{FF}(\Omega)}{\mathcal{U}+1} + \frac{\mathcal{U}\hat{S}_{F^\bullet F^\bullet}(\Omega)}{\mathcal{U}+1}, \tag{34}$$

$$\frac{S_{AB}(\Omega)}{S_{AA}(\Omega)} = 1 - \frac{2}{1 + \mathcal{U}\frac{\hat{S}_{F^\bullet F^\bullet}(\Omega)}{\hat{S}_{FF}(\Omega)}}. \tag{35}$$

where $\mathcal{U} = \widetilde{F^{*/2}}/\widetilde{F^{*2}}$. Following the same procedure as outlined above, Eq. (33) yields:

$$\mathcal{U} = 1 - \frac{\Gamma^2(\frac{2}{q})}{q\Gamma(\frac{3}{q})\Gamma(\frac{q+1}{q})}. \tag{36}$$

This implies that the parameter $\mathcal{U}(q)$ is in the approximate range $0.25 \leq \mathcal{U} \leq 1$, depending on the degree of the exponential at the asymptotic stage of mixing. For $q = 2$, the value $\mathcal{U} = 0.36$ is that suggested by Kosály (1993).

Based on the results presented here, we recommend Eqs. (29)-(30) for relating the autospectral and the cross-spectral density functions of the reacting scalars to the spectrum of the mixture fraction in homogeneous flows with symmetric pdf of the mixture fraction. These results are valid if the asymptotic stage of mixing yields gaussian statistics. For the general family of the exponential scalar pdfs, the corresponding relations are given by Eqs. (34)-(36). Again, it is emphasized that these relations (and also those provided by Kosály (1993)) are only valid in the limit of equilibrium chemistry. It is impossible to generalize these results for non-equilibrium chemistry flows. Also, it is very difficult, perhaps impossible, to provide

analogous relations when the pdf is non-symmetric, *i.e.* at off-center regions of the laboratory flow and/or in other homogeneous flows where the local compositional structure is not in stoichiometric proportions.

4 Results

4.1 Modeling of the Reactant Conversion

The results of our parametric study indicates that the best overall match between the model predictions of the mixture fraction and the experimental data of BSK is established with $C_1 = 0.89$ and $C_2 = 5.72$. LaRue *et al.* (1981) suggest $C_1 = 0.89$, $C_2 = 2.25$. The difference in the magnitude of C_2 is attributed to the observation that the peak of the scalar variance in the measurements of LaRue *et al.* (1981) is about 30% higher than that in BSK. In BSK, data are provided of reacting flows with several values of the Damköhler numbers, stoichiometric mixture fractions, and the Reynolds number. In all the cases, the measured results for the mean value of the mixture fraction agree well with model predictions as shown in Fig. 3(a). In this and subsequent figures $\eta^* = \eta/\delta$, where $\delta = \eta(\tilde{f} = 0.9) - \eta(\tilde{f} = 0.1)$. The measured variance of the mixture fraction show a dependence on the Reynolds number. The results in Fig. 3(b) indicate a reasonable agreement between the predicted results and the experimental data for $Re = 5,300$. For $Re = 11,700$, the model fails to capture the "valley" at the center of the layer. This is due to the gradient diffusion closure and also the independency of the model to the Reynolds number. Transverse variations of the skewness and kurtosis of the mixture fraction are shown in Figs. 4 and 5 for $Re = 11,700$. The model results are based on the Beta frequency yielding closed form analytical expressions for higher order moments. While the accordance of the predicted results with experimental data is encouraging, the local minima and maxima portrayed by the data are not well-predicted. Noticeably, the "kink" in the skewness profiles as suggested experimentally is not captured. The results based on this pdf for predicting the statistics of reacting scalars under equilibrium condition are given in Figs. 6 and 7. These results are obtained by closed-form analytical expressions

based on Eqs. (4)-(5). In Fig. 6, the cross-stream variations of the normalized mass fractions of the reactants are in reasonable accord with measured data. A somewhat similar level of agreement is observed in the profiles of the reactants' standard deviations as Fig. 7 shows that both the distribution and the peak of the deviations are predicted well. The maximum deviation is near the center of the layer.

Of greater interest is the statistical behavior of the reactants' mass fractions in the non-equilibrium chemistry flow. On account of the fact that the statistics of mixture fraction should be invariant with the reaction rate, it is required to tailor the model accordingly. Therefore, in this case the magnitudes of the empirical constants C_1 and C_2 are prescribed in such a way as to yield the best match to the first two measured moments of the reactants' mass fractions, of course in accord with the respective parameterization scheme. The statistics of the mixture fraction are evaluated subsequently. This procedure is followed for both of the cases reported in the BSK experiments: $Da = 0.3$ and $Da = 1.81$. The comparison between the predicted standard deviation of the mixture fraction and the measure data is shown in Fig. 8. With the degree of freedom available in the matching, the Dirichlet density parameterized by the scalar-energy yields better overall agreements. However, the results are not Damköhler number invariant. The consequence of this will be discussed later. Figures 9 and 10 show the profiles of skewness and kurtosis of the mixture fraction. Both Dirichlet closures perform well and the results are in a better agreement with data than those based on the univariate Beta density (Figs. 4-5). It is appropriate here to note that the multivariate gaussian pdf yields uniform values of higher order moments (skewness = 0, and kurtosis = 3); thus despite possessing more statistical information, *i.e.* a higher-degree of freedom for parameterization, this pdf is less superior to the Dirichlet density. The final performance test of the models is their capability of predicting the statistics of the reacting scalars under non-equilibrium conditions. In Figs. 11 and 12 results are presented of the mean product mass fraction and the scalar-energy, respectively. For consistency, the empirical constants are optimized for each model such that the predicted statistics of the mixture fraction are in accord with the experimental data. These figures also confirm the relative better performance of the scalar-energy parameterized Dirichlet.

A more elaborate validation of the models requires examination of the higher-order joint moments. Since these moments are not measured in the experiments, they are provided here by DNS of the spatially developing mixing layer. The structure of this layer as depicted by DNS is shown in Fig. 13, where a plot of the instantaneous mixture fraction contours is presented. Statistical analyses of the data are conducted at regions far away from the inflow so that the influence of random perturbations are sufficiently sensed. For statistical sampling, 4,000 realizations are used. The sufficiency of this number of realizations was confirmed by detailed comparisons against results obtained at higher sampling rates. The conclusions drawn from the trends discussed below are independent of the streamwise location considered. Thus results are presented here only for $x = 47.5\delta_w$ denoted by station I in Fig. 13.

A detailed assessment of both Dirichlet closures indicates the superiority of the one parameterized with the scalar-energy. For example, Figs. 14 and 15 show the cross-stream variation of the moment $\widetilde{Y_A''^4 Y_B''^2}$ for two values of the Damköhler number. These results support the use of the scalar-energy for pdf parameterization. Also, the figures suggest that the agreement improves somewhat as the Damköhler number is increased. However, the use of neither of these models can be recommended when the chemistry is in complete equilibrium. In the limit of infinitely large Damköhler number all the joint moments of the scalar are identically zero. The use of the covariance $\widetilde{Y_A'' Y_B''} = -\widetilde{Y}_A \widetilde{Y}_B$ yields $\xi_1 = \xi_2 = \xi_3 = 0$; thus the model fails. The use of the scalar-energy avoids this failure but is incapable of satisfying the orthogonality condition (Eq. 4). In non-equilibrium flows, as the rate of reaction is increased but with finite Damköhler numbers, the covariance-quantified distribution quickly approaches the singularity. This is demonstrated by a comparison of Figs. 14 and 15 where the results indicate a mild improvement in the scalar-energy parameterized model, but little or no change in the model based on the covariance.

Despite the caveat on the use of Dirichlet density for flows under equilibrium chemistry, it is useful to examine its behavior in modeling of higher order moments. Figures 16-17 show the profiles of the joint central moments $\widetilde{Y_A''^2 Y_B''^2}$, and $\widetilde{Y_A''^3 Y_B''}$. The results indicate that the Dirichlet multivariate density parameterized by the scalar-energy and the univariate Beta frequency yield a similar level of agreement with the DNS data. No distinct superiority is

established via the use of either of the closures. However, due to univariate nature of the Beta pdf, the orthogonality condition is identically satisfied.

Finally, it is useful to compare the predicted statistics of the mixture fraction with the DNS data in non-equilibrium flows. This comparison is made in Figs. 18 and 19 for the skewness for both Damköhler numbers. The results are also compared with the predictions based on the univariate Beta pdf as parameterized by the DNS data. These figures indicate that both closures behave somewhat similarly without a dominant superiority of any of the two. This trend is observed for all the other moments of the mixture fraction (not shown here). However, the Dirichlet density does not yield an exact Beta frequency for the mixture fraction. It is straightforward to demonstrate that with the assumption of a Dirichlet density for the reacting scalars, the univariate pdf of the mixture fraction is a Beta density if the chemistry is frozen. That is, along the line $\psi_1 + \psi_2 = 1$ for $n = 2$ in Eq. (7). The Dirichlet density yields a marginal Beta pdf for each of the scalars; thus a Beta distribution cannot be obtained for the mixture fraction. Therefore, in the limit of infinitely large Damköhler number, the use of the univariate Beta density is more appropriate. An optimum value of a finite Damköhler number below which the Dirichlet density is to be recommended, cannot be specified. Due to computational limitations, it is not possible to perform DNS of very large (but finite) Damköhler numbers. For the highest reaction rate considered in the BSK experiments, the Dirichlet density performs reasonably well.

4.2 Frequency-Spectra of Reacting Scalars

Many important spectral features of the reacting scalars can be exhibited by results extracted from the DNS of the spatially developing mixing layer. Here these results are presented of the layer under the conditions of frozen, equilibrium and non-equilibrium chemistry. The normalized autospectrum of scalar A is shown in Fig. 20 for several values of the Damköhler number at streamwise locations of $x = 4\delta_\omega$ and $x = 16\delta_\omega$ (stations II and III in Fig. 13) along the centerline ($y = 0$). This figure indicates that at low frequencies, the influence of chemical reaction is not significant as the spectrum is influenced primarily by hydrodynamics.

At $\Omega = 0$ the amplitude must decrease as the Damköhler number is increased in order to accommodate for the decrease of the integral time-scale due to chemistry. An opposite trend is observed at the other end of the spectrum. At high frequencies, the autospectral density becomes more energetic as the magnitude of the Damköhler number is increased, and at the equilibrium limit the spectrum range extends to very high frequencies. This behavior is not observed in the results of BSK and Kosály (1993) since a small frequency range, limited at the smallest scales to the hydrodynamics frequency is considered. In all the cases, the autospectrum exhibits local peaks at $\Omega = 1.086$Hz (for $x = 4\delta_\omega$) and at $\Omega = 0.543$Hz (for $x = 16\delta_\omega$). These values correspond approximately to the most unstable frequency of the mean flow and its first subharmonic (Michalke, 1965). Note that $x = 4\delta_\omega$ corresponds to the approximate location where the first vortical roll-up occurs, and at $x = 16\delta_\omega$ the pairing of neighboring vortical structures is observed. After this point, the additional vortex pairings which occur downstream yield the shift of the spectra peaks towards higher frequencies. Since the area under the normalized autospectrum must be identical in all the cases (Bendat and Piersol, 1986), the increase of energies at high frequencies must be compensated by an energy decrease at low frequencies. This causes the curves of the spectral density functions to cross over each other at some intermediate values of the frequency. This behavior is observed in Fig. 20 and also in the results of BSK and Kosály (1993).

In Fig. 21 results are presented of the normalized autospectral density function of F, F^*, and the reactant A under equilibrium condition. Although $\hat{S}_{AA}$ and $\hat{S}_{F^\bullet F^\bullet}$ can be determined from the F-time series data, they cannot be calculated from $\hat{S}_{FF}$ directly unless the exact two-time pdf of the F-process is known. Note that unlike the conditions at the center of the symmetric configuration in the BSK experiments, here $\hat{S}_{FF^\bullet} \neq 0$. Thus, Eq. (29) or Eq. (34) cannot be used. However, the DNS results do indicate that the amplitude of $\hat{S}_{AA}$ falls between $\hat{S}_{FF}$ and $\hat{S}_{F^\bullet F^\bullet}$ at high frequencies. At low frequencies, due to the influence of hydrodynamics in causing asymmetric effects, the use of our analytical relations is not appropriate. These figures also show that the local peaks in the F- and A-autospectra are not observed in the F^*-autospectrum. This is expected since the spectrum of the absolute value of a process forced at a single particular frequency (like the process corresponding to

the transport of a single-eddy), contains energy at all the harmonics of that frequency. Since the absolute value of a process represents a non-linear system, the analytical determination of its spectrum is difficult. However, it is reasonable to expect that the autospectrum of F^* decays slower than that of F at high frequencies and the results in Fig. 21 do show this behavior.

The cross-spectral density function is characterized by the coherence function and the phase. High coherence between two random processes usually indicates that the two processes are either exactly in phase or out of phase ($\Theta = 0,$ or π). Low coherence implies indeterminate phase values (Bendat and Piersol, 1986). In Figs. 22 and 23 results are presented of the coherence and the phase in the cross-spectral density functions of scalars A and B for different magnitudes of the Damköhler number. In the frozen chemistry limit, the coherence is unity and phase is equal to π at all frequencies. This is expected as the reactants are completely out of phase. At low frequencies the coherence is high and the non-equilibrium chemistry results are bounded by those corresponding to the frozen and equilibrium limits. In this range, the magnitudes of the phase for all cases are near π. At frequencies which correspond to the local peaks of the autospectra (Fig. 20), there are also high local coherence peaks. At the intermediate frequencies where the autospectra curves cross, the coherence drop and also cross over each other. The magnitude of the phase in this frequency range is random and as speculated by BSK this behavior is associated with the reactive-diffusive balance in the spectral transfer due the large-scale eddies and chemical reaction. After dropping to near zero at intermediate frequencies, the coherence rise at higher frequencies with a reverse effect of the Damköhler number. That is, the coherence increases as the Damköhler number increases. In this range, the phase is near zero ($\Theta = 0, 2\pi$) for all reacting cases. This behavior is in fact predicted by Eq. (35) in that as $\hat{S}_{FF} \rightarrow 0, \hat{S}_{F^*F^*} \neq 0$ ($\hat{S}_{F^*F^*} >> \hat{S}_{FF}$), then $S_{AB} = S_{AA}$. Kosály (1993) also recognizes the possibility of increasing coherence with a zero phase at high frequency. However, due to lack of experimental data this behavior could not be observed. The DNS results here capture this trend.

5 Concluding Remarks

The experiments of Bilger *et al.* (1991) provide an extensive data set for assessing the role of turbulence fluctuations on the rate of reactant conversion and on the spectra of reactive scalars in turbulent shear flows. The objective here is to provide mathematical models to reproduce these data with the hope of suggesting simple working relations for predictive applications. Based on comparative assessment against these measured data and additional data generated here by direct numerical simulation, we recommend the Pearson family of probability density functions for statistical description of scalar transport in flows of this type. In particular, the Dirichlet frequency parameterized by the scalar-energy is recommended, in the absence of better alternatives, for modeling of the reactant conversion rate in non-premixed reacting mixing layers under non-equilibrium conditions. In the limit of frozen chemistry this density yields a Beta frequency for the marginal pdf of each of the reactants. This univariate frequency is recommended for stochastic treatment of both frozen and equilibrium flows.

In the context considered, the models do not yield a consistent limiting condition for equilibrium flows. In this limit, the Dirichlet density does not satisfy the orthogonality condition of the reactants and also does not yield a Beta density for the mixture fraction. This is due to inability of the distribution to include all the first and second order moments in its parameterization. This problem is well-recognized in statistics and (classical) biometric literature (Johnson, 1949a). In principle, it is possible to construct a modified multivariate Pearson density which overcomes this predicament (Johnson, 1987). However, the parameters of the model cannot be algebraically related to input moments (that is, the pdf cannot be analytically integrated); thus the model cannot be recommended for practical applications. The other known multivariate frequencies such as the joint gaussian (and distributions generated by the JET and other schemes), do not share this problem but they do not possess appropriate physical properties to justify their use for combustion applications.

The other alternative for pdf description is to utilize a transport equation governing its evolution (Pope, 1985). However, despite concentrated recent efforts it is not yet clear what

physical closure and/or computational schemes are to be used in the implementation of this scheme. Currently, the most promising methodology for this purpose is the Amplitude Mapping Closure (Chen *et al.*, 1989; Kraichnan, 1989), but it is not yet at a level suitable for modeling of multi-scalar transport in non-homogeneous flows (Pope, 1991). The results of extensive recent work (Miller *et al.*, 1993; Frankel *et al.*, 1993; Madnia *et al.*, 1992) indicate that at situations where the AMC can be enacted, other schemes based on the PF and the JET perform equally well. Amongst all available schemes, the PF is the simplest to use and until the shortcomings associated with the use of the pdf transport equation are resolved, the PF (or other parameterized pdfs prescribed based on known physics) will likely remain as the method of choice for practical applications.

With the use of the PF family of pdfs, the spectral density functions of the reacting scalars are related to the frequency-spectrum of the mixture fraction. These results are more general than those provided previously in that the evolution of the mixture fraction pdf from an initial double-delta profile to an asymptotic gaussian distribution is taken into account. In the asymptotic limit of mixing completion, the results are in accord with those suggested by Kosály (1993). The corrections to the frequency spectra for asymptotic exponential pdfs are also provided. These mathematical relations are valid for applications in homogeneous mixing layers such as the configuration considered by BSK. However, the trends portrayed by these relations are also in accord with those provided by DNS of the spatially developing reacting mixing layer.

At this point it is instructive to reiterate the limitations of the model in the format utilized in this work. The primary drawbacks are associated with: (1) modeling of turbulent fluxes, (2) the single-point nature of the statistical description (3) the restrictive applicability of the equations governing the spectral densities, and (4) the non-generality of the frequencies. The first three problems are also encountered in approaches based on a pdf transport; the last problem is particular to the model here. The first problem manifests itself in the limitations of the gradient diffusion closure and is present in any pdf approach in which the statistics of the velocity field are not included (Givi and McMurtry, 1988). It is now well-recognized that this closure is not capable of capturing the spatial transport of the scalar

pdf in non-homogeneous turbulence, particularly when the flow is dominated by organized coherent structures (Koochesfahani and Dimotakis, 1986). To remedy this problem, one can potentially use higher order models such as spectral closures (Frankel *et al.*, 1992); but the implementation of these models in non-homogeneous flows is extremely difficult, if not impossible. The second problem infers that the errors associated with modeling of the first two moments of the scalar result in the contamination of the pdf and thus all the higher order moments. To rectify the situation, one can use multi-point statistical closures; but again their use is not practical at this point (Pope, 1990). The third limitation is understandable as the spectral manipulation of nonlinear systems is a challenging task, which sometimes is not even recommended (Bendat, 1990). Here with the assumption of equilibrium chemistry and with the spatial symmetry of the problem, it is possible to relate the spectra of the reactants to the frequency spectrum of the mixture fraction. For problems without such a symmetry, the final results can be only obtained by the numerical integration of the equations relating the correlation functions. In non-equilibrium flows it is impossible to provide analogous relations due to closure problems encountered in determining the correlation functions (Corrsin, 1958; Lee, 1966; Corrsin, 1981). Even in the form presented, the final equations require the knowledge of the spectral densities of the absolute value of the mixture fraction. Without pertinent available data (from laboratory experiments or DNS), the evaluation of these densities require the knowledge of "two-time process" of the signal. Note that for the simple case of an ergodic gaussian stochastic process, an analytical evolution of these spectral densities is infeasible as realized in the literature on nonlinear system identifications (Bendat and Piersol, 1986; Bendat, 1990). Finally, the drawbacks associated with the non-generality of the present model, or other approaches based on parameterized pdfs, are well-recognized. In applying the PF generated pdf for modeling of other types of turbulent combustion systems (*e.g* premixed flames, temperature dependent reaction rates, *etc.*) one must have some knowledge of the systems before utilizing *a priori* schemes.

References

Abramowitz, M. and Stegun, I. A. (1972). *Handbook of Mathematical Functions and Formulas, Graphs, and Mathematical Tables.* Government Printing Office, Washington, D.C.

Bendat, J. S. (1990). *Nonlinear System Analysis & Identification from Random Data.* John Wiley and Sons, New York, NY.

Bendat, J. S. and Piersol, A. G. (1986). *Random Data.* John Wiley and Sons, New York, NY, 2nd edition.

Bilger, R. W. (1980). Turbulent flows with nonpremixed reactants. In Libby, P. A. and Williams, F. A., editors, *Turbulent Reacting Flows*, chapter 3, pages 65–113. Springer-Verlag, Heidelberg.

Bilger, R. W. (1989). Turbulent diffusion flames. *Ann. Rev. Fluid Mech.* **21**, 101–135.

Bilger, R. W., Saetran, L. R., and Krishnamoorthy, L. V. (1991). Reaction in a scalar mixing layer. *J. Fluid Mech.* **233**, 211–242.

Bockhorn, H. (1988a). Finite chemical reaction rate and local equilibrium effects in turbulent hydrogen-air diffusion flames. In *Proceedings of the 22nd Symp. (Int.) on Combustion*, pages 665–664. The Combustion Institute, Pittsburgh, PA.

Bockhorn, H. (1988b). Modeling of turbulent diffusion flames with detailed chemistry. In Brauner, C. M. and Schmidt-Laine, C., editors, *Mathematical Modeling in Combustion and Related Topics*, pages 411–420. Martinus Nijhoff Publishers, Dordrecht.

Carpenter, M. H. (1990). A high-order compact numerical algorithm for supersonic flows. In Morton, K. W., editor, *Twelfth International Conference on Numerical Methods in Fluid Dynamics*, volume 371 of *Lecture Notes in Physics*, pages 254–258. Springer-Verlag, New York, NY.

Castaing, B., Gunaratne, G., Heslot, F., Kadanoff, L., Libchaber, S., Thomae, S., Wu, X. Z., Zaleski, S., and Zanetti, G. (1989). Scaling of hard thermal turbulence in Rayleigh-Bernard convection. *J. Fluid Mech.* **204**, 1–30.

Castaing, B., Gagne, Y., and Hopfinger, E. J. (1990). Velocity probability density functions of high Reynolds number turbulence. *Physica D* **46**, 177–200.

Chen, H., Chen, S., and Kraichnan, R. H. (1989). Probability distribution of a stochastically advected scalar field. *Phys. Rev. Lett.* **63**, 2657–2660.

Corrsin, S. (1958). Statistical behavior of a reacting mixture in isotropic turbulence. *Phys. Fluids* **1**, 42–47.

Corrsin, S. (1961). The reactant concentration spectrum in turbulent mixing with a first-order reaction. *J. Fluid Mech.* **11**, 407–416.

Corrsin, S. (1981). Some statistical properties of the product of a turbulent, first-order reaction. In Diaz, J. B. and Pai, S. I., editors, *Fluid Dynamics and Applied Mathematics, Proceedings of the Symposium Sponsored by the Institute of Fluid Dynamics and Applied Mathematics*, pages 105–124.

Curl, R. L. (1963). Dispersed phase mixing: I. Theory and effects in simple reactors. *AIChE J.* **9**, 175–181.

Dopazo, C. and O'Brien, E. E. (1976). Statistical treatment of non-isothermal chemical reactions in turbulence. *Combust. Sci. and Tech.* **13**, 99–112.

Edgeworth, F. Y. (1907). On the representation of statistical frequency by a series. *Journal of the Royal Statistical Society, Series A.* **70**, 102–106.

Frankel, S. H., Jiang, T.-L., and Givi, P. (1992). Modeling of isotropic reacting turbulence by a hybrid Mapping-EDQNM closure. *AIChE J.* **38**, 535–543.

Frankel, S. H., Madnia, C. K., and Givi, P. (1993). Comparative assessment of closures for turbulent reacting flows. *AIChE J.* **39**, 899–903.

Gao, F. (1991). An analytical solution for the scalar probability density function in homogeneous turbulence. *Phys. Fluids A* **3**, 511–513.

Givi, P. (1989). Model free simulations of turbulent reactive flows. *Prog. Energy Combust. Sci.* **15**, 1–107.

Givi, P. (1994). Spectral and random vortex methods in turbulent reacting flows. In Libby and Williams (1994), chapter 8. in press.

Givi, P. and Jou, W.-H. (1988). Direct numerical simulations of a two-dimensional reacting, spatially developing mixing layer by a spectral element method. In *Proceedings of 22nd Symp. (Int.) on Combustion*, pages 635–643. The Combustion Institute, Pittsburgh, PA.

Givi, P. and Madnia, C. K. (1993). Spectral methods in combustion. In Chung, T. J., editor, *Numerical Modeling in Combustion*, chapter 8, pages 409–452. Taylor & Francis, Washington, D.C.

Givi, P. and McMurtry, P. A. (1988). Direct numerical simulation of the PDFs of a passive scalar in a forced mixing layer. *Combust. Sci. and Tech.* **57**, 141–147.

Gollub, J. P., Clarke, J., Gharib, M., Lane, B., and Mesquita, O. N. (1991). Fluctuations and transport in a stirred fluid with a mean gradient. *Phys. Rev. Lett.* **67**, 3507–3510.

Janicka, J. and Peters, N. (1982). Prediction of turbulent jet diffusion flame lift-off using a PDF transport equation. In *Proceedings of 19th Symp. (Int.) on Combustion*, pages 367–374. The Combustion Institute, Pittsburgh, PA.

Janicka, J., Kolbe, W., and Kollmann, W. (1979). Closure of the transport equation for the probability density function of turbulent scalar field. *J. Nonequil. Thermodyn.* **4**, 47–66.

Jayesh and Warhaft, Z. (1991). Probability distribution of a passive scalar in grid-generated turbulence. *Phys. Rev. Lett.* **67**, 3503–3506.

Jayesh and Warhaft, Z. (1992). Probability distribution, conditional dissipation, and transport of passive temperature fluctuations in grid-generated turbulence. *Phys. Fluids A* **4**, 2292–2307.

Jiang, T.-L., Gao, F., and Givi, P. (1992). Binary and trinary scalar mixing by Fickian diffusion-Some mapping closure results. *Phys. Fluids A* **4**, 1028–1035.

Jiang, T.-L. (1992), *Turbulent Mixing in Non-Reacting and Reacting Flows: A PDF Approach at the Two-Point Level.* Ph.D. Thesis, Department of Mechanical Engineering, State University of New York at Stony Brook, Stony Brook, NY.

Johnson, N. L. and Kotz, S. (1972). *Distributions in Statistics: Continious Multivariate Distributions.* John Wiley and Sons, New York, NY.

Johnson, N. L. (1949a). Bivariate distributions based on simple translation systems. *Biometrika* **36**, 297–304.

Johnson, N. L. (1949b). Systems of frequency curves generated by methods of translation. *Biometrika* **36**, 149–176.

Johnson, M. E. (1987). *Multivariate Statistical Simulation.* John Wiley and Sons, New York, NY.

Jones, W. P. and Priddin, C. H. (1978). Predictions of the flowfield and local gas composition in gas turbine combustors. In *17th Symp. (Int.) on Combustion*, pages 399–409. The Combustion Institute, Pittsburgh, PA.

Kerstein, A. R. (1991). Linear-eddy modeling of turbulent transport. Part 6. Microstructure of diffusive scalar mixing fields. *J. Fluid Mech.* **231**, 361–394.

Kimura, Y. and Kraichnan, R. H. (1993). Statistics of an advected passive scalar. *Phys. Fluids A.* **5**, 2264–2277.

Kollmann, W. (1990). The pdf approach to turbulent flow. *Theoret. Comput. Fluid Dynamics* **1**, 249–285.

Komori, S. K., Hunt, J. C., Kanzaki, T., and Murakami, Y. (1991). The effects of turbulent mixing on the correlation between two species and on concentration fluctuations in non-premixed reacting flows. *J. Fluid Mech.* **228**, 629–659.

Koochesfahani, M. M. and Dimotakis, P. E. (1986). Mixing and chemical reactions in a turbulent liquid mixing layer. *J. Fluid. Mech.* **170**, 83–112.

Kosály, G. and Givi, P. (1987). Modeling of turbulent molecular mixing. *Combust. Flame* **70**, 101–118.

Kosály, G. (1993). Frequency spectra of reactant fluctuations in turbulent flows. *J. Fluid. Mech.* **246**, 489–502.

Kraichnan, R. H. (1989). Closures for probability distributions. *Bull. Amer. Phys. Soc.* **34**, 2298.

Lane, B. R., Mesquita, O. N., Meyers, S. R., and Gollub, J. P. (1993). Probability distributions and thermal transport in a turbulent grid flow. *Phys. Fluids A* **5**, 2255–2263.

LaRue, J. C. and Libby, P. A. (1981). Thermal mixing layer downstream of half-heated turbulence grid. *Phys. Fluids* **24**, 597–604.

LaRue, J. C., Libby, P. A., and Seshardi, D. V. R. (1981). Further results on the thermal mixing layer downstream of half-heated turbulence grid. *Phys. Fluids* **24**, 1927–1933.

Lee, J. (1966). Isotropic turbulent mixing under a second order chemical reaction. *Phys. Fluids* **9**, 1753–1763.

Leemis, L. M. (1986). Relations among common univariate distributions. *American Statistician* **40**, 143–146.

Lesieur, M. (1990). *Turbulence in Fluids.* Kluwer Academic Publishers, Boston, MA. Second Revised Edition.

Libby, P. A. and Williams, F. A., editors. (1980). *Turbulent Reacting Flows*, volume 44 of *Topics in Applied Physics.* Springer-Verlag, Heidelberg.

Libby, P. A. and Williams, F. A., editors. (1994). *Turbulent Reacting Flows.* Academic Press, London, UK. in press.

Libby, P. A. (1975). Diffusion of heat downstream of a turbulence grid. *Acta Astronautica* **2**, 867–878.

Lockwood, F. C. and Moneib, H. A. (1980). Fluctuating temperature measurement in a heated round free jet. *Combust. Sci. and Tech.* **22**, 63–81.

Lundgren, T. S. (1967). Distribution functions in the statistical theory of turbulence. *Phys. Fluids* **10**, 969–975.

Lundgren, T. S. (1969). Model equation for nonhomogeneous turbulence. *Phys. Fluids* **12**, 485–497.

Madnia, C. K., Frankel, S. H., and Givi, P. (1992). Reactant conversion in homogeneous turbulence: Mathematical modeling, computational validations and practical applications. *Theoret. Comput. Fluid Dynamics* **4**, 79–93.

Masutani, S. M. and Bowman, C. T. (1986). The structure of a chemically reacting plane mixing layer. *J. Fluid Mech.* **72**, 93–126.

McMurtry, P. A. and Givi, P. (1992). Direct numerical simulations of a reacting, turbulent mixing layer by a pseudospectral-spectral element method. In Chung, T. J., editor, *Finite Elements in Fluids*, chapter 14, pages 361–384. Hemisphere Publishing Corporation, Washington, D.C.

Metais, O. and Lesieur, M. (1992). Spectral large-eddy simulation of isotropic and stably stratified turbulence. *J. Fluid Mech.* **239**, 157–194.

Michalke, A. (1965). On spatially growing disturbances in an inviscid shear layer. *J. Fluid Mech.* **23**, 521–544.

Miller, R. S., Frankel, S. H., Madnia, C. K., and Givi, P. (1993). Johnson-Edgeworth translation for probability modeling of binary mixing in turbulent flows. *Combust. Sci. and Tech.* **91**, 21–52.

Narumi, S. (1923). On the general form of bivariate frequency distributions which are mathematically possible when regression and variation are subjected to limiting conditions, I. *Biometrika* **15**, 77–88.

Norris, A. T. and Pope, S. B. (1991). Turbulent mixing model based on ordered pairing. *Combust. Flame* **83**, 27–42.

O'Brien, E. E. (1960), *On the Statistical Behavior of a Dilute Reactant in Isotropic Turbulence.* Ph.D. Thesis, The Johns Hopkins University, Baltimore, MD.

O'Brien, E. E. (1980). The probability density function (PDF) approach to reacting turbulent flows. In Libby, P. A. and Williams, F. A., editors, *Turbulent Reacting Flows*, chapter 5, pages 185–218. Springer-Verlag, Heidelberg.

O'Brien, E. E. (1985). The spectra of single reactants in homogeneous turbulence. In Davis, S. W. and Lumley, J. L., editors, *Frontiers in Fluid Mechanics*, pages 113–122. Springer-Verlag, New York, NY.

Orszag, S. A. (1977). Lectures on the statistical theory of turbulence. In Balian, R. and Peube, J. L., editors, *Fluid Dynamics*, pages 237–374. Gordon and Breach Science Publishers, New York, NY.

Pearson, K. (1895). Contributions to the mathematical theory of evolution: II. skew variations in homogeneous material. *Philos. Trans. of the Royal Soc. of London, Series A.* **186**, 343–414.

Peters, N. (1984). Laminar diffusion flamelet models in non-premixed turbulent combustion. *Prog. Energy Combust. Sci.* **10**, 319–339.

Pope, S. B. (1981). A Monte Carlo method for the PDF equations of turbulent reactive flow. *Combust. Sci. and Tech.* **25**, 159–174.

Pope, S. B. (1982). An improved turbulent mixing model. *Combust. Sci. and Tech.* **28**, 131–145.

Pope, S. B. (1985). PDF methods for turbulent reacting flows. *Prog. Energy Combust. Sci.* **11**, 119–192.

Pope, S. B. (1990). Computations of turbulent combustion: Progress and challenges. In *Proceedings of 23rd Symp. (Int.) on Combustion*, pages 591–612. The Combustion Institute, Pittsburgh, PA.

Pope, S. B. (1991). Mapping closures for turbulent mixing and reaction. *Theoret. Comput. Fluid Dynamics* **2**, 255–270. Presented at the NASA Langley Research Center on the occasion of the sixtieth birthday of John Lumley.

Pope, S. B. (1994). Lagrangian pdf methods for turbulent flows. *Ann. Rev. Fluid Mech.* **26**, 23–63.

Priddin, C. H. (1991). Turbulent combustion modeling-A review. In Johansson, A. V. and Alfredsson, P. H., editors, *Advances in Turbulence 3*, pages 279–299. Springer-Verlag, Berlin.

Pumir, A., Shraiman, B., and Siggia, E. D. (1991). Exponential tails and random advection. *Phys. Rev. Lett.* **3**, 2838–2840.

Rhodes, P. R. (1975). A probability distribution function for turbulent flows. In Murthy, S. N. B., editor, *Turbulent Mixing in Non-Reactive and Reactive Mixing*, pages 235–241. Plenum Press, New York, NY.

Saetran, L. R., Honnery, D. R., Straner, S. H., and Bilger, R. W. (1989). Scalar mixing layer in grid turbulence with transport of passive and reactive species. In *Turbulent Shear Flows 6*, pages 109–118. Springer-Verlag, New York, NY.

Sano, M., Wu, X. Z., and Libchaber, A. (1989). Turbulence in helium gas free convection. *Phys. Rev. A* **40**, 6421–6430.

Stanisić, M. M. (1988). *The Mathematical Theory of Turbulence.* Springer-Verlag, New York, NY.

Taylor, G. I. (1938). The spectrum of turbulence. *Proc. Royal Soc. London* **164**, 476–490.

Toor, H. L. (1962). Mass transfer in dilute turbulent and nonturbulent systems with rapid irreversible reactions and equal diffusivities. *AIChE J.* **8**, 70–78.

Wilks, S. S. (1962). *Mathematical Statistics.* Wiley, New York, NY, 2nd edition.

Williams, F. A. (1985). *Combustion Theory.* The Benjamin/Cummings Publishing Company, Menlo Park, CA, 2nd edition.

Figure captions

Figure 1. Schematic diagrams of (a) the homogenous scalar mixing layer, and (b) the spatially developing mixing layer.

Figure 2. Variation of the parameters of Eqs. (29)-(30). The points identified by • correspond to the results of Kosály (1993).

Figure 3(a). Cross-stream variation of the mean value of the mixture. Frozen chemistry.

Figure 3(b). Cross-stream variation of the standard deviation of the mixture fraction. Frozen chemistry.

Figure 4. Cross-stream variation of the skewness of the mixture fraction. Frozen chemistry.

Figure 5. Cross-stream variation of the kurtosis of the mixture fraction. Frozen chemistry.

Figure 6. Cross-stream variation of the mean values of the reactants' mass fractions under equilibrium chemistry.

Figure 7. Cross-stream variation of the standard deviations of the reactants' mass fractions under equilibrium chemistry.

Figure 8. Cross-stream variation of the standard deviation of the mixture fraction.

Figure 9. Cross-stream variation of the skewness of the mixture fraction.

Figure 10. Cross-stream variation of the kurtosis of the mixture fraction.

Figure 11. Cross-stream variation of the mean product mass fraction.

Figure 12. Cross-stream variation of the scalar-energy.

Figure 13. Plot of the mixture fraction contours.

Figure 14. Cross-stream variation of the moment $\widetilde{Y_A'^4 Y_B'^2}$ for $Da = 0.3$.

Figure 15. Cross-stream variation of the moment $\widetilde{Y_A'^4 Y_B'^2}$ for $Da = 10$.

Figure 16. Cross-stream variation of the moment $\widetilde{Y_A'^2 Y_B'^2}$. Equilibrium chemistry.

Figure 17. Cross-stream variation of the moment $\widetilde{Y_A'^3 Y_B'}$. Equilibrium chemistry.

Figure 18. Cross-stream variation of the skewness of the mixture fraction ($Da = 0.3$).

Figure 19. Cross-stream variation of the skewness of the mixture fraction ($Da = 10$).

Figure 20. Autospectrum density function of the mass fraction of species A at (a) $x =$

$4\delta_\omega, y = 0$, (b) $x = 16\delta_\omega, y = 0$.

Figure 21. Autospectra of F, F^* and A ($Da \to \infty$) at (a) $x = 4\delta_\omega, y = 0$, (b) $x = 16\delta_\omega, y = 0$.

Figure 22. Coherence between reactants A and B at (a) $x = 4\delta_\omega, y = 0$, (b) $x = 16\delta_\omega, y = 0$.

Figure 23. Phase between reactants A and B at (a) $x = 4\delta_\omega, y = 0$, (b) $x = 16\delta_\omega, y = 0$.

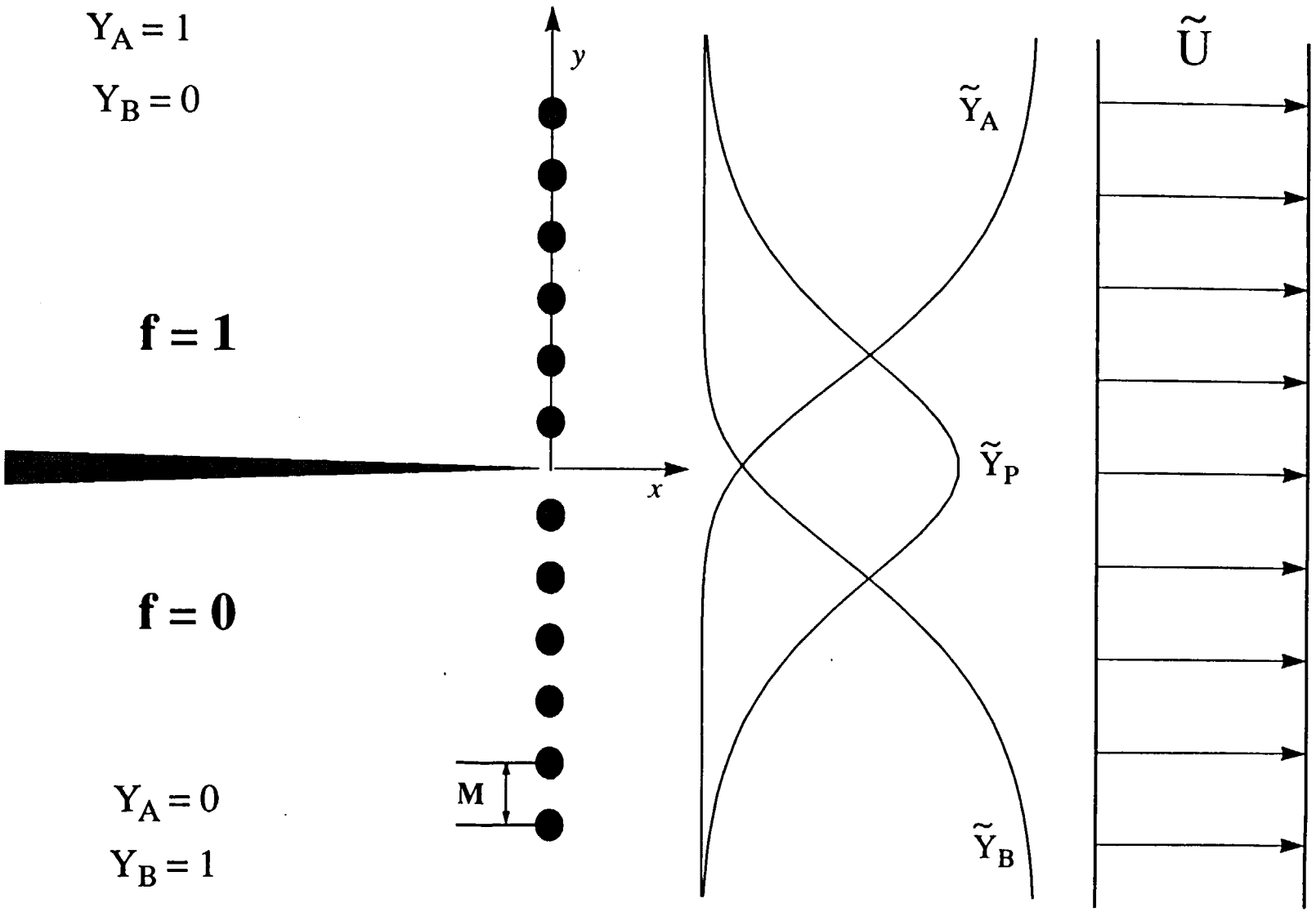

Figure 1(a)

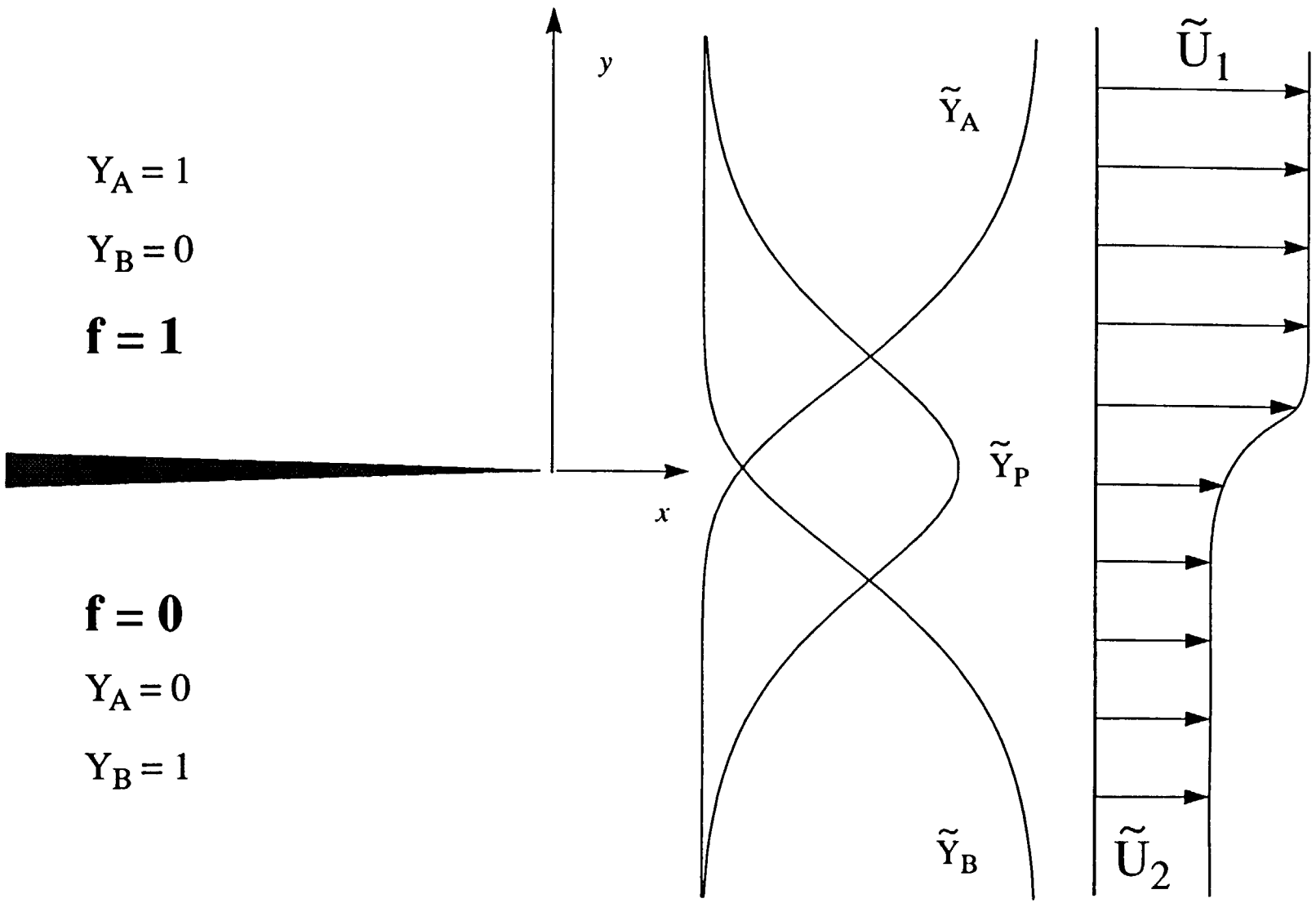
$Y_A = 1$
$Y_B = 0$
f = 1
f = 0
$Y_A = 0$
$Y_B = 1$
y
x
$\tilde{Y}_A$
$\tilde{Y}_P$
$\tilde{Y}_B$
$\tilde{U}_1$
$\tilde{U}_2$

Figure 1(b)

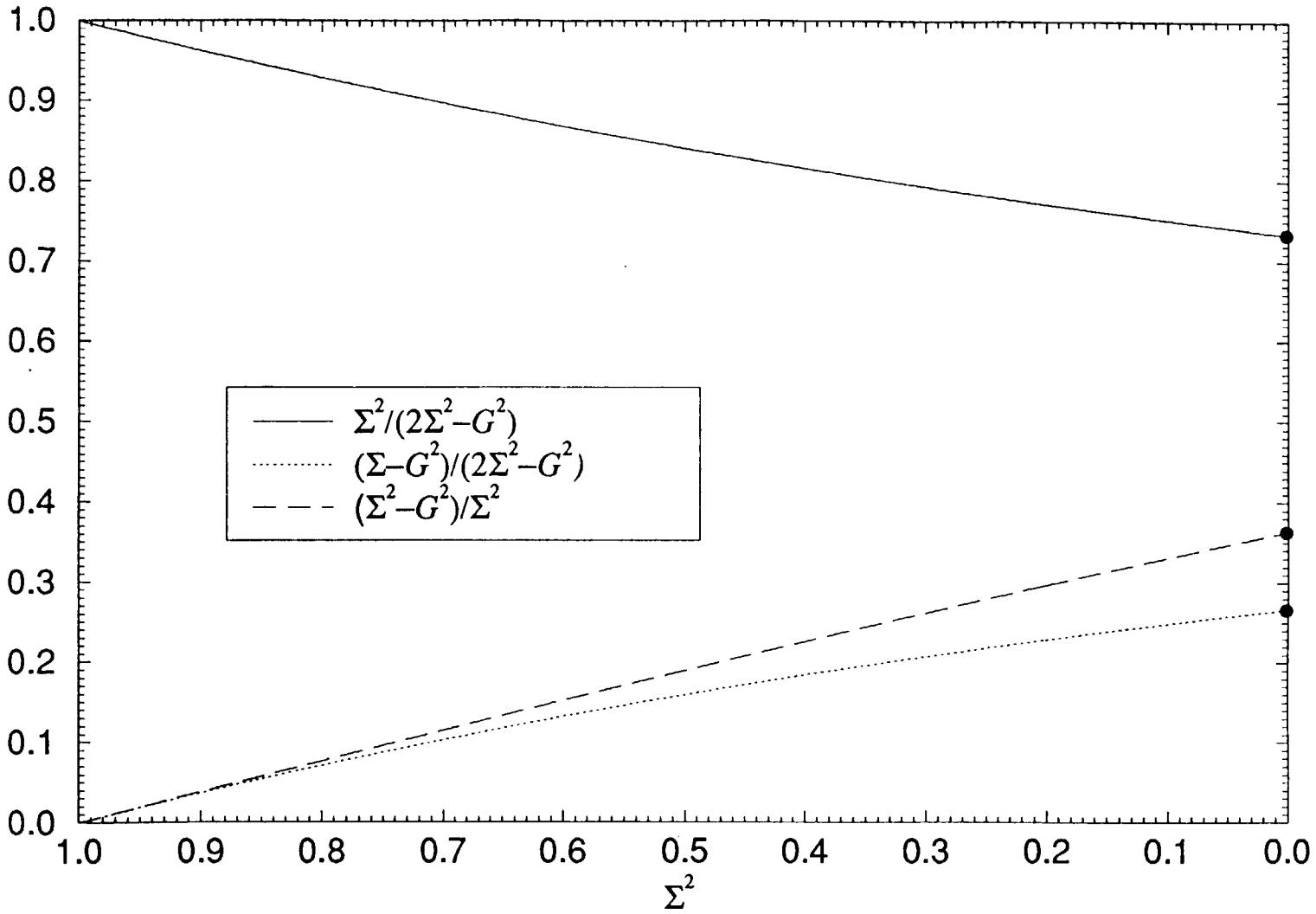
1.0
0.9
0.8
0.7
0.6
0.5
0.4
0.3
0.2
0.1
0.0
1.0 0.9 0.8 0.7 0.6 0.5 0.4 0.3 0.2 0.1 0.0
Σ^2
$\Sigma^2/(2\Sigma^2-G^2)$
$(\Sigma-G^2)/(2\Sigma^2-G^2)$
$(\Sigma^2-G^2)/\Sigma^2$
Mixing Progression

Figure 2

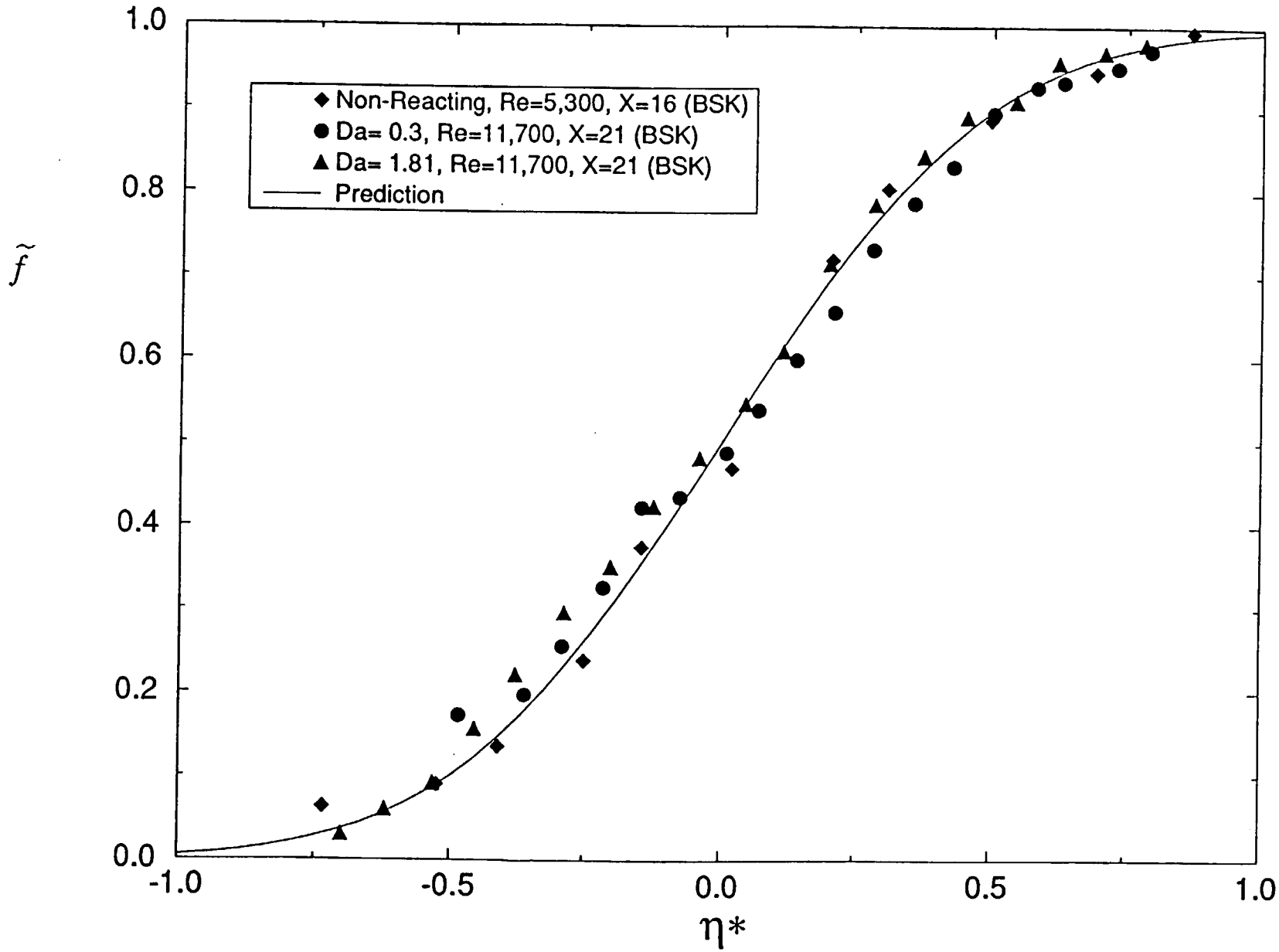
Non-Reacting, Re=5,300, X=16 (BSK)
Da= 0.3, Re=11,700, X=21 (BSK)
Da= 1.81, Re=11,700, X=21 (BSK)
Prediction
$\tilde{f}$
1.0
0.8
0.6
0.4
0.2
0.0
-1.0
-0.5
0.0
0.5
1.0
η^*

Figure 3(a)

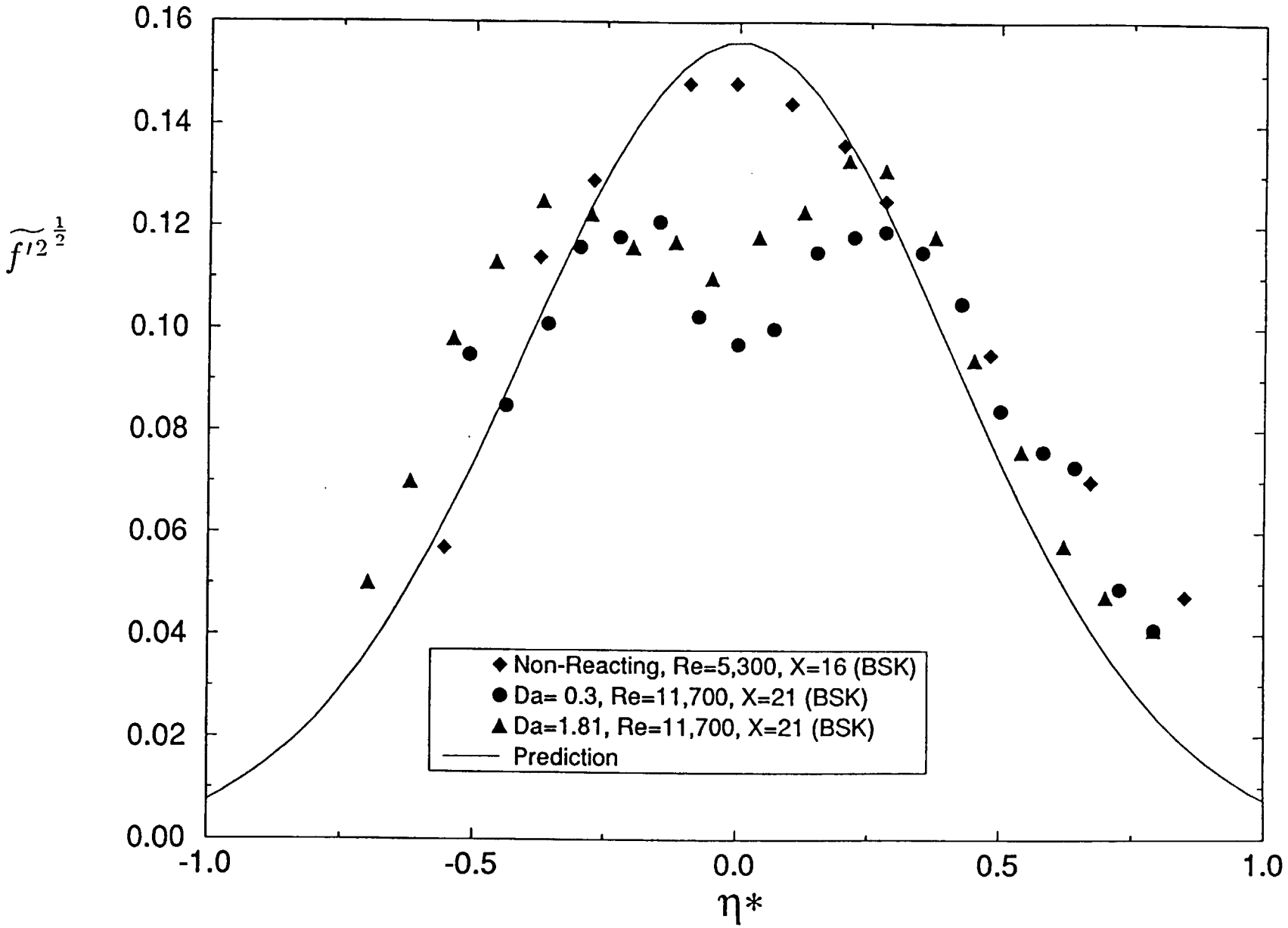
0.16
0.14
0.12
0.10
0.08
0.06
0.04
0.02
0.00
$\widetilde{f'^2}^{\frac{1}{2}}$
-1.0
-0.5
0.0
0.5
1.0
η*
◆ Non-Reacting, Re=5,300, X=16 (BSK)
● Da= 0.3, Re=11,700, X=21 (BSK)
▲ Da=1.81, Re=11,700, X=21 (BSK)
Prediction

Figure 3(b)

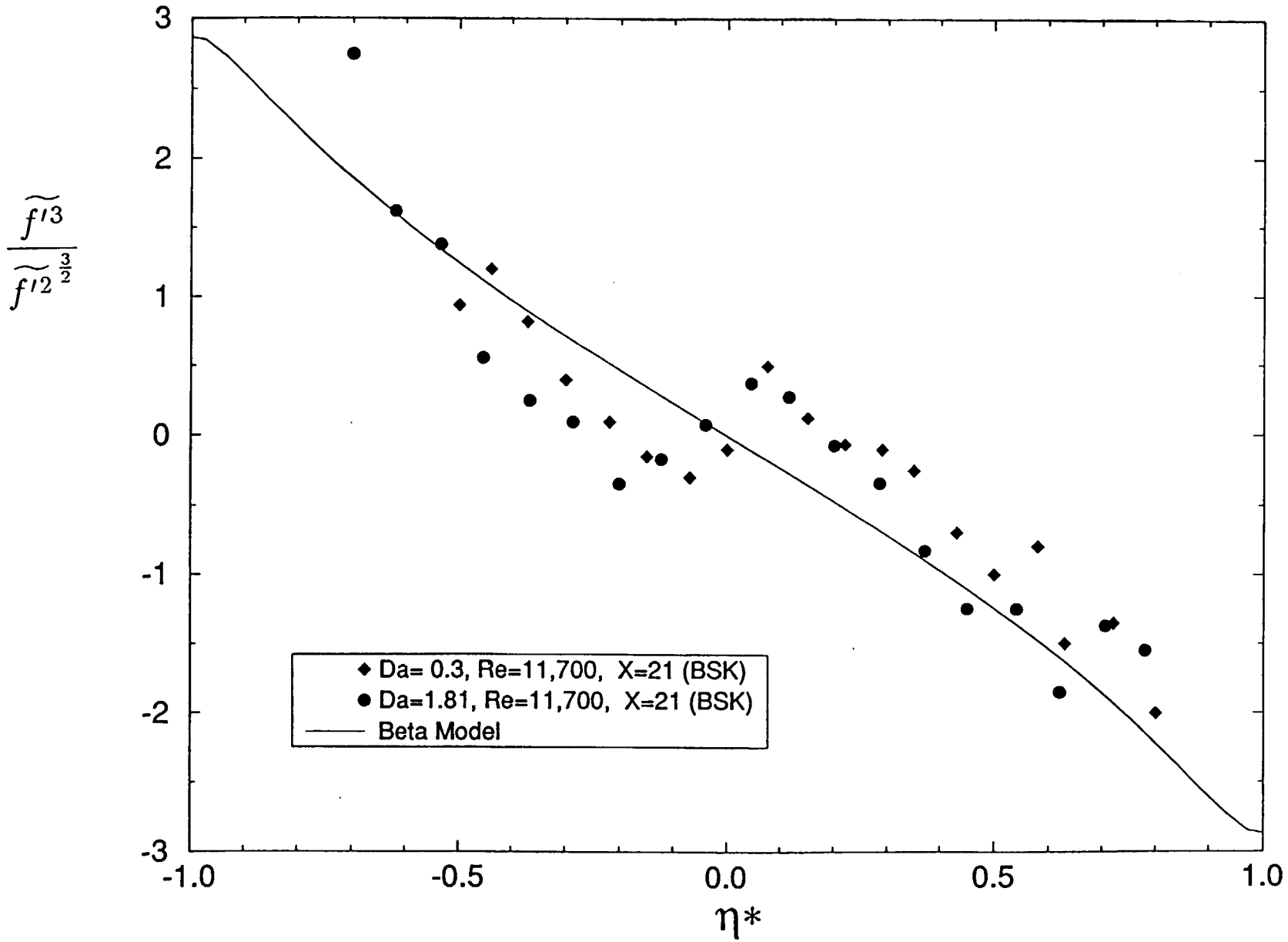
$\frac{\widetilde{f'^3}}{\widetilde{f'^2}^{\frac{3}{2}}}$
3
2
1
0
-1
-2
-3
-1.0
-0.5
0.0
0.5
1.0
η*
◆ Da= 0.3, Re=11,700, X=21 (BSK)
● Da=1.81, Re=11,700, X=21 (BSK)
Beta Model

Figure 4

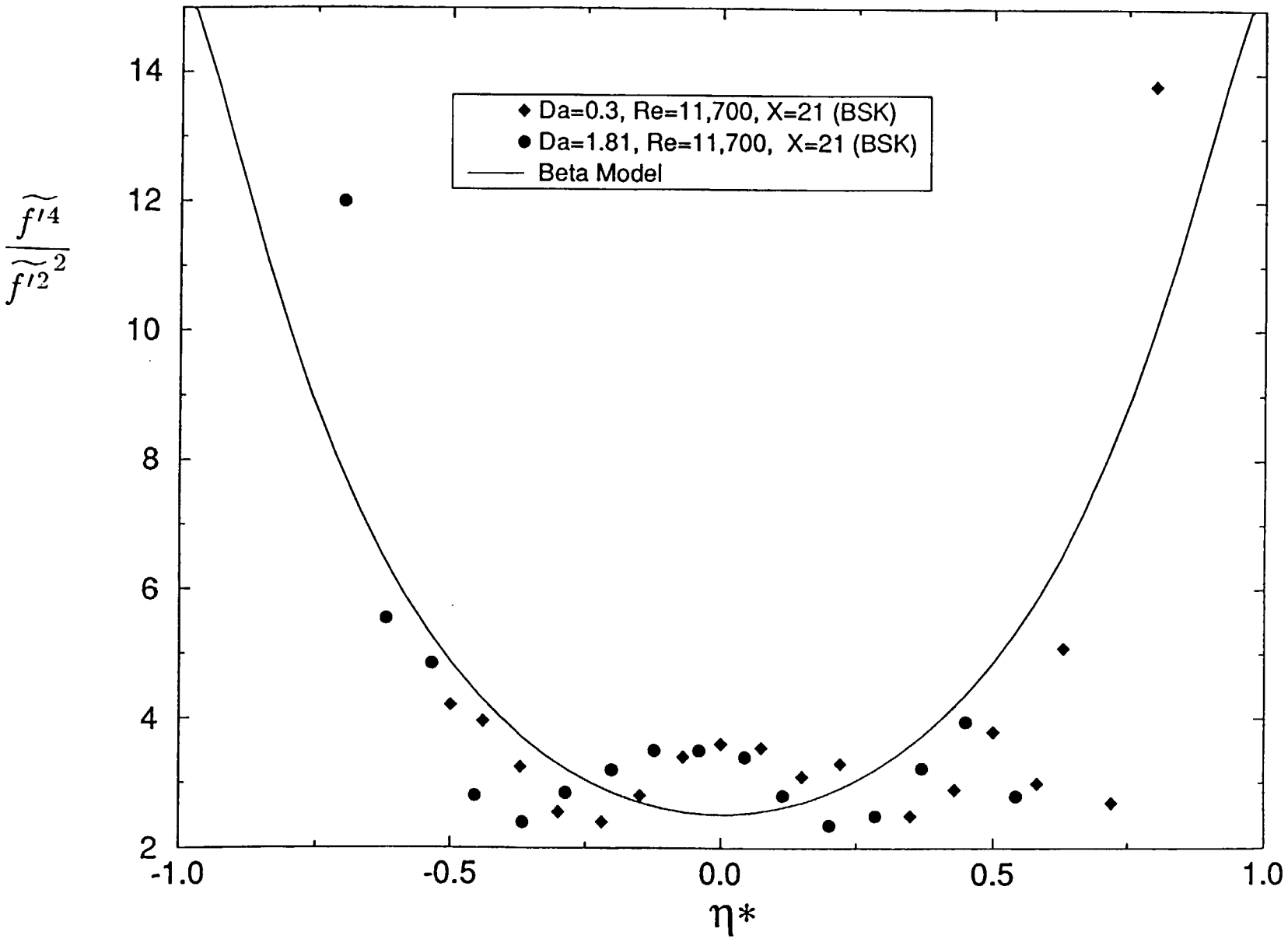
◆ Da=0.3, Re=11,700, X=21 (BSK)
● Da=1.81, Re=11,700, X=21 (BSK)
Beta Model
$\frac{\widetilde{f'^4}}{\widetilde{f'^2}^2}$
14
12
10
8
6
4
2
-1.0
-0.5
0.0
0.5
1.0
η*

Figure 5

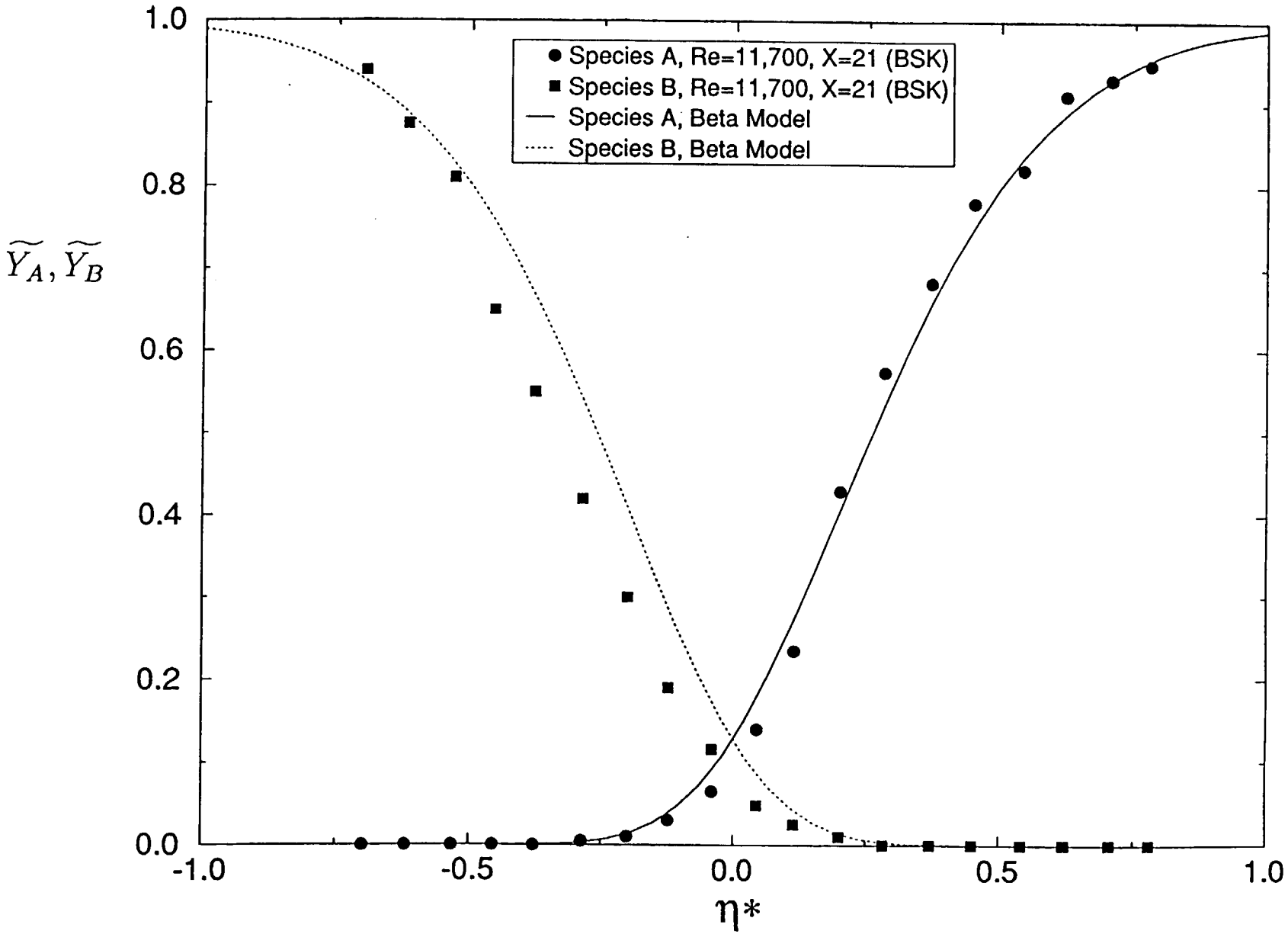
Species A, Re=11,700, X=21 (BSK)
Species B, Re=11,700, X=21 (BSK)
Species A, Beta Model
Species B, Beta Model
$\widetilde{Y_A}, \widetilde{Y_B}$
1.0
0.8
0.6
0.4
0.2
0.0
-1.0
-0.5
0.0
0.5
1.0
η^*

Figure 6

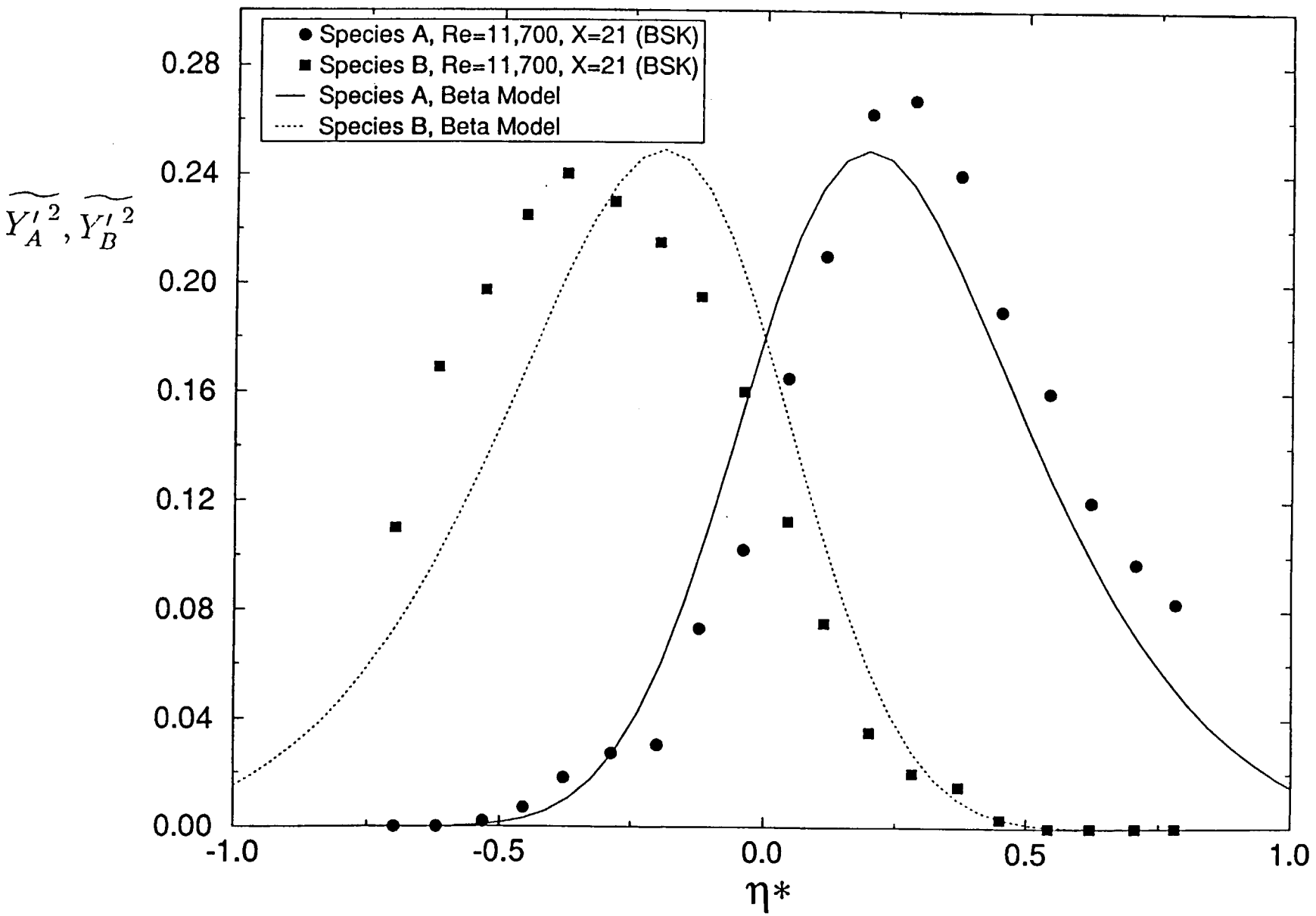
Species A, Re=11,700, X=21 (BSK)
Species B, Re=11,700, X=21 (BSK)
Species A, Beta Model
Species B, Beta Model
$\widetilde{Y_A'^2}, \widetilde{Y_B'^2}$
0.28
0.24
0.20
0.16
0.12
0.08
0.04
0.00
-1.0
-0.5
0.0
0.5
1.0
η^*

Figure 7

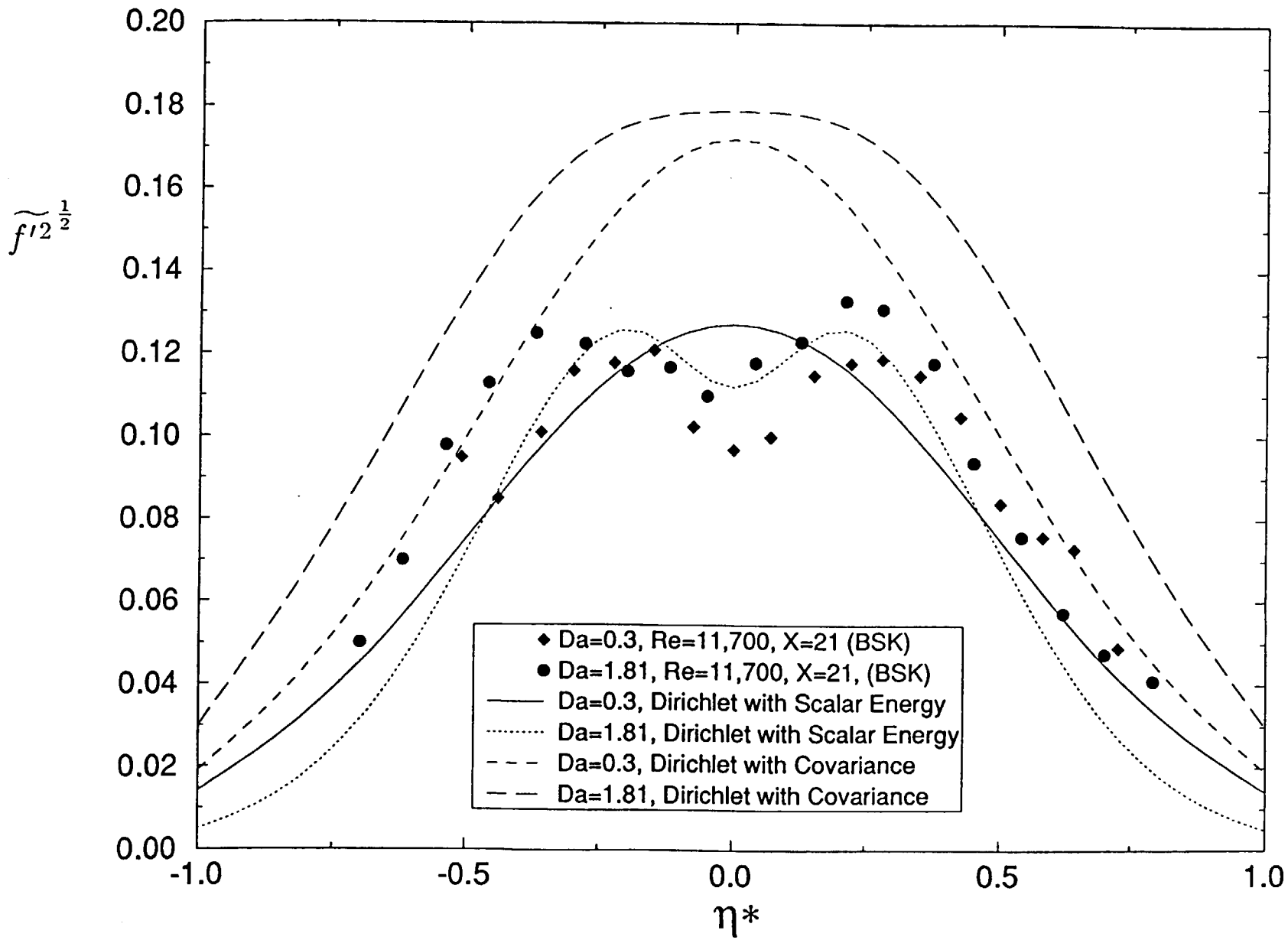
0.20
0.18
0.16
0.14
0.12
0.10
0.08
0.06
0.04
0.02
0.00
-1.0
-0.5
0.0
0.5
1.0
η*
$\widetilde{f'^2}^{\frac{1}{2}}$
Da=0.3, Re=11,700, X=21 (BSK)
Da=1.81, Re=11,700, X=21, (BSK)
Da=0.3, Dirichlet with Scalar Energy
Da=1.81, Dirichlet with Scalar Energy
Da=0.3, Dirichlet with Covariance
Da=1.81, Dirichlet with Covariance

Figure 8

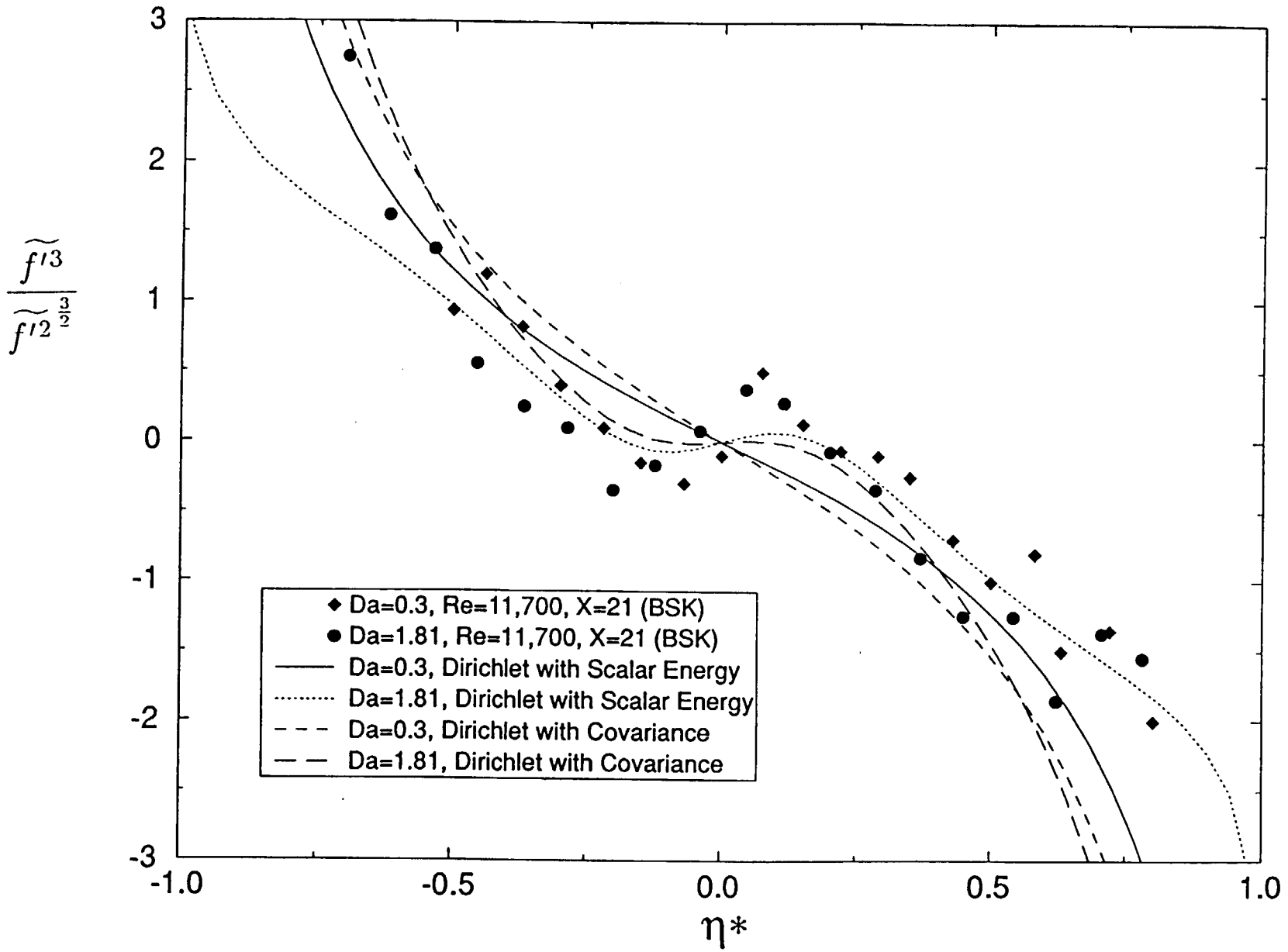
$\frac{\widetilde{f'^3}}{\widetilde{f'^2}^{\frac{3}{2}}}$
3
2
1
0
-1
-2
-3
-1.0
-0.5
0.0
0.5
1.0
η*
Da=0.3, Re=11,700, X=21 (BSK)
Da=1.81, Re=11,700, X=21 (BSK)
Da=0.3, Dirichlet with Scalar Energy
Da=1.81, Dirichlet with Scalar Energy
Da=0.3, Dirichlet with Covariance
Da=1.81, Dirichlet with Covariance

Figure 9

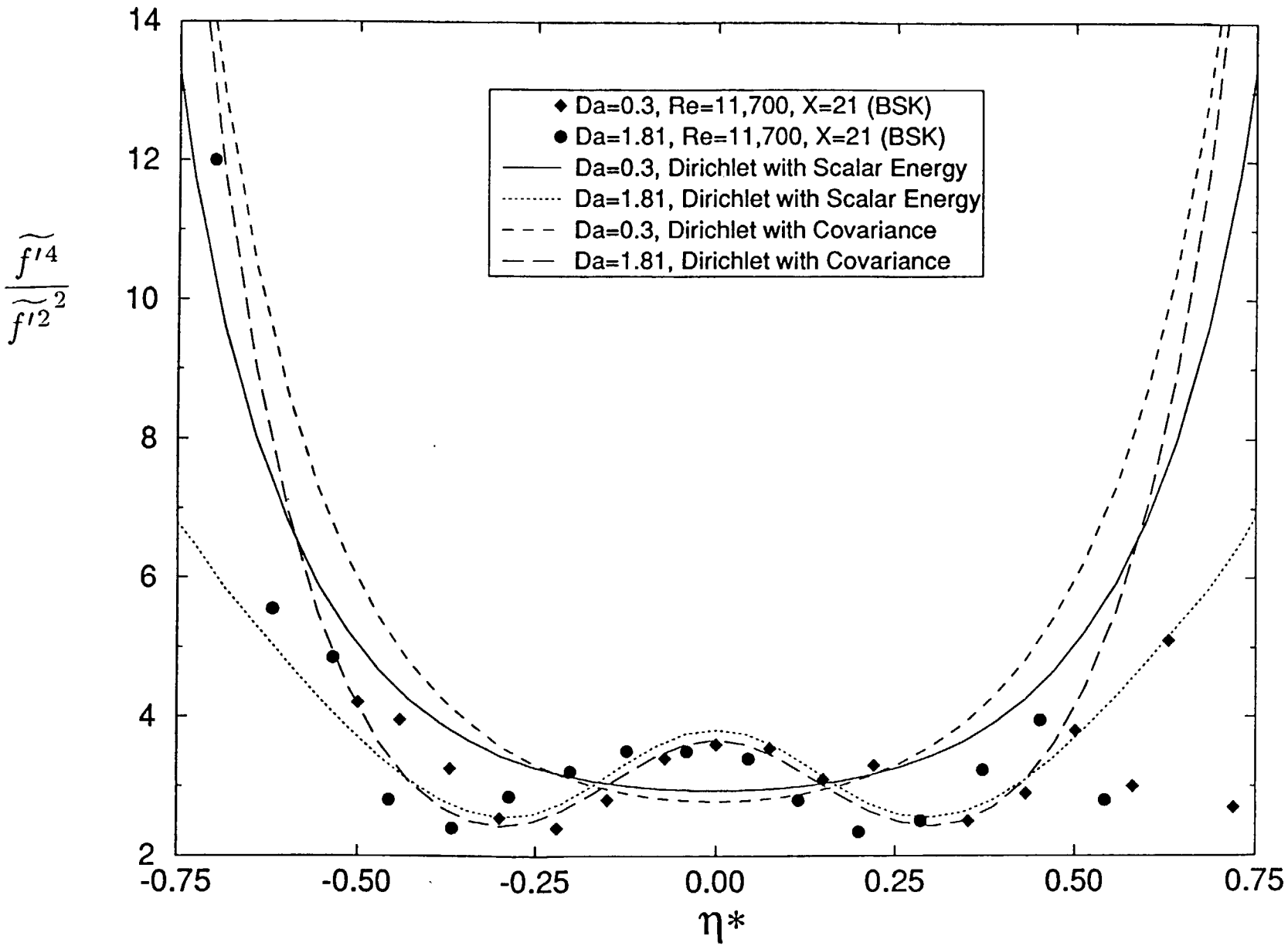
◆ Da=0.3, Re=11,700, X=21 (BSK)
● Da=1.81, Re=11,700, X=21 (BSK)
Da=0.3, Dirichlet with Scalar Energy
Da=1.81, Dirichlet with Scalar Energy
Da=0.3, Dirichlet with Covariance
Da=1.81, Dirichlet with Covariance
$\frac{\widetilde{f'^4}}{\widetilde{f'^2}^2}$
14
12
10
8
6
4
2
-0.75
-0.50
-0.25
0.00
0.25
0.50
0.75
η*

Figure 10

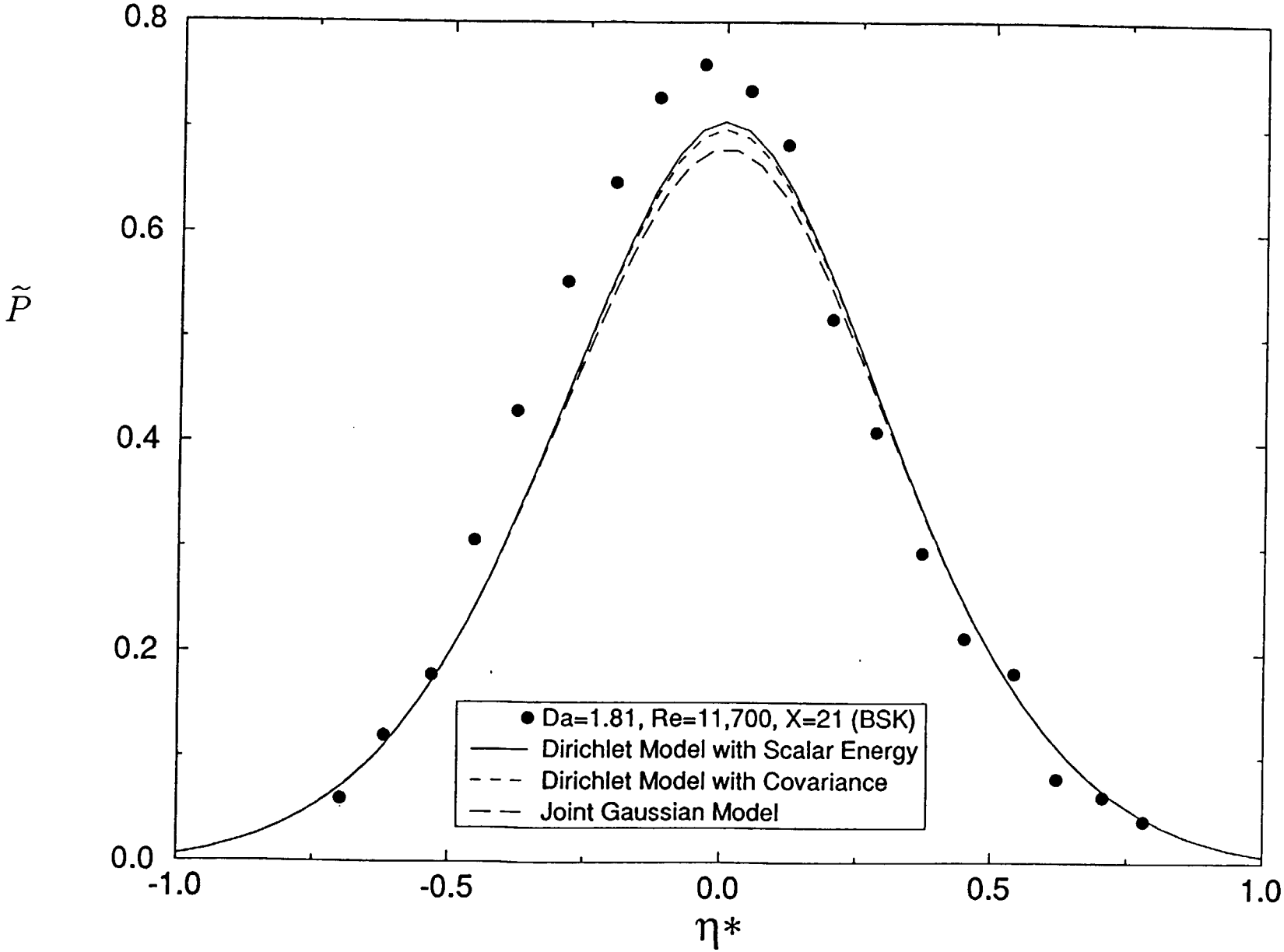
0.8
0.6
0.4
0.2
0.0
$\widetilde{P}$
-1.0
-0.5
0.0
0.5
1.0
η^*
Da=1.81, Re=11,700, X=21 (BSK)
Dirichlet Model with Scalar Energy
Dirichlet Model with Covariance
Joint Gaussian Model

Figure 11

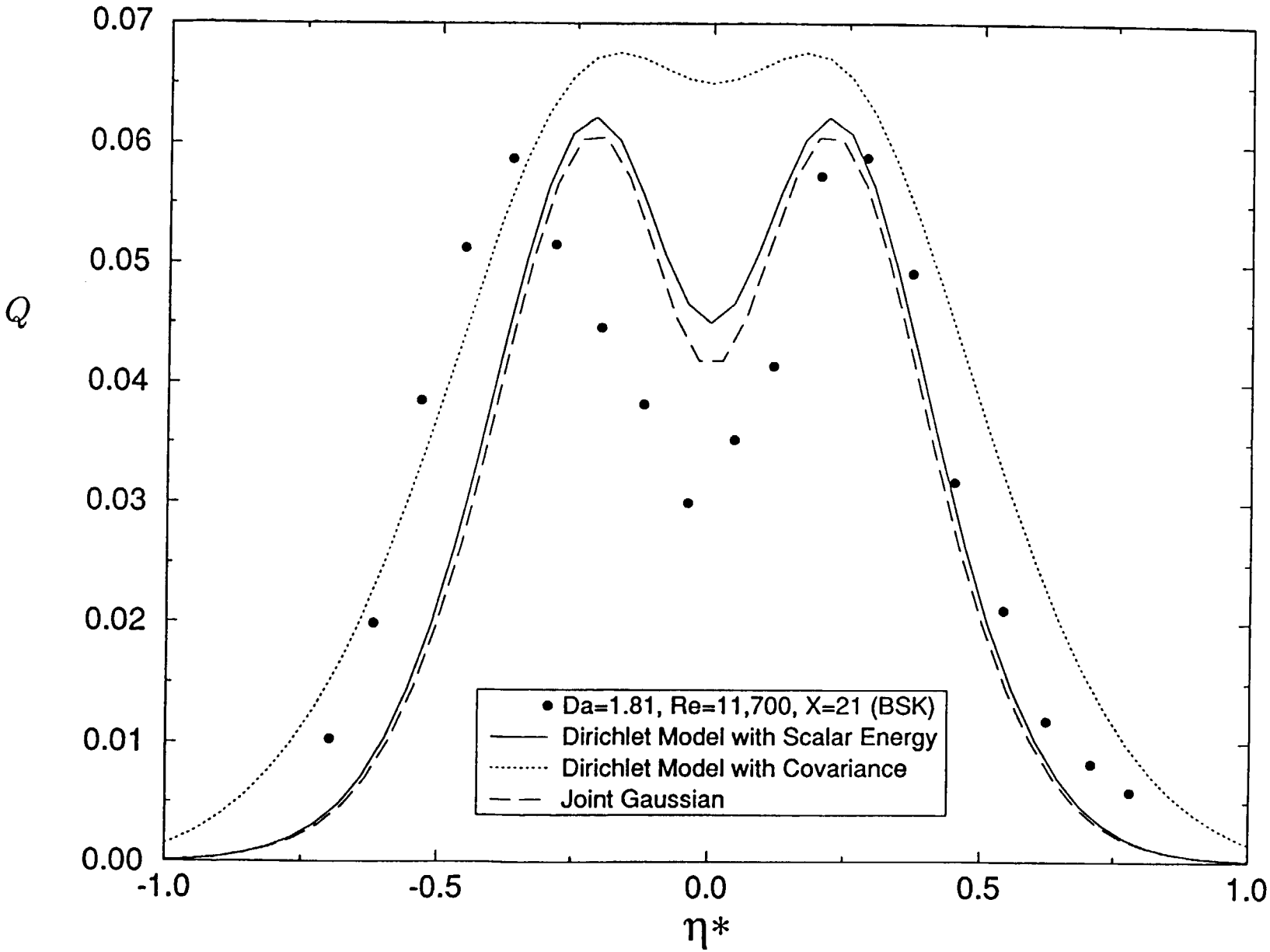
0.07
0.06
0.05
0.04
0.03
0.02
0.01
0.00
Q
-1.0
-0.5
0.0
0.5
1.0
η*
Da=1.81, Re=11,700, X=21 (BSK)
Dirichlet Model with Scalar Energy
Dirichlet Model with Covariance
Joint Gaussian

Figure 12

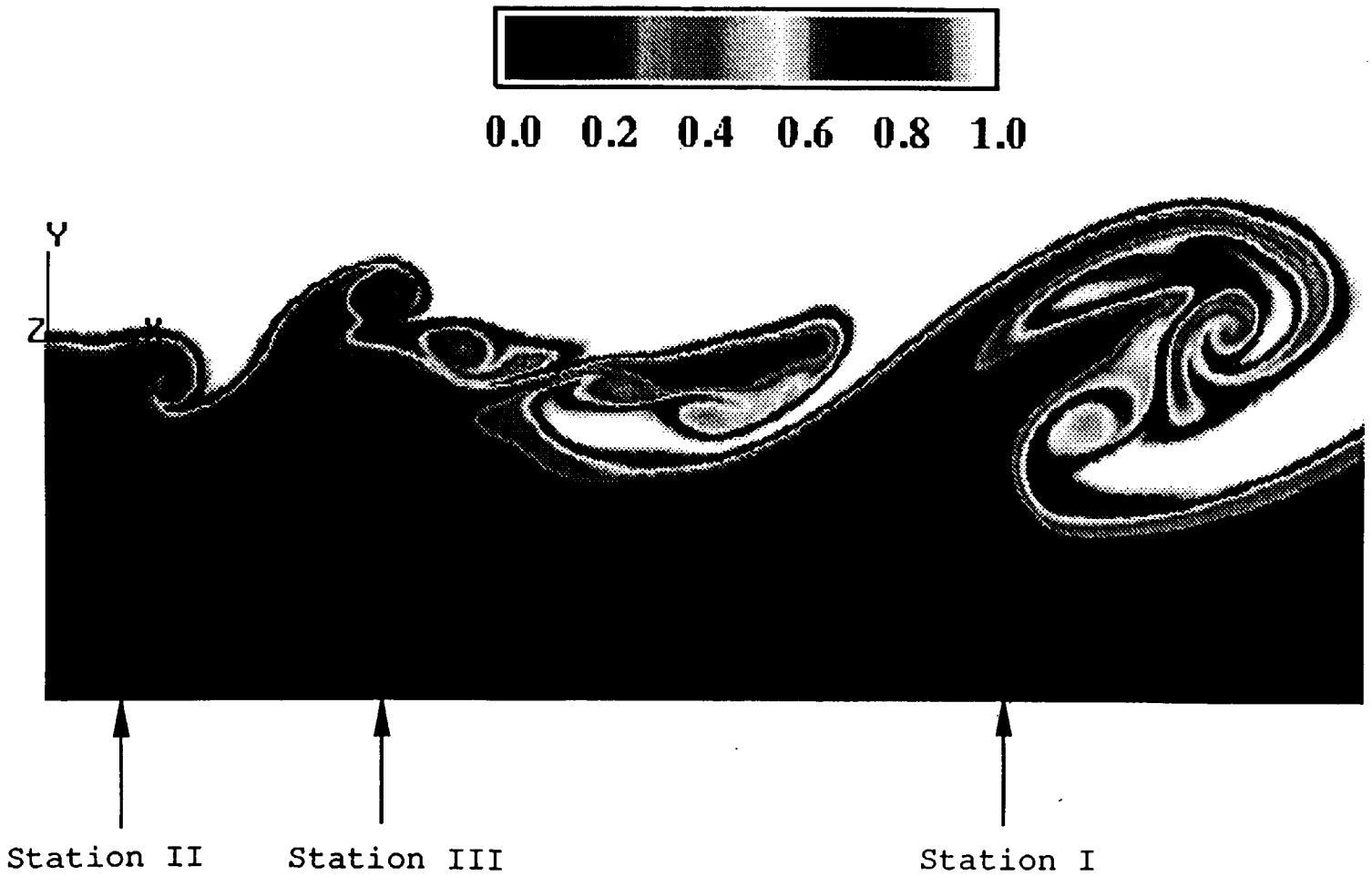

Figure 13

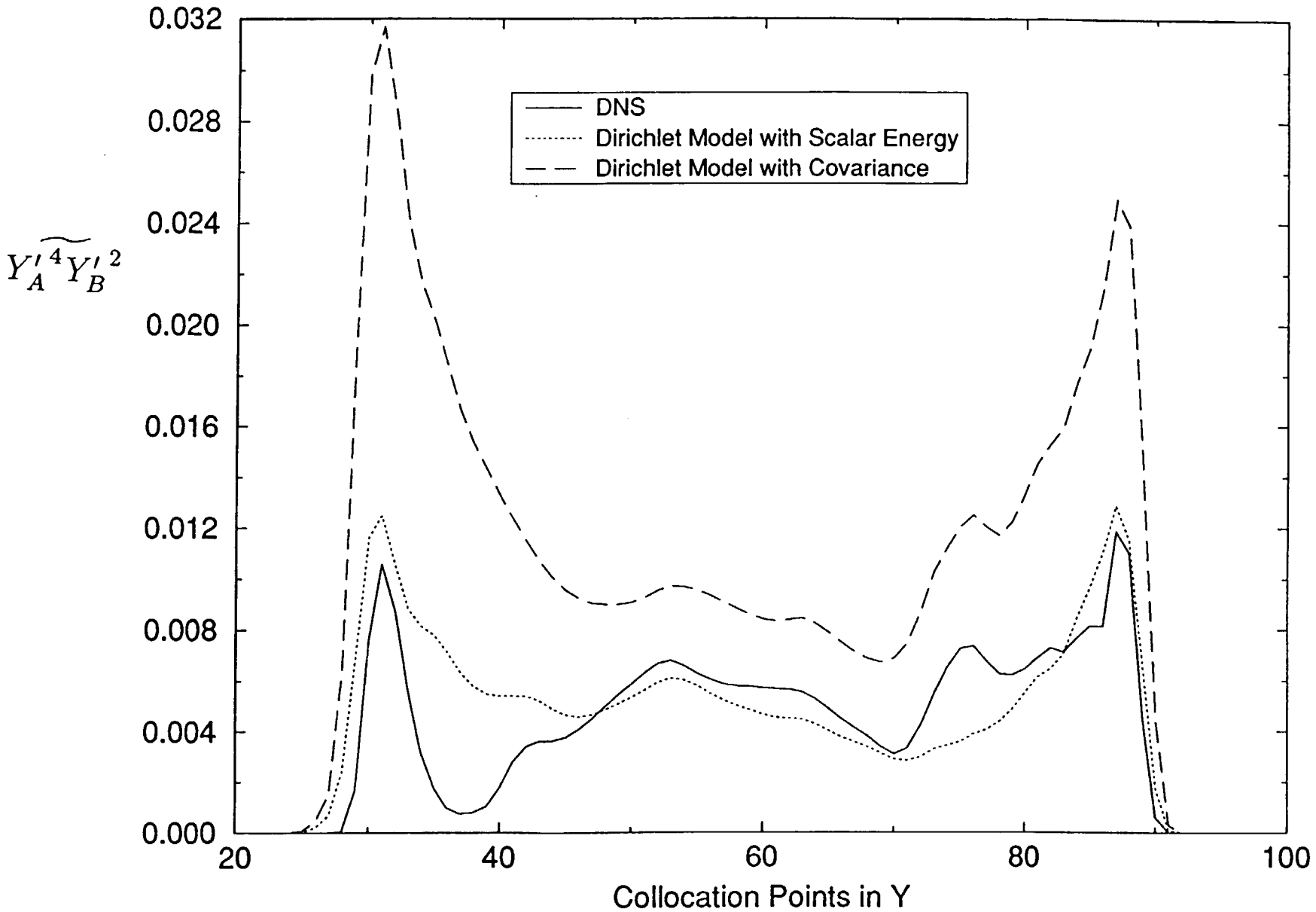
0.032
0.028
0.024
0.020
0.016
0.012
0.008
0.004
0.000
$\widetilde{Y_A'^4 Y_B'^2}$
DNS
Dirichlet Model with Scalar Energy
Dirichlet Model with Covariance
20
40
60
80
100
Collocation Points in Y

Figure 14

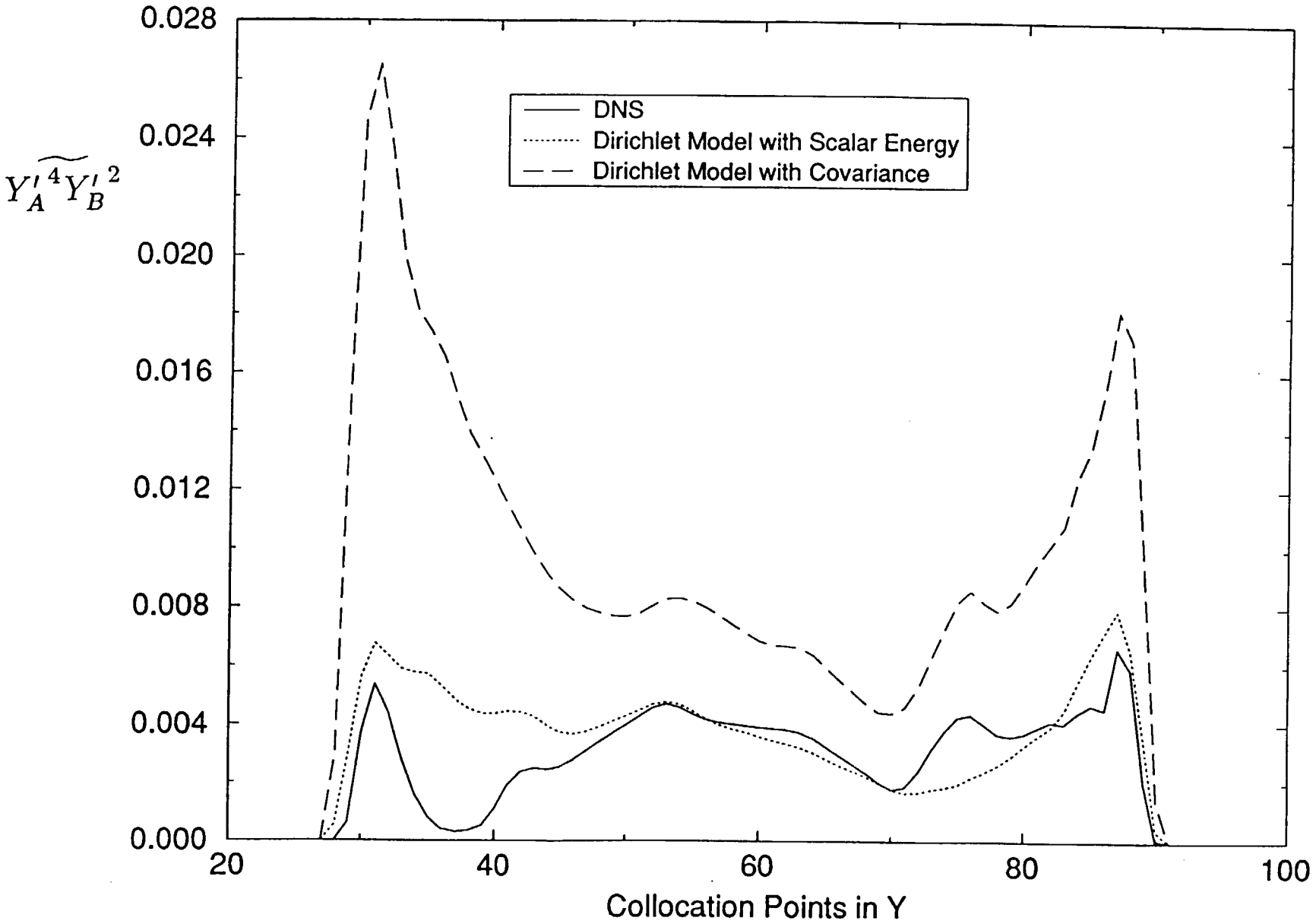
0.028
0.024
0.020
0.016
0.012
0.008
0.004
0.000
$\widetilde{Y_A'^4 Y_B'^2}$
DNS
Dirichlet Model with Scalar Energy
Dirichlet Model with Covariance
20
40
60
80
100
Collocation Points in Y

Figure 15

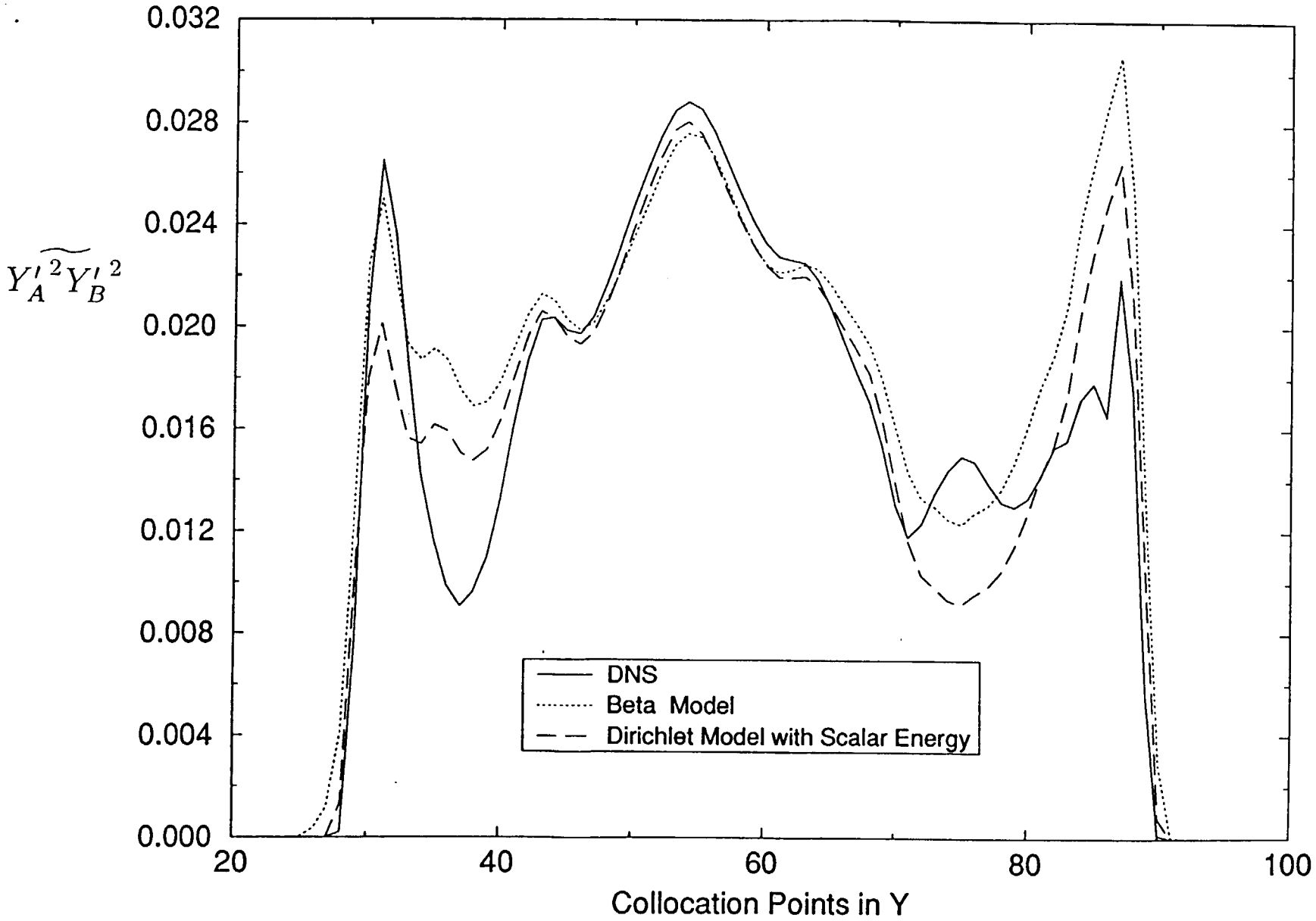
0.032
0.028
0.024
0.020
0.016
0.012
0.008
0.004
0.000
$\widetilde{Y_A'^2 Y_B'^2}$
20
40
60
80
100
Collocation Points in Y
DNS
Beta Model
Dirichlet Model with Scalar Energy

Figure 16

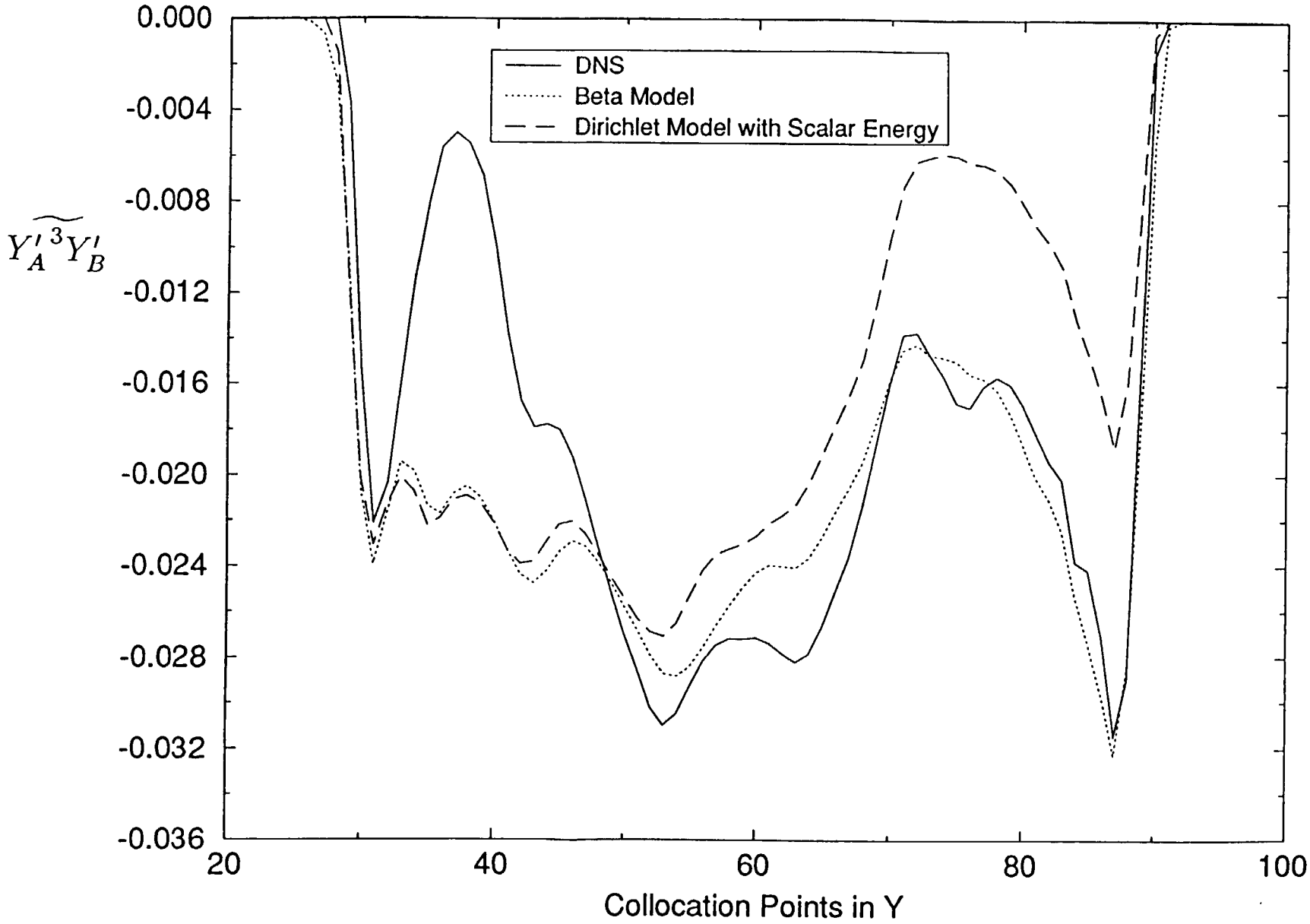
DNS
Beta Model
Dirichlet Model with Scalar Energy
$\widetilde{Y_A'^3 Y_B'}$
0.000
-0.004
-0.008
-0.012
-0.016
-0.020
-0.024
-0.028
-0.032
-0.036
20
40
60
80
100
Collocation Points in Y

Figure 17

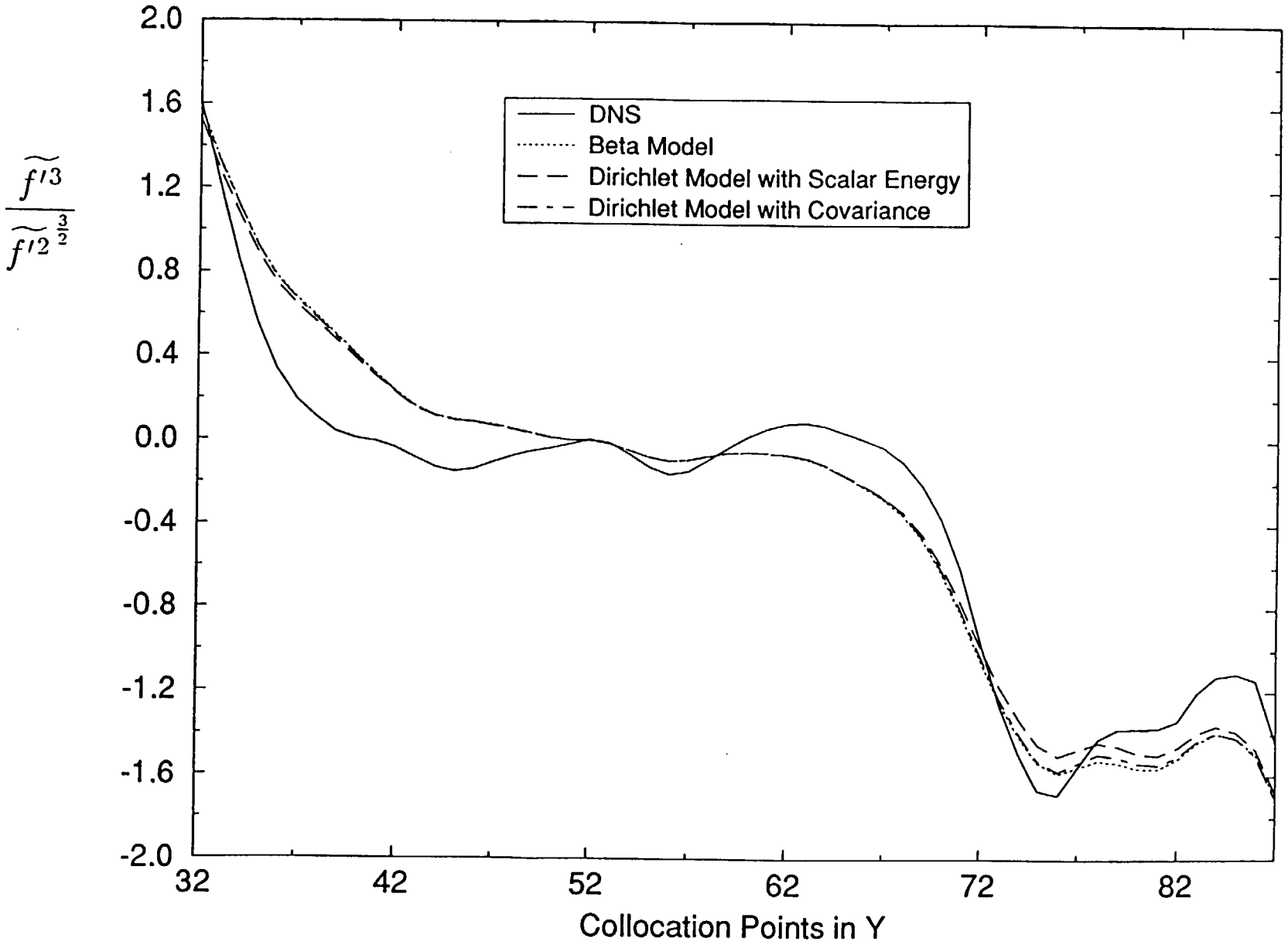
$\frac{\widetilde{f'^3}}{\widetilde{f'^2}^{\frac{3}{2}}}$
2.0
1.6
1.2
0.8
0.4
0.0
-0.4
-0.8
-1.2
-1.6
-2.0
32
42
52
62
72
82
Collocation Points in Y
DNS
Beta Model
Dirichlet Model with Scalar Energy
Dirichlet Model with Covariance

Figure 18

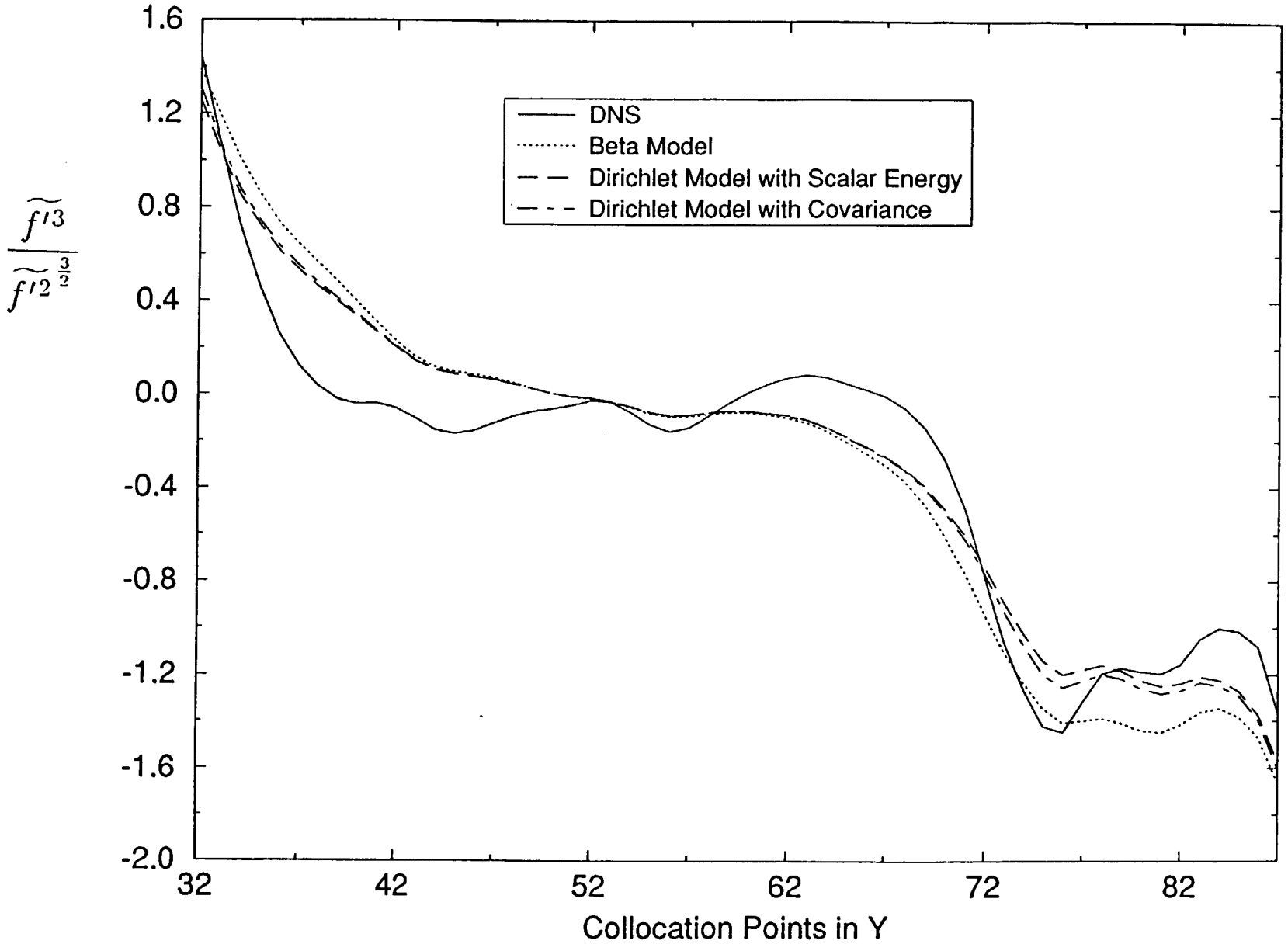
$\frac{\widetilde{f'^3}}{\widetilde{f'^2}^{\frac{3}{2}}}$
1.6
1.2
0.8
0.4
0.0
-0.4
-0.8
-1.2
-1.6
-2.0
32
42
52
62
72
82
Collocation Points in Y
DNS
Beta Model
Dirichlet Model with Scalar Energy
Dirichlet Model with Covariance

Figure 19

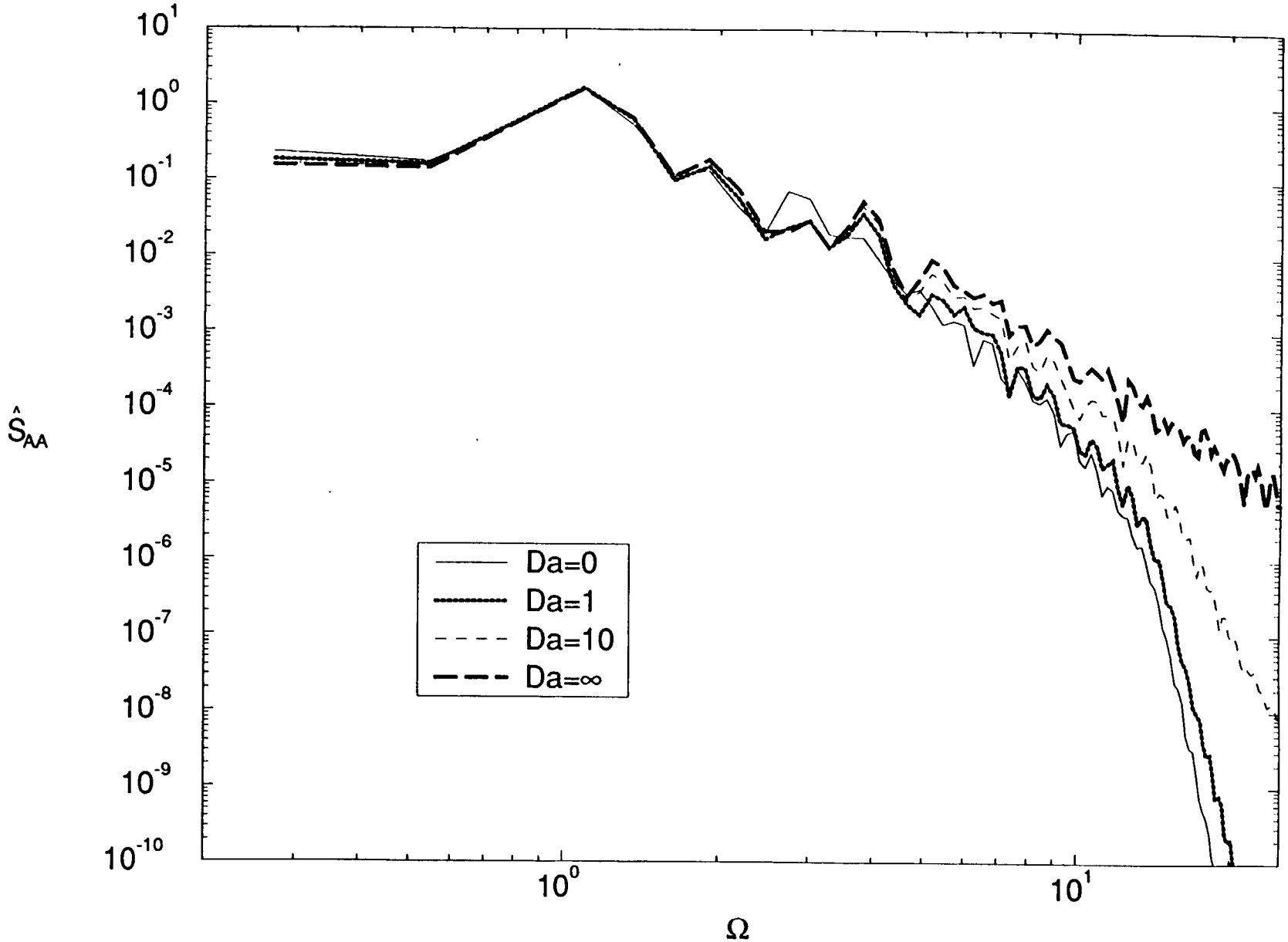
10^{1}
10^{0}
10^{-1}
10^{-2}
10^{-3}
10^{-4}
10^{-5}
10^{-6}
10^{-7}
10^{-8}
10^{-9}
10^{-10}
$\hat{S}_{AA}$
10^{0}
10^{1}
Ω
Da=0
Da=1
Da=10
Da=∞

Figure 20(a)

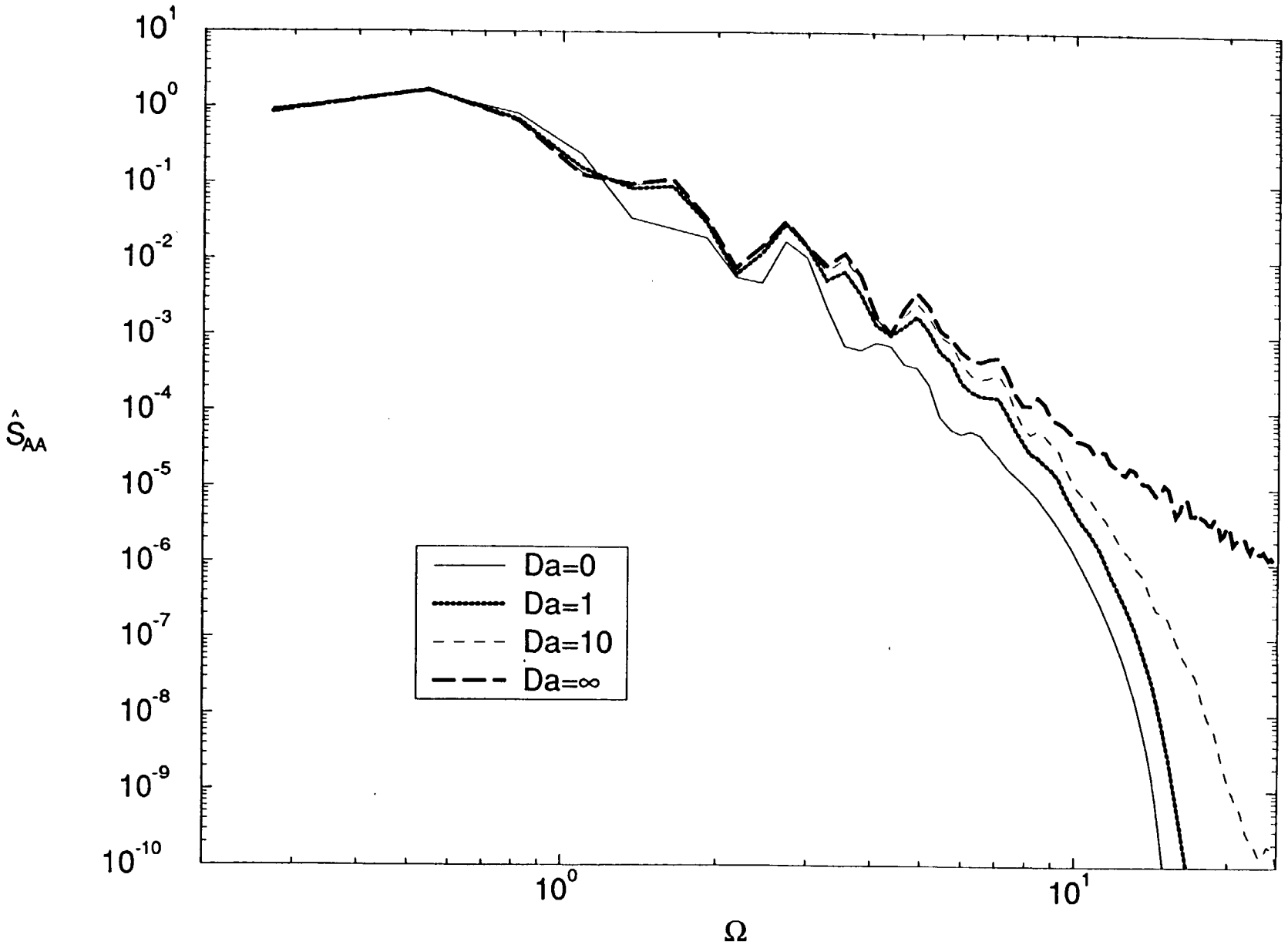
10^{1}
10^{0}
10^{-1}
10^{-2}
10^{-3}
10^{-4}
10^{-5}
10^{-6}
10^{-7}
10^{-8}
10^{-9}
10^{-10}
$\hat{S}_{AA}$
10^{0}
10^{1}
Ω
Da=0
Da=1
Da=10
Da=∞

Figure 20(b)

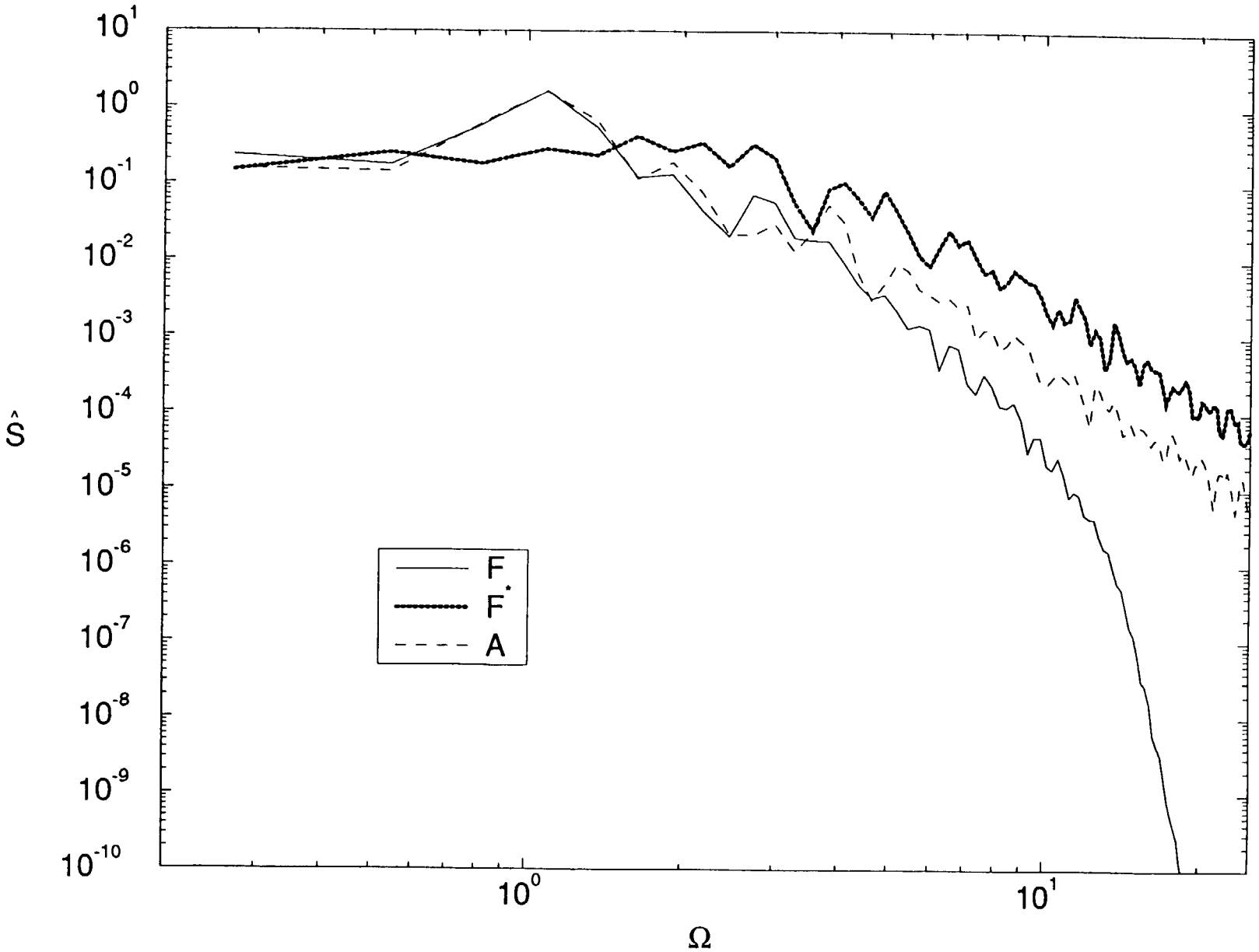
10^{1}
10^{0}
10^{-1}
10^{-2}
10^{-3}
10^{-4}
10^{-5}
10^{-6}
10^{-7}
10^{-8}
10^{-9}
10^{-10}
$\hat{S}$
10^{0}
10^{1}
Ω
F
F*
A

Figure 21(a)

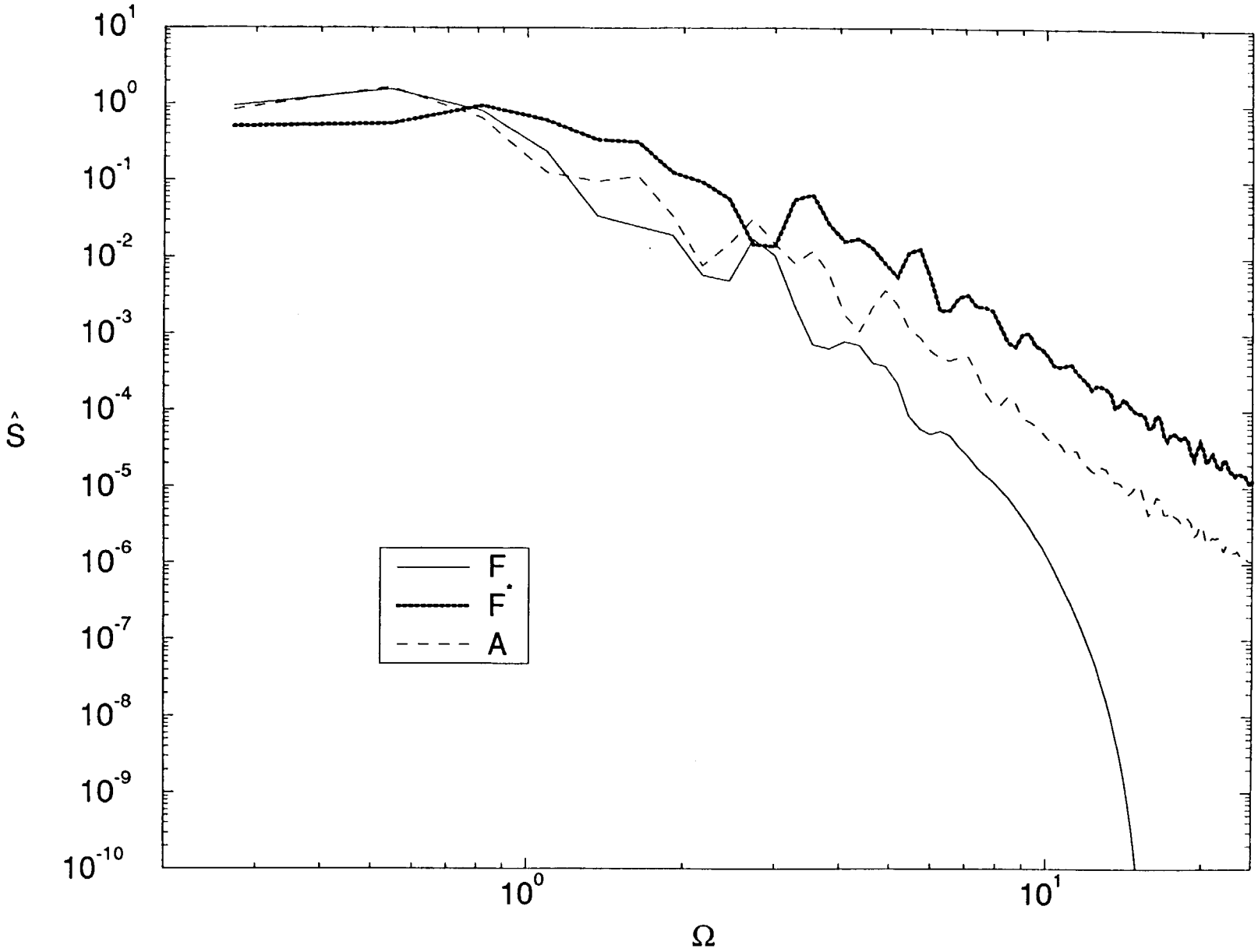
10^{1}
10^{0}
10^{-1}
10^{-2}
10^{-3}
10^{-4}
10^{-5}
10^{-6}
10^{-7}
10^{-8}
10^{-9}
10^{-10}
$\hat{S}$
10^{0}
10^{1}
Ω
F
F
A

Figure 21(b)

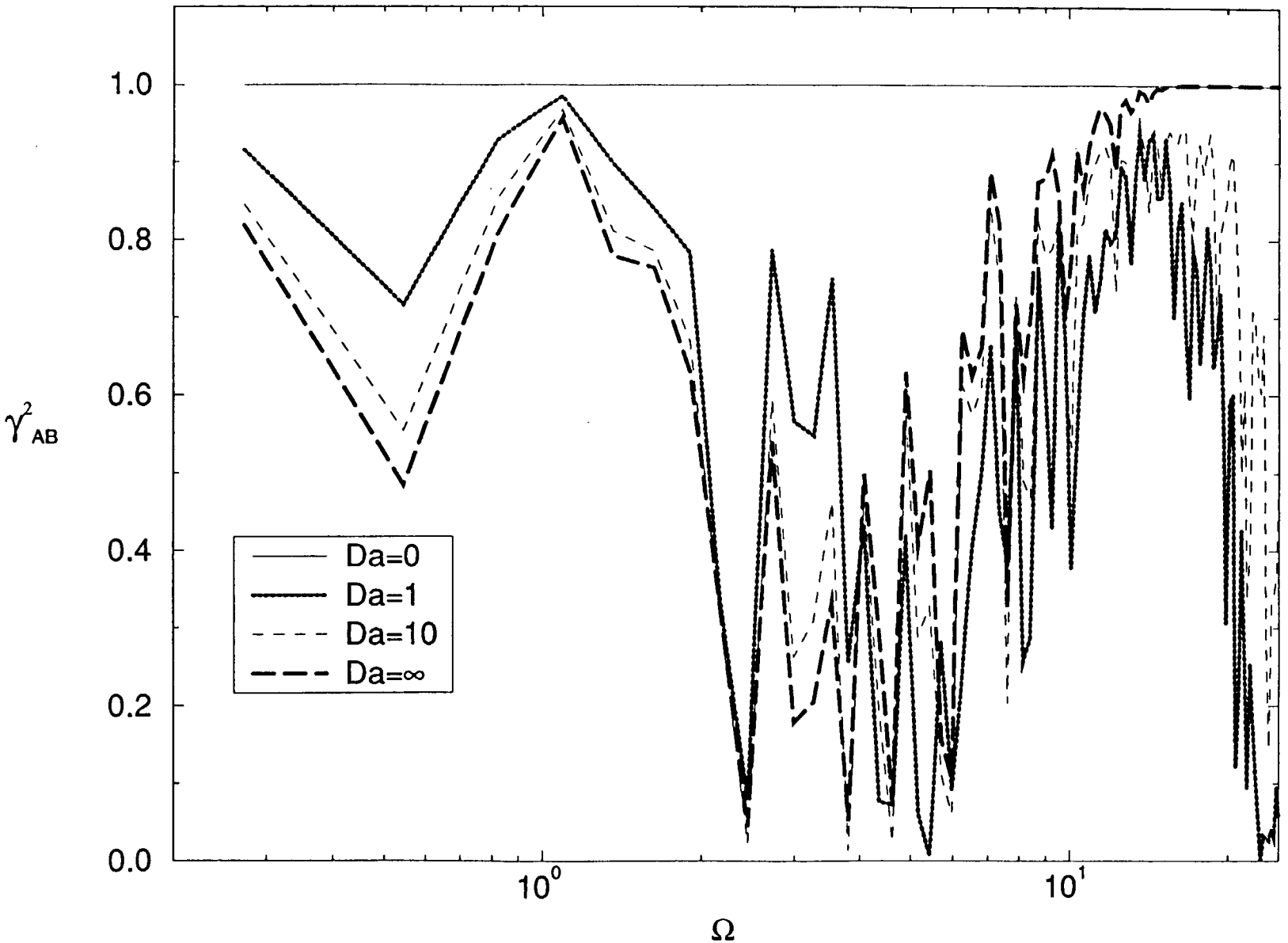

Figure 22(a)

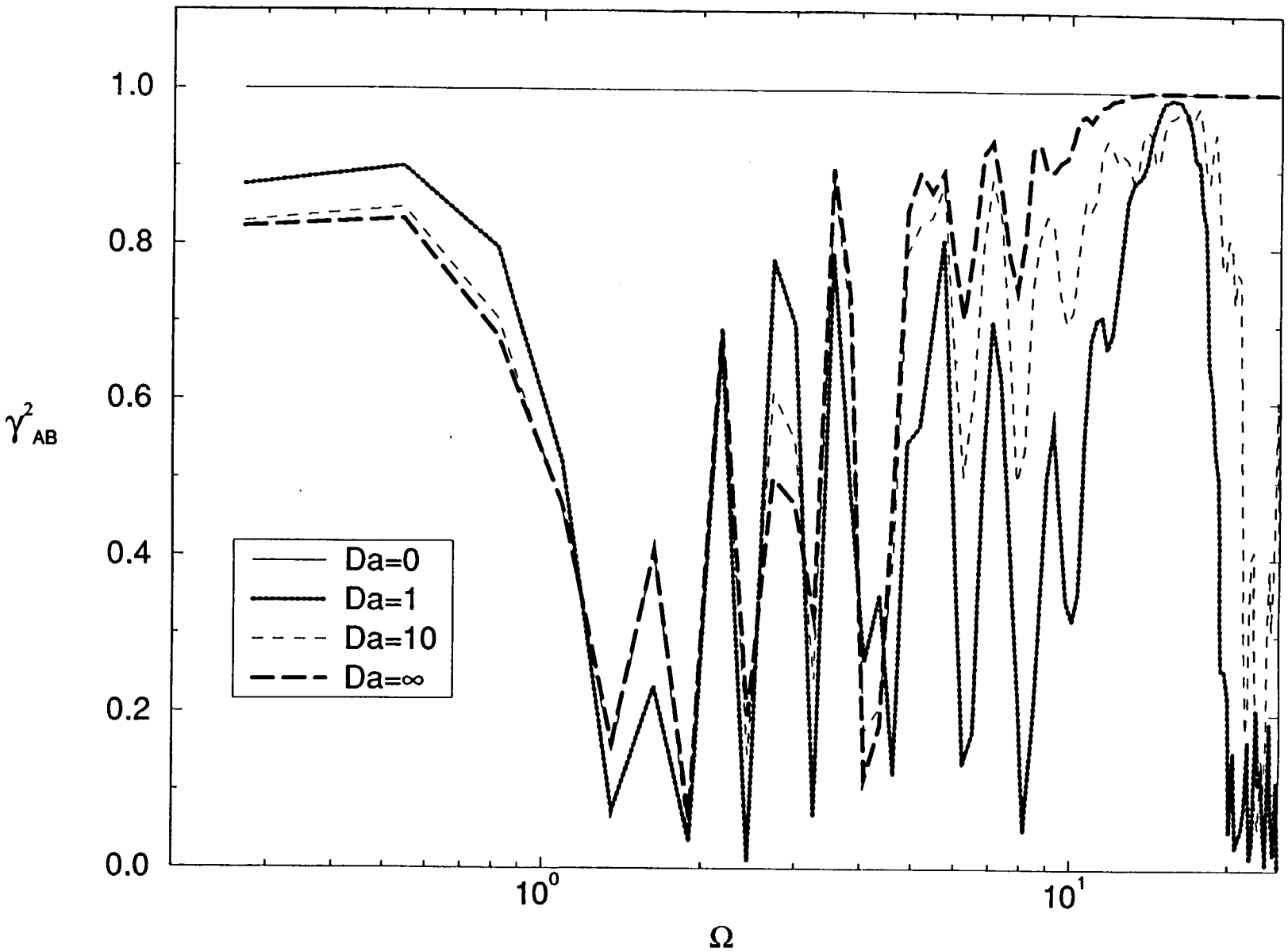

Figure 22(b)

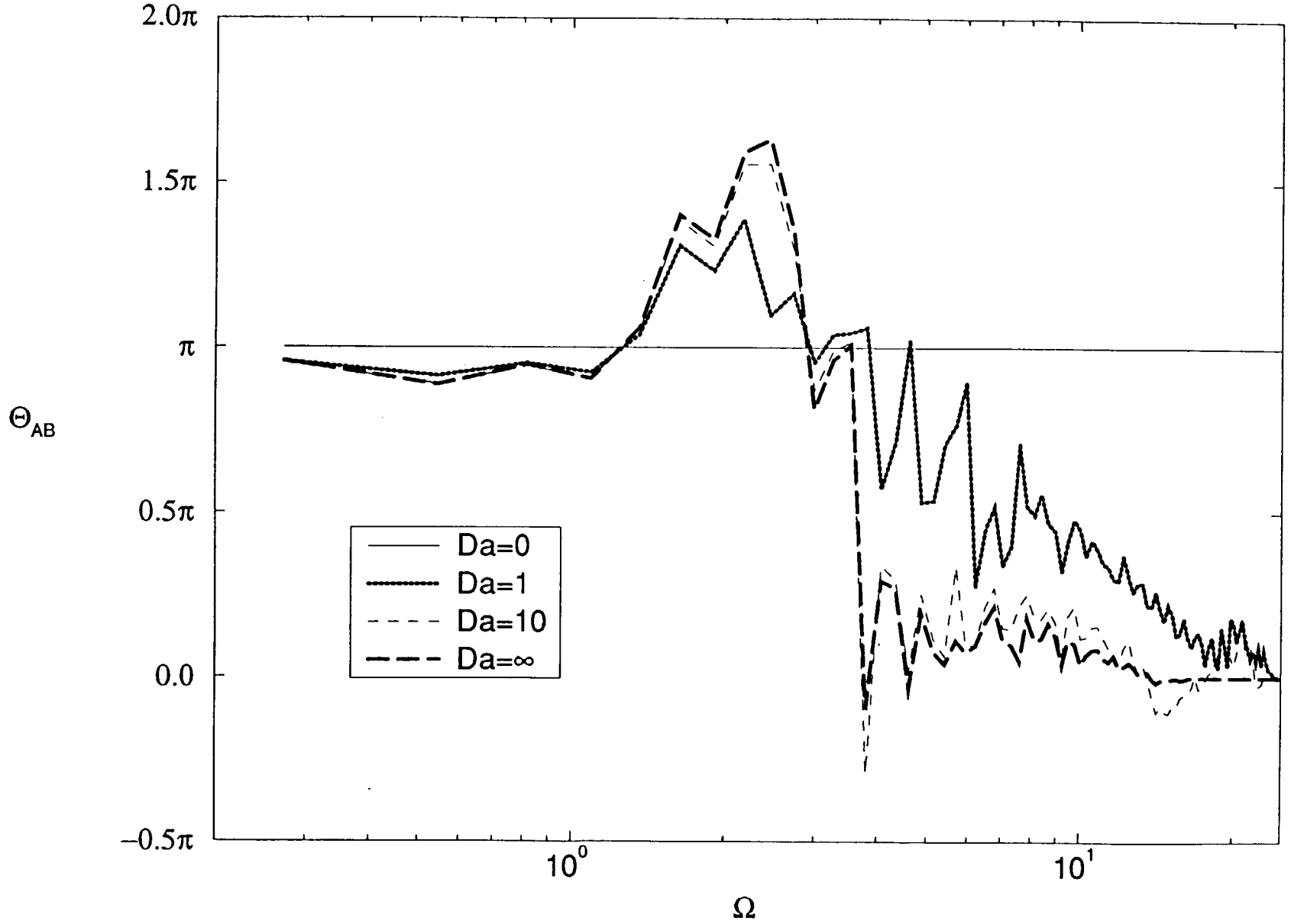

Figure 23(a)

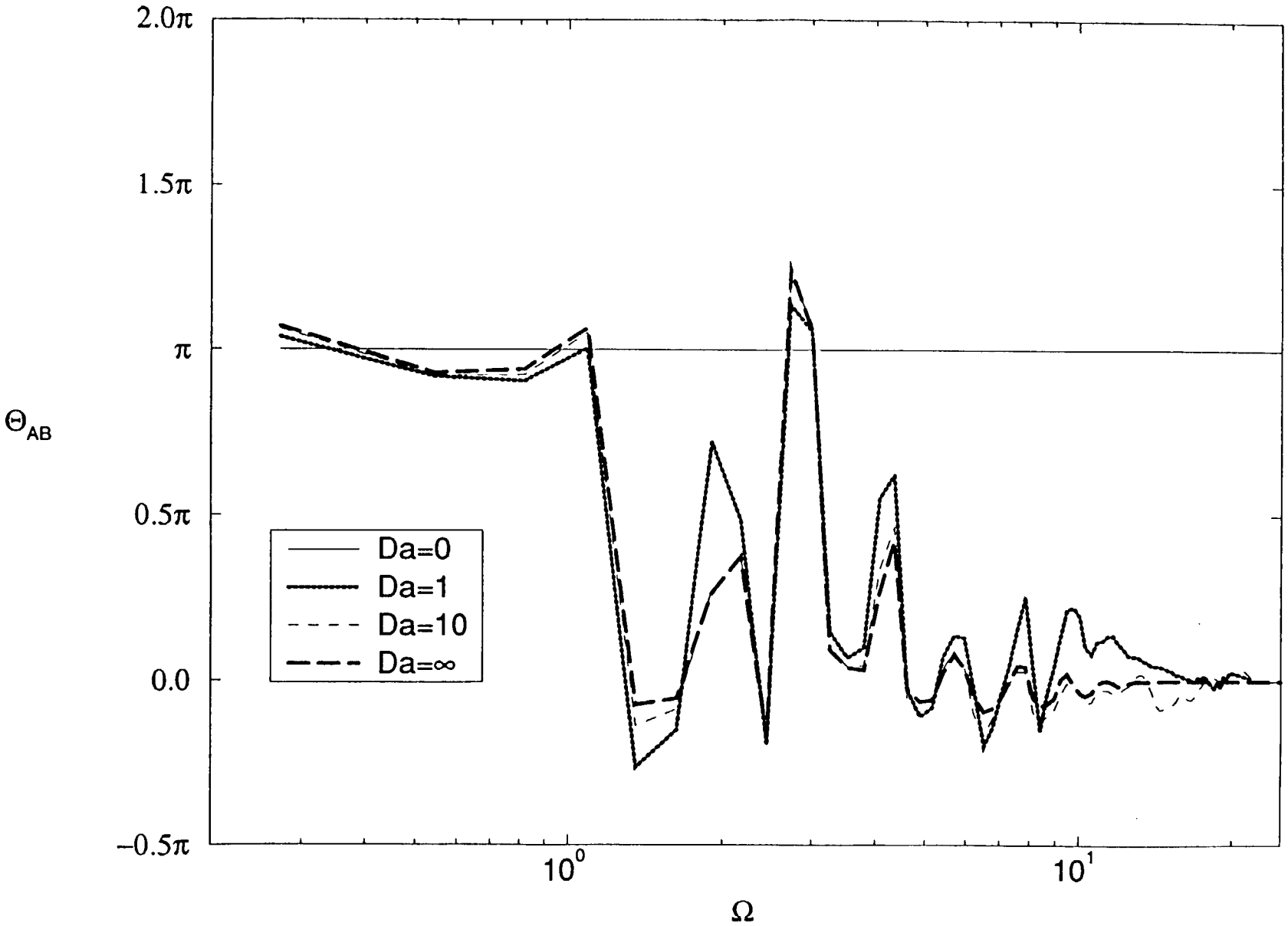

Figure 23(b)